THE APPLICATION OF ADVANCED SIGNAL PROCESSING TECHNIQUES TO THE CONDITION MONITORING OF ELECTRICAL MACHINE DRIVE SYSTEMS

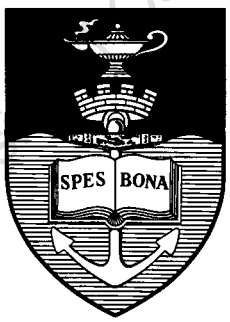

By: Paul Stanley Barendse

Thesis submitted to the Department of Electrical Engineering, University of Cape Town, in complete fulfilment of the requirements for the degree of
Doctor of Philosophy

August 2007

DECLARATION

This dissertation is submitted to the Department of Electrical Engineering, University of Cape Town, in complete fulfilment of the requirements for the degree of Doctor of Philosophy. It has not been submitted before for any degree or examination at this or any other university. The author confirms that this thesis is based on his own work. Portions of this work have been published in peer-reviewed journals and at refereed international conferences.

Signature: Signed by candidate Date: 26/11/07

Paul S. Barendse

ACKNOWLEDGEMENTS

My sincere thanks to my supervisor, Professor P. Pillay. The support and guidance he offered through my graduate career was truly invaluable.

My sincere gratitude is extended to my family, whose unconditional love, understanding, encouragement and support could not be surpassed. They include Mr Stanley Barendse (father), Mrs Doreen Barendse (mother), Ms Jackie Barendse (sister), Mr Dennis Barendse (grandfather), Mrs Isabel Barendse (grandmother), Mr Dennis Barendse (uncle) and Ms Mervynne Barendse (aunt).

I would like to thank my girlfriend, Ms Michelle Cotton, who has supported me and who is a very important part of my life.

My thanks and appreciation extends to my colleagues and friends in Professor Pillay's research group at the University of Cape Town (UCT). These include: Dr Ben Sebitosi, Dr Azeem Khan, Dr Hugh Douglas, Dr Lotten Mthombeni, Raj Naidoo, Marubini Manyage, Dave Johnson.

I am grateful for the technical assistance from Mr Chris Wozniak at the University of Cape Town.

ABSTRACT

Condition monitoring of electrical machines is a field which continuously demands improvement, especially as the tasks performed by these machines become more demanding and complex. Presently, the well established condition monitoring techniques are based on steady-state analysis of various diagnostic variables (i.e. current, voltage, power, etc.). These steady-state techniques are currently being applied to most machine-related applications, however it is well known that machine diagnostic variables behave typically as non-stationary signals. Therefore, it is difficult distinguishing fault conditions from normal operating conditions using steady-state analysis techniques. The most popular of these steady-state techniques employs the Fourier Transform as the analysis tool. Although there are numerous diagnostic variables which may be utilized for condition monitoring purposes, e.g. thermal and vibration monitoring have been quite popular, the most recent research is directed towards electrical monitoring of the motor.

The thesis examines the use of two time-frequency domain signal processing tools in its application to condition monitoring of electrical machine drive systems. The mathematical and signal processing tools which are explored are wavelet analysis and a non-stationary adaptive signal processing algorithm. Four specific applications are identified for the research. These applications were specifically chosen to encapsulate important issues in condition monitoring of variable speed drive systems. The main aim of the project is to highlight the need for fault detection during machine transients and to illustrate the effectiveness of incorporating and adapting these new class of algorithms to detect faults in electrical machine drive systems during non-stationary conditions.

The first application investigates the use of an adaptive algorithm for fault detection of inverter-fed permanent magnet (PM) machines during non-stationary conditions using the stator currents. The detection technique is based on the non-stationary adaptive signal processing algorithm which has been cascaded to extract fault associated sinusoids using the current signals. The machine faults examined include permanent magnet damage, inter-coil shorts and static

eccentricity. The results indicate that the algorithm's predictive ability is capable of extracting fault information under non-stationary operating conditions.

This second application examines the collaborative use of the non-stationary adaptive algorithm and the Wavelet Transform for the detection of mechanical imbalances in inverter-fed induction machines. The fault frequency components for induction machines are dependant on two variables, unlike the single variable dependence by permanent magnet machines. This poses too much of a challenge for the predictive capability of the cascaded adaptive algorithms proposed for the PM case and an alternate approach is explored. The Wavelet Transform is incorporated into the final detection scheme and it is shown that imbalanced faults in inverter-fed induction machines can be identified by decomposing transient inrush currents. This is significant, since most fault detection schemes fail or operate at a diminished level when drives are connected to the machine. The detection algorithm is load dependent, however it only requires a minimum load of approximately 30% at the desired speed. This is a considerable improvement from steady-state analysis techniques where heavier load conditions are required, particularly in the case of inverter-fed machines.

The third application investigates the detection of inter-turn stator faults in doubly-fed induction generators (DFIG), which are typically used in wind generator applications. The decision to analyze the system is based on their popularity in utility wind generator applications and because these generators can operate in both synchronous and asynchronous modes. A new non-stationary method of detecting inter-turn stator faults is proposed. The proposed fault detection method is a combination of Extended Park's Vector Approach and the non-stationary adaptive algorithm. The new method shows that inter-turn stator faults can unambiguously be identified during non-stationary conditions while also providing insight into the severity of the fault.

In the previous applications, the faults stem from machine failure, however it is important for this research to incorporate at least one fault, which is not machine related, but which could have an impact on the health of the machine and drive. The doubly-fed induction generator proves to be an ideal candidate, whereby a sag in the grid voltage could cause large induced currents

within the rotor circuit. This would be catastrophic to the power electronics and machine. The voltage sag therefore needs to be detected almost immediately. The sag detection technique is based on the non-stationary adaptive algorithm and is shown to detect sags faster than previous sag detection techniques. A simple mitigation strategy is employed to illustrate the effectiveness of diverting the excess energy once the sag is detected. The proposed strategy is simple and easy to incorporate as part of an existing control system.

TABLE OF CONTENTS

LIST OF ILLUSTRATIONS

TABLES **PAGE**

LIST OF ABBREVIATIONS

CWT	– Continuous Wavelet Transform
DFIG	– Doubly-Fed Induction Generator
DFT	– Discrete Fourier Transform
DWT	– Discrete Wavelet Transform
EPVA	– Extended Park's Vector Approach
FFT	– Fast Fourier Transform
FOC	– Field Orientated Control
MCSA	– Motor Current Signature Analysis
MUSIC	– Multiple Signal Classification Estimator
PM	– Permanent Magnet
RMS	– Root Mean Square
STFT	– Short Time Fourier Transform
WECS	– Wind Energy Conversion System
WRIM	– Wound Rotor Induction Machine

Chapter 1

1. INTRODUCTION

1.1 Overview

The thesis examines the use of two time-frequency domain signal processing tools in its application to condition monitoring of electrical machine drives. The mathematical and signal processing tools which are explored are wavelet analysis and a non-stationary adaptive signal processing algorithm. Four specific applications are identified for the research. These applications were specifically chosen to encapsulate important issues in variable speed drives. The project highlights the need for fault detection during machine transients and to illustrate the effectiveness of incorporating and adapting these new class of algorithms to detect faults in electrical machine drives during non-stationary conditions.

1.2 Research Background

Condition monitoring as applied to electrical machines, is the use of different technologies and algorithms to assess the machine health in an attempt to diagnose faults at their inception. The ability to detect faults at a very early stage is critical, since it facilitates a proactive response which minimizes downtime, maximizes productivity and reduces cost. There are many techniques and tools available, however the field of fault diagnosis continuously demands improvement as tasks performed by machines become increasingly more complex [1].

There are numerous faults which may be experienced by an electrical machine, however they may be broadly categorized as follows:

1) stator winding faults
2) broken rotor bars or cracked end rings for induction machines
3) static or dynamic eccentricity
4) unbalanced rotor
5) bearing failures.

Numerous fault detection methods have already been developed to identify particular faults [1]. Some of these methods are invasive and some are non-invasive. These condition monitoring techniques typically proceed in the following sequence of events:

1) a particular diagnostic variable, i.e. voltage, current, vibration, etc., is monitored using a sensor,
2) the monitored signal is coupled to an algorithm which analyses the data,
3) based on the analyzed results, a decision is made on the condition of the machine.

The following lists some of the condition monitoring techniques available:

1) temperature measurements
2) oil analysis
3) motor current signature analysis
4) neural-network-based techniques
5) electromagnetic field monitoring
6) vibration analysis.

The papers referred to in [1]-[3], provide an overview of work already covered in this area of research. [1] highlights the more common faults and their most suitable fault detection techniques.

One very popular method of analyzing the fault-related signal is to monitor the steady-state spectral components of the signal. Presently, many techniques that are based on steady-state analysis are being applied to almost all applications. However, many applications exist where the machine operates predominately in the transient, which holds particularly true in cases where the machine is connected to a drive, e.g. wind generators, motor operated valves, etc.

1.3 Objectives

The objectives of the thesis are to:

- conduct a thorough literature review on current condition monitoring techniques and time-frequency domain signal processing tools

- identify four drive-related applications which encapsulates the important issues in variable speed-electrical machine drives
- design, model and experimentally implement each of the identified applications
- identify possible faults which may be implemented on each of the applications
- develop methods to implement the faults on the systems
- conduct various transient tests and capture results
- perform an in-depth analysis on the attained results and conduct a comparative investigation into the most suitable combination of the signal processing/mathematical tools for fault detection in each of the applications
- draw conclusions and make recommendations

1.4 Literature Survey on Condition Monitoring Techniques

There are numerous tools and techniques which have been developed for condition monitoring purposes. Although thermal and vibration monitoring have been quite popular, the most recent research is directed towards electrical monitoring of the motor. Some of the more popular electrical monitoring techniques will now be discussed in greater detail.

1.4.1 Spectral Analysis

The more popular electrical monitoring techniques utilize the steady-state spectral components of various diagnostic variables of the machine. There are numerous diagnostic variables which may be used, i.e. voltage, power, flux, current, etc. These signals are transformed from the time domain to the frequency domain using the Fourier Transform. The accuracy of the technique is dependant upon a number of factors, these include:

1) the speed of the machine is constant and known
2) the slip is accurately measured
3) the stator fundamental is constant

4) the load is constant.

Any change in these constraints renders the information attained to be questionable. It is also well known that the diagnostic variables are typically non-stationary signals. As a result, it is considerably difficult to distinguish fault conditions from normal operating conditions using Fourier analysis.

Another challenge faced by the Fourier Transform is that it only provides the spectral content of the signal and does not provide any information regarding where in time these spectral components occur. Therefore different time-domain signals may produce identical spectrums, as illustrated by the following example. Figures 1.1(a) and 1.1(b) shows the time domain representation of two signals. Fig. 1.1(a) shows the summation of two sine waves of frequencies 20Hz and 40Hz, for the 0.2sec duration. Fig. 1.1(b) shows the 40Hz sine wave from 0 to 0.1sec and the 20Hz sine wave from 0.1sec to 0.2sec. These are two different signals in the time domain, however they produce the same frequency spectrum, as shown in Fig. 1.2.

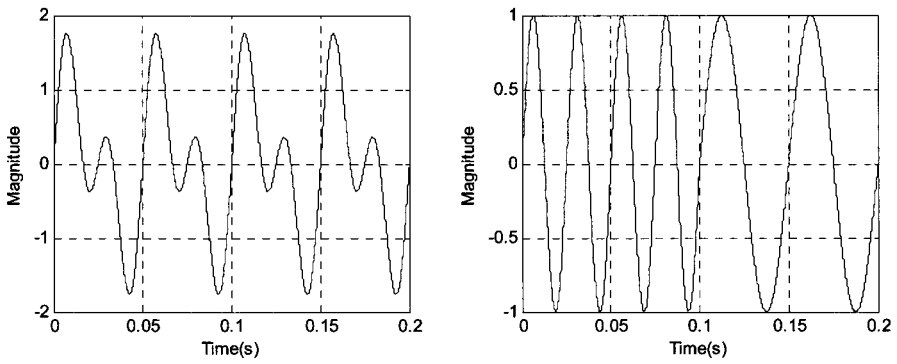

(a) **(b)**

Figure 1.1: Time representation of signals with two frequency components, 20Hz and 40Hz, whereby (a) is the summation of the two sinusoids for the entire duration, (b) the 40Hz sinusoid occurs for half the time and the 20Hz sinusoid occurs for the remaining time

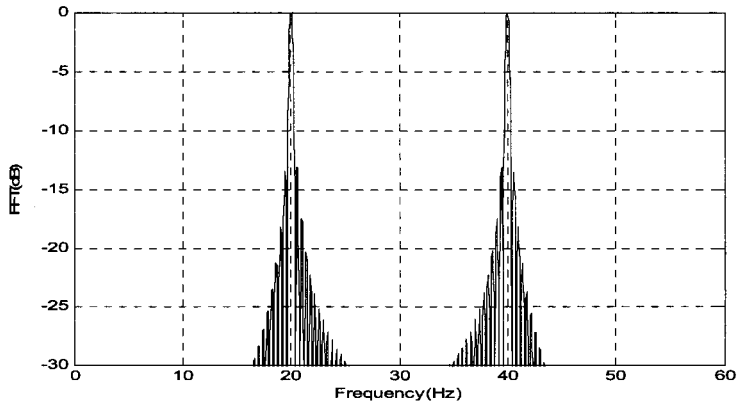

Figure 1.2: Current spectrums for the two signals are identical

1.4.1.1. Motor Current Signature Analysis

The prevalent technique used for the condition monitoring of electrical machines is Motor Current Signature Analysis (MCSA), which utilizes the stator currents of the motor as a diagnostic variable. Fig. 1.3 shows a typical current monitoring scheme for a 3-phase inverter-fed induction machine. The current signal is transformed from the time domain to the frequency domain using the Fourier Transform. The objective is to then identify specific current spectral components that are characteristic of faults.

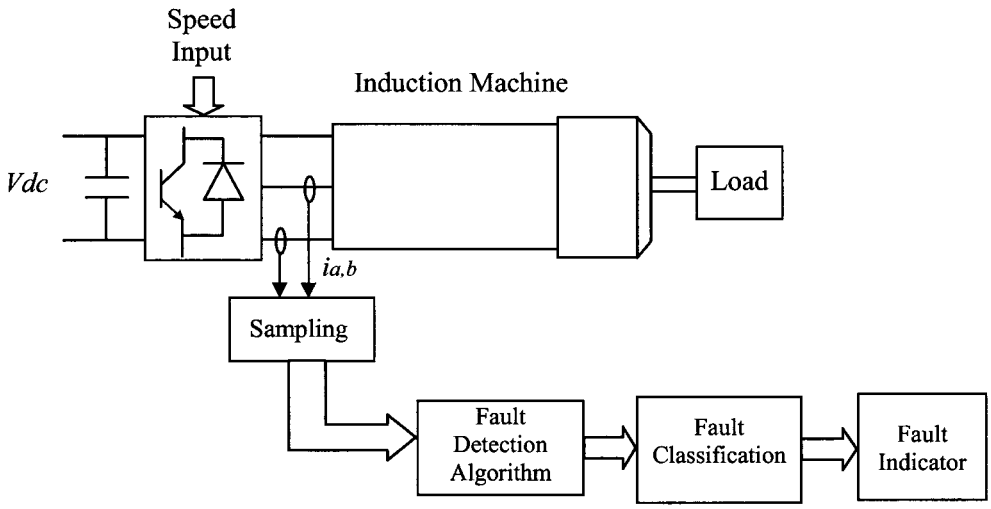

Figure 1.3: Stator current condition monitoring scheme

would appear at $2sf_s$ and $4sf_s$ [1]. This is particularly useful since the fault components are clear from the any other components.

1.4.1.2. Instantaneous Power Spectral Analysis

With this technique, the stator currents are replaced with the instantaneous power as the diagnostic variable for motor signature analysis. Therefore, the stator currents and voltages need to be monitored, which increases the hardware costs since extra sensors need to be incorporated into the monitoring system. The advantage of this technique is that the instantaneous power, which is the multiplication of the currents and voltages, would possess a greater amount of information than would be deduced from the currents alone. All fault information is also constrained in the frequency band 0-$2f_s$ Hz. Table 1.1 illustrates the relationship between the line currents frequency components and the instantaneous power frequency components, for the case of broken rotor bars [4]. Fig. 1.5 illustrates the instantaneous power spectrum for an induction machine with healthy rotor bars. The DC and 100Hz components are evident. Fig. 1.6 shows the instantaneous power spectrum for an induction machine with broken rotor bars. The DC and 100Hz components are again evident, however they are also accompanied by the broken rotor bar fault components located at $2sf_s$ and $(1\pm s)\,2f_s$.

Table 1.1: Relationship between Line Currents and Instantaneous Power Frequency Components

Frequency components in the line current	Frequency components in the instantaneous power
f_s	DC
	$2f_s$
$(1\pm 2ks)f_s$	$2ksf_s$
	$(1\pm ks)\,2f_s$

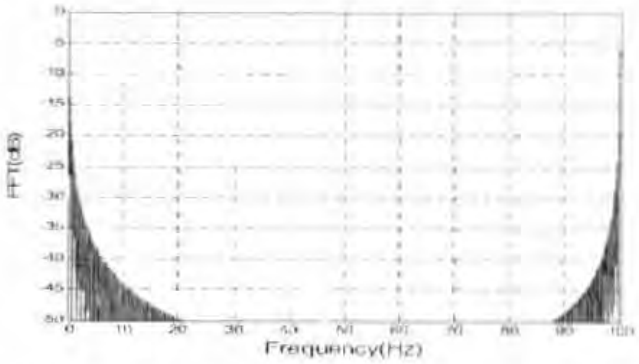

Figure 1.5: Typical instantaneous power spectrum for an induction machine with healthy rotor bars

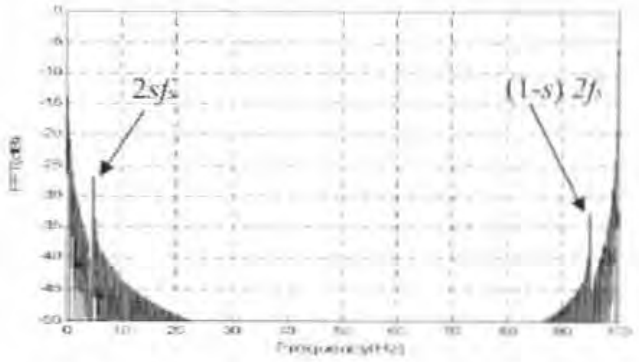

Figure 1.6: Typical instantaneous power spectrum for an induction machine with broken rotor bars

1.4.1.3. Bispectrum

Bispectrum, also known as third-order moment spectrum, was introduced to overcome some of the shortcomings faced by the power spectrum. While the power spectrum retains the magnitude information of a signal, the phase information is suppressed. Spectra of order three and higher must be used to preserve both magnitude and phase information, thus enriching the information preserved. The bispectrum is defined as "the 2-dimensional Fourier Transform of the 3rd-order moment", [5], [6], [7]. Very promising results are indicated in [8], however the results seem to suggest that the technique is better suited for electrical type faults rather than mechanical faults. The machines vibration signals served as the diagnostic variable in [8],

As an example, the fault harmonics to be monitored for broken rotor bars are given by

$$f_{brb} = (1 \pm 2ks) f_s \qquad (1.1)$$

f_{brb} are the sideband frequency components associated with broken rotor bars, f_s is the stator fundamental frequency, $k = 1,2,3,\ldots$, s is the slip [1].

Fig. 1.4(a) shows a typical current spectrum for an induction machine with healthy rotor bars. Fig. 1.4(b) shows a typical current spectrum for an induction machine with broken rotor bars, operating at a slip of 0.05. The sideband components which are characteristic of the broken rotor bars are clearly evident in Fig. 1.4(b).

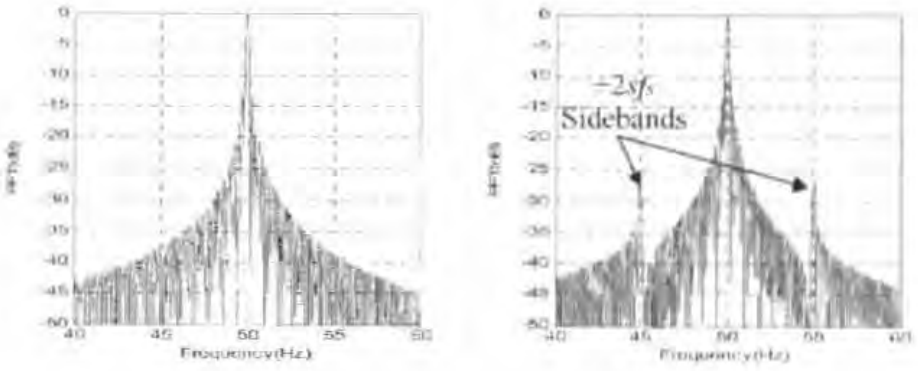

(a) (b)

Figure 1.4: Typical current spectrum for an induction machine with (a) healthy rotor bars and (b) broken rotor bars

Recent advances in MCSA, shows the 3-phase currents being mapped to the stationary reference plane using the Park's Transform, whereby the real and imaginary components are tracked to provide information about the type and extent of the fault. This is useful since it provides information about all three phases. An extension of this method is to monitor the frequency components of the current Park's vector modulus, which is known as the Extended Park's Vector Approach (EPVA). For a healthy machine, only a dc component would appear in the spectrum, however for the case of a machine with broken rotor bars, the dc component would be accompanied by the fault components which

however this was incorrectly referenced in [5], whereby the author claims the stator currents were analysed instead.

1.4.1.4.High Resolution Spectral Analysis

Another spectral technique which is presented in [9], attempts to solve one of the major disadvantages of classical spectral analysis techniques, i.e. the effect of side lobe leakages due to the inherent windowing effect of finite data sets. Window weighting is proposed as a possible solution, however the spectral resolution is drastically diminished through this process. [9] further investigates a class of spectral techniques which are based on eigenanalysis of the autocorrelation matrix. It is indicated that without sacrificing much stability, these techniques may enrich or maintain high resolution. This is achieved by only keeping the more dominant spectral components, thus offering greater resistance to noise [3].

Two well known eigenanalysis-based frequency estimators are the Multiple Signal Classification Estimator (MUSIC) and ROOT-MUSIC. Although these methods have shown to have definite advantages over the classic FFT spectral analysis for fault detection purposes, i.e. incorporating the stator current model into the algorithm and increasing noise resistance, the disadvantages are that these techniques are computationally intensive and may only be used for identifying faults which modify main spectral components [5].

1.4.2 Recently Developed Fault Detection Techniques

The more recently developed signal processing techniques indicates a shift to a new class of algorithms, which provide both time and frequency information of the signal. This is considerably important since the previous techniques were limited to steady-state operation, and signals that displayed transitory characteristics could not be analysed. As mentioned earlier, signals attained from machines typically display a non-stationary behaviour. To overcome the problem, the Short Time Fourier Transform (STFT) was incorporated into fault diagnosis. The signal is segmented into small sections and analysed using the Fourier Transform. The process translates the signal into the two-

dimensional time-frequency domain. Although the technique proved to provide promising results, the fixed size window which is used to segment the signal, limits the resolution. Wavelet Analysis was introduced to overcome the resolution-related difficulties faced by the STFT. There has been considerable development in the area of fault detection due to the introduction to wavelet analysis, since fault detection has been extended to non-stationary conditions, some of these are listed in [10]-[15]. Very little has been done on detecting faults in variable speed drives during transients using these new class of algorithms. This does pose a considerable challenge, however the advancement in signal processing techniques makes it possible to begin exploring these areas.

1.5 Summary and Discussion of the Project

The research conducted in this thesis explores the use of recent mathematical and signal processing algorithms, discussed in greater depth in Chapter 2, for the detection of machine-drive faults during transients. This is achieved by examining four drive-related applications. These applications were specifically selected to broadly cover key classes/types of machine drives. These are primarily classified according to the type of electrical machine employed. AC electrical machines can broadly be classified into two types:

1) Synchronous machines
2) Asynchronous machines.

The first application therefore investigates the use of a permanent magnet machine drive as an example of the synchronous machine type, which is presented in Chapter 3. The second application examines the implementation of an induction machine drive as an asynchronous machine type. Since the above mentioned applications operate as motors, it is thought to be of importance to include an application where the machine operates as a generator. The third application therefore examines the use of a doubly-fed induction generator, which is typically used in wind generator applications. The decision to analyze the system is based on their popularity in utility wind generator applications and because these generators can operate in both synchronous and asynchronous modes. In these applications, the faults stem

from machine failure, however it is important for this research to incorporate at least one fault, which is not machine related, but which could have an impact on the health of the machine and drive. The doubly-fed induction generator proves to be an ideal candidate for the above mentioned scenario, whereby a sag in the grid voltage could cause large induced currents within the rotor circuit, which would be catastrophic to the power electronics and machine. The voltage sag therefore needs to be detected almost immediately.

The above-mentioned applications are all modeled and implemented experimentally. The more common faults are then implemented on each of the systems and various transient tests are performed. The diagnostic signals are captured and the results are analysed using the various combinations of the signal processing techniques. The combination of techniques which produced the most prominent results for each of the applications are presented and discussed in the respective chapters, after which conclusions are drawn.

1.6 Contributions of this Dissertation

The research methods associated with this thesis are mainly analytical and experimental. The performance and design of drive systems are modeled analytically. The models are validated through simulation, using Matlab, and implemented experimentally. The models are used to analyse the performance and to optimise the design of the systems.

The specific contributions made by this thesis include the following:

- Chapter 3 proposes a fault detection strategy for an inverter-fed PM synchronous machine. The control strategy used for the drive is modeled and validated through simulations. The system is then implemented experimentally. The proposed fault detection technique combines the concept of the MCSA technique and the non-stationary adaptive mathematical tool, described in Chapter 2, to produce a strategy capable of extracting fault information during non-stationary conditions. The faults which are examined include damage to the permanent magnet, static

eccentricity and inter-turn stator faults. Methods for implementation of these faults are fully described and illustrated.

- Chapter 4 examines a fault detection strategy for detecting mechanical rotor imbalances in inverter-fed induction machines. Unlike the PM machine, the fault components which appear in the stator currents of induction machines are not only dependant on the fundamental frequency, but also slip. This adds to the complexity of monitoring these components, which poses too much of a challenge for the predictive capabilities of the proposed technique for the PM case and an alternative approach is investigated. The technique investigated was first proposed in [10] for the detection of broken rotor bars in induction machines during direct-online start-ups, where the slip component is considerably large. The large slip separates the broken rotor bar frequencies from the fundamental frequency, making them easier to detect. The work done in this chapter extends the concept to inverter-fed induction machines. This poses a challenge since the slip is kept considerably small due to the soft starting capabilities of the drive. The findings indicate that the fault detection strategy is capable of detecting the fault by analysing transient in-rush currents. Although the technique is load dependant, there is a considerable improvement to the loading requirements compared to the MCSA technique.
- In Chapter 5, a method of detecting inter-turn stator faults in doubly-fed wind generators during non-stationary conditions is proposed. The doubly-fed wind generator is developed from fundamental principles. The system is firstly modeled, simulated and then implemented experimentally. A method for simulating inter-turn stator faults is also described and implemented. Changes in the load and the wind speed, affects the magnitude of the stator currents. These changes could have a considerable impact on the ability of the existing steady-state fault detection techniques in effectively diagnosing faults. The most effective steady-state fault detection technique for detecting inter-turn stator faults is the Extended Park's Vector Approach. In [16], it is shown that wavelet analysis performed on the modulus of the Park's Vector representation of the stator

current, could serve as a means for diagnosing the fault during non-stationary conditions. This chapter proposes a more efficient fault detection scheme which is capable of indicating the severity of the fault while reducing the computational requirements of the final detection scheme. The proposed scheme replaces the wavelet analysis performed on the modulus of the Park's Vector representation of the stator current with the use of the non-stationary adaptive algorithm, described in Chapter 2.

- Chapter 6 proposes a fault ride-through strategy for doubly-fed wind generators during voltage sags. A voltage sag at the terminals of the doubly-fed wind generator, causes large transient currents in the rotor circuit which could damage the back-to-back converter. Although fault mitigation techniques exist for the doubly-fed wind generator, the deciding factor that could prevent catastrophic failure is the time required to detect the sag. The sag detection technique in [17] utilises the non-stationary adaptive algorithm for rapid sag detection. This is shown to detect sags faster than current techniques. This technique is incorporated into the final fault ride-through strategy for the doubly-fed wind generator. Once the sag is detected using this technique, a simple method of mitigating the fault is proposed whereby a resistor is switched across the DC-link capacitor to absorb the excess energy transmitted through the rotor. Simulated and experimental results are shown and discussed.

1.7 References

[1] S. Nandi, H. A. Toliyat, X. Li, "Condition Monitoring and Fault Diagnosis of Electrical Motors-A Review," IEEE Trans. on Energy Conversion, vol. 20, no. 4, pp 719 – 729, December 2005.

[2] W. T. Thomson, M. Fenger, "Current Signature Analysis to Induction Motor Faults," IEEE Industry Applications Magazine, May/June 2001, pp. 26-34.

[3] M.E. H. Benbouzid, "A Review of Induction Motors Signature Analysis as a Medium for Faults Detection," IEEE Trans. on Ind. Electronics, vol. 47, no. 5, Sept. 2000, pp 984-993.

[4] Zhenxing Liu, Xinaggen Yin, Deshu Chen, "Online Rotor Mixed Fault Diagnosis Way Based on Spectrum Analysis of Instantaneous Power in Squirrel Cage Induction Motors," IEEE Trans. in Energy Conversion, vol. 19, no. 3, September 2004.

[5] M. E. H. Benbouzid, G. B. Kliman, "What Stator Current Processing-Based Technique to Use for Induction Motor Rotor Faults Diagnosis?," IEEE Trans on Energy Conversion, col. 18, no. 2, June 2003.

[6] A. P. Petropulu and H. Pozidis "Phase Reconstruction from Bispectrum Slices," IEEE Trans. on Signal Processing, vol. 46, no. 2, pp 527-530, Feb. 1998.

[7] Ji-Wu Zhang, Chong-Xun Zheng, An Xie, "Bispectrum Analysis of Focal Ischemic Cerebral EEG Signal Using Third-Order Recursion Method," IEEE Trans. on Biomedical Engineering, vol. 47, no. 3, pp 527-530, March 2000.

[8] T. W. S. Chow, G. Fei, "Three Phase Induction Machines Asymmetrical Faults Identification Using Bispectrum," IEEE Trans. on Industrial Electronics, vol. 51, no. 3, pp 558-565, June 2004.

[9] M. E. H. Benbouzid, M. Vieira, C. Theys, "Induction Motors' Faults Detection and Localization Using Stator Current Advanced Signal Processing Techniques," IEEE Trans. on Power Electronics, vol. 14, no. 1, Jan. 1999.

[10] H. Douglas, P. Pillay, A. K. Ziarani, "Broken Rotor Bar Detection in Induction Machines with Transient Operating Speeds," IEEE Trans. on Energy Conversion, vol. 20, no. 1, March 2005.

[11] H. Douglas, P. Pillay, A. K. Ziarani, "A New Algorithm for Transient Motor Current Signature Analysis using Wavelets," IEEE Trans. on Industry Appl., vol. 40, no. 5, 30 Sept/ Oct 2004.

[12] H. Douglas, P. Pillay, A. K. Ziarani, "The Impact of Wavelet Selection on Transient Motor Current Signature Analysis," IEEE-International Conference on Electrical Machines and Drives IEMDC, 2005, pp 80-85.

[13] Faliang Niu, Jin Huang, "Rotor Broken Bars Fault Diagnosis for Induction Machines based on Wavelet Ridge Energy Spectrum,"

Proceedings of the Eighth International Conference on Electrical Machines and Systems ICEMS 2005, vol. 3, pp 2274-2277, Sept. 2005.

[14] T. W. S. Chow, Shi Hai, "Induction Machine Fault Diagnostic Analysis with Wavelet Technique," IEEE Trans. on Industrial Electronics, vol. 51, Issue 3, pp 558-565, June 2004.

[15] J. A. Antonino-Daviu, M. Riera-Guasp, J. R. Folch, M.P.M. Palomares, "Validation of a New Method for the Diagnosis of Rotor Bar Failures via Wavelet Transform in Industrial Induction Machines," IEEE Trans. on Industry Applications, vol. 42, no. 4, pp: 990-996, July-Aug. 2006.

[16] H. Douglas, P. Barendse, P. Pillay, "The Detection of Inter-Turn Stator Faults in Doubly-Fed Induction Generators", Proc. IEEE Ind. Appl. Soc. (IAS'05), Hong Kong 2005, vol. 2, pp 1097 – 1102, 2-6 Oct. 2005.

[17] R. M. Naidoo, P. Pillay, "A New Algorithm for Voltage Sag Analysis and Mitigation", IEEE Power Engineering Society General Meeting, 2005, 12-16 June 2005 Page(s):2935 - 2938 Vol. 3.

Chapter 2

2. TIME-FREQUENCY DOMAIN SIGNAL PROCESSING TECHNIQUES

2.1 Introduction

Due to the limitations in signal processing techniques, fault diagnosis of electrical machines have primarily been based on steady-state analysis, e.g. Discrete Fourier Transform (DFT). However, these techniques lose their effectiveness when the analysed signal exhibits transitory characteristics, i.e. drifts, abrupt changes, etc. The advancement in signal processing techniques has produced a new class of algorithms, the development of which do not follow conventional methods, making it possible to analyse non-stationary signals. The ability of the algorithms to analyse non-stationary signals is indicative of their capacity to extract time and frequency information from the signal. These are therefore known as time-frequency domain signal processing techniques. These new algorithms have already found applications in diverse areas of electrical engineering ranging from power systems to biomedical applications [1]-[9].

Some of these techniques have already been applied to the condition monitoring of electrical machines. Although the research in this area is still in its infancy, it has been shown that there is tremendous scope for these algorithms in its application to condition monitoring [10]-[15]. This chapter presents one such algorithm in addition to a recently developed mathematical technique which lends itself to the analysis of non-stationary signals. Section 2.2 formulates and evaluates the performance of the non-linear adaptive algorithm. Section 2.3 presents the fundamental concepts behind Wavelet analysis. Conclusions are drawn in Section 2.4.

2.2 An Algorithm for Extracting Non-Stationary Sinusoids

This section presents a signal processing algorithm capable of extracting non-stationary sinusoids, by estimating the amplitude, phase and frequency of the input signal over time and accommodating variations in these parameters.
The algorithm has found application in diverse areas of engineering. Examples include frequency estimation, active noise and vibration control, power systems and sinusoidal disturbance rejection [1]-[9]. A set of non-linear differential equations govern the performance and dynamics of the algorithm [1]. The algorithm exhibits a high degree of noise immunity and robustness. The functionality of the algorithm is enhanced by it's very simple structure, which is suitable for both hardware and software implementation. Section 2.2.1 presents the mathematical derivation of the algorithm's governing equations and Section 2.2.2 evaluates the performance of the algorithm.

2.2.1 Formulation of the Algorithm

Let *u(t)* represent a signal comprising of a dominant sinusoidal component polluted by a number of additional sinusoidal components and noise. This would typically represent a voltage or current signal. A sinusoidal component of this function which is of interest is $y(t) = A\sin(\omega t + \delta)$, where A is the constant amplitude, ω represents the constant frequency, δ is constant phase and $\phi(t) = \omega t + \delta$ represents the total phase of this component. In practice, the amplitude, frequency and phase terms of all constituting sinusoids could vary with time. Consider a general form for *u(t)* [1],

$$u(t) = \sum_{i=0}^{\infty} A_i \sin\phi_i + n(t) \tag{2.1}$$

in which *n(t)* denotes the superimposed noise. To incorporate the concept of instantaneous frequency into the total phase, the output is defined as

$$y(t) = A(t)\sin\left(\int^{t}\omega(\tau) + \delta(t)\right) \tag{2.2}$$

Let $\mathfrak{M}$ represent a manifold containing all sinusoidal signals defined as

$$\mathfrak{M}=\left\{A(t)\sin\left(\int^{t}\omega(\tau)+\delta(t)\right)\middle|A(t)\in[A_{\min},A_{\max}],\omega(t)\in[\omega_{\min},\omega_{\max}],\delta(t)\in[\delta_{\min},\delta_{\max}]\right\}$$

where $\theta(t)=[A(t),\omega(t),\delta(t)]^T$ is the vector of parameters which belong to the parameter space

$$\Theta=\left\{[A,\omega,\delta]^T\middle|A\in[A_{\min},A_{\max}],\omega\in[\omega_{\min},\omega_{\max}],\delta\in[\delta_{\min},\delta_{\max}]\right\}$$

and T denotes the matrix transposition, [1].

The output is defined as the desired sinusoidal component, i.e.

$$y(t,\theta(t))=A(t)\sin\left(\int^{t}\omega(\tau)+\delta(t)\right) \tag{2.3}$$

To produce the optimum solution in extracting the desired sinusoidal component, the element selected has to minimise the distance function d between the desired sinusoid, $y(t,\theta(t))$ and the input, $u(t)$, i.e.,

$$\theta_{opt}=\arg\min_{\theta(t)\in\Theta} d[y(t,\theta(t)),u(t)] \tag{2.4}$$

The instantaneous distance function d is given as

$$d(t,\theta(t))=[u(t)-y(t,\theta(t))]=e(t) \tag{2.5}$$

Therefore, the cost function is defined as

$$J(t,\theta(t))=d^2(t,\theta(t)) \tag{2.6}$$

The gradient descent method is used to minimise the least-squares error between the input signal and the desired sinusoidal signal by estimating the parameter vector θ, this is given by equation (2.7),

$$\frac{\mathrm{d}\theta(t)}{\mathrm{d}t}=-\mu\frac{\partial[J(t,\theta(t))]}{\partial\theta(t)} \tag{2.7}$$

where μ represents the algorithms regulating constant diagonal matrix [1]. The rate of convergence and stability of the algorithm are governed by the values of the entries to this matrix. The direct mathematical proofs of convergence and stability are discussed and fully presented in [1]. The diagonal matrix μ is defined as

$$\mu=\begin{bmatrix}m_1 & 0 & 0\\ 0 & m_2 & 0\\ 0 & 0 & m_3\end{bmatrix} \tag{2.8}$$

From here on, $\hat{A}(t), \hat{\omega}(t)$ and $\hat{\delta}(t)$ will denote the estimated values of the parameter vector $\theta(t)$, i.e.,

$$\hat{\theta}(t) = \left[\hat{A}(t), \hat{\omega}(t), \hat{\delta}(t)\right]^T \tag{2.9}$$

Expanding equation (2.7), the following arises, [1]

$$\begin{bmatrix} \frac{d\hat{A}(t)}{dt} \\ \frac{d\hat{\omega}(t)}{dt} \\ \frac{d\hat{\delta}(t)}{dt} \end{bmatrix} = -\begin{bmatrix} m_1 & 0 & 0 \\ 0 & m_2 & 0 \\ 0 & 0 & m_3 \end{bmatrix} \begin{bmatrix} \frac{\partial}{\partial \hat{A}(t)}\left[u(t) - \hat{A}(t)\sin\left(\int^t \hat{\omega}(\tau)d\tau(t) + \hat{\delta}(t)\right)\right]^2 \\ \frac{\partial}{\partial \hat{\omega}(t)}\left[u(t) - \hat{A}(t)\sin\left(\int^t \hat{\omega}(\tau)d\tau(t) + \hat{\delta}(t)\right)\right]^2 \\ \frac{\partial}{\partial \hat{\delta}(t)}\left[u(t) - \hat{A}(t)\sin\left(\int^t \hat{\omega}(\tau)d\tau(t) + \hat{\delta}(t)\right)\right]^2 \end{bmatrix} \tag{2.10}$$

By solving the above differential equation, the equations below are derived, [1].

$$\frac{d\hat{A}(t)}{dt} = 2m_1 e(t)\sin\left(\int^t \hat{\omega}(\tau)d\tau(t) + \hat{\delta}(t)\right) \tag{2.11}$$

$$\frac{d\hat{\omega}(t)}{dt} = 2m_2 e(t)\hat{A}(t)t\cos\left(\int^t \hat{\omega}(\tau)d\tau(t) + \hat{\delta}(t)\right) \tag{2.12}$$

$$\frac{d\hat{\delta}(t)}{dt} = 2m_3 e(t)\hat{A}(t)\cos\left(\int^t \hat{\omega}(\tau)d\tau(t) + \hat{\delta}(t)\right) \tag{2.13}$$

where *e(t)* is defined as

$$e(t) = u(t) - \hat{A}(t)\sin\left(\int^t \hat{\omega}(\tau)d\tau(t) + \hat{\delta}(t)\right) \tag{2.14}$$

Since $\hat{\phi}(t) = \int^t \hat{\omega}(\tau)d\tau(t) + \hat{\delta}(t)$, therefore

$$\frac{d\hat{\phi}(t)}{dt} = \hat{\omega}(t) + \frac{d\hat{\delta}(t)}{dt} \tag{2.15}$$

A time-variable is explicitly attained in equation (2.12), when solving the matrix in equation (2.10). It is stated in [1], that the time-varying system has been observed to be unstable and practically of no value. This is to be expected since the non-convex cost function formulation of the algorithm does conform well to the performance attributes rendered by the gradient descent method. A heuristic method is implemented to ensure the system is time-

invariant, which performs very well in practice, as described in [1]. This conversion process is achieved by replacing t by a constant number m_4.

As a result, the following set of non-linear differential equations, which represent the governing equations of the algorithm, may be written as

$$\frac{d\hat{A}(t)}{dt} = 2\mu_1 e(t)\sin\hat{\phi}(t) \tag{2.16}$$

$$\frac{d\hat{\omega}(t)}{dt} = 2\mu_2 e(t)\hat{A}(t)\cos\hat{\phi}(t) \tag{2.17}$$

$$\frac{d\hat{\phi}(t)}{dt} = \hat{\omega}(t) + \mu_3 \frac{d\hat{\omega}(t)}{dt} \tag{2.18}$$

where error $e(t)$ remains as

$$e(t) = u(t) - \hat{A}(t)\sin\hat{\phi}(t)$$

and the parameters μ_1, μ_2 and μ_3 are formed from constants m_1, m_2 and m_3 as shown below

$$\mu_1 = m_1 \tag{2.19}$$

$$\mu_2 = m_2 m_4 \tag{2.20}$$

$$\mu_3 = \frac{m_3}{m_2 m_4} \tag{2.21}$$

As mentioned in [1], although the formulation of the algorithm stems from the minimisation of least squares error and gradient descent method, the final derivation does not conform to the conditions under which these method operate. This implies that the properties surrounding the proposed algorithm, i.e., it's rate of convergence, stability and it's value to the engineering application, needs to be examined. Some of the key properties will be investigated and findings presented in the next section. In [1], the stability of the theorem is proven mathematically and a further investigation into the properties of the algorithm is presented.

A block diagram representation of the algorithm is given in Fig. 2.1. ω_o represents the initial conditions of the predicted frequency. The algorithm will then track the most dominant frequency component of the input sinusoid which is closest to ω_o. This version of the algorithm will be referred to as the varying-frequency sinusoid tracking algorithm.

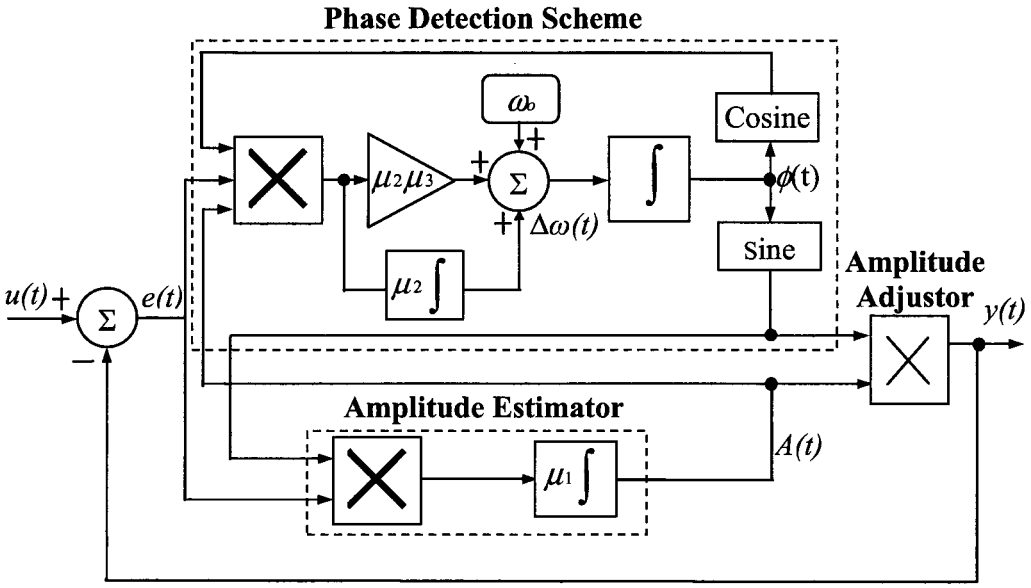

Figure 2.1: Varying–frequency sinusoid tracking algorithm

In [1], [3] and [4], the algorithm is slightly reconfigured to track and extract sinusoids of a fixed frequency ω_0. The adapted algorithm is described by the following differential equations,

$$\frac{d\hat{A}(t)}{dt} = 2\mu_1 e(t)\sin\hat{\phi}(t) \tag{2.22}$$

$$\frac{d\hat{\phi}(t)}{dt} = 2\mu_2 e(t)\hat{A}(t)\cos\hat{\phi}(t) + \omega_0 \tag{2.23}$$

The gains of the system μ_1 and μ_2 are responsible for the response speed of the amplitude and phase angle estimation, respectively. The system does not accommodate changes in frequency and extracts the sinusoid centred around ω_0. The space in which the desired signal lies is two-dimensional since the only variables which accommodate time-variations are $\hat{A}(t)$ and $\hat{\phi}(t)$. Fig. 2.2 shows the block diagram of the fixed-frequency tracking algorithm.

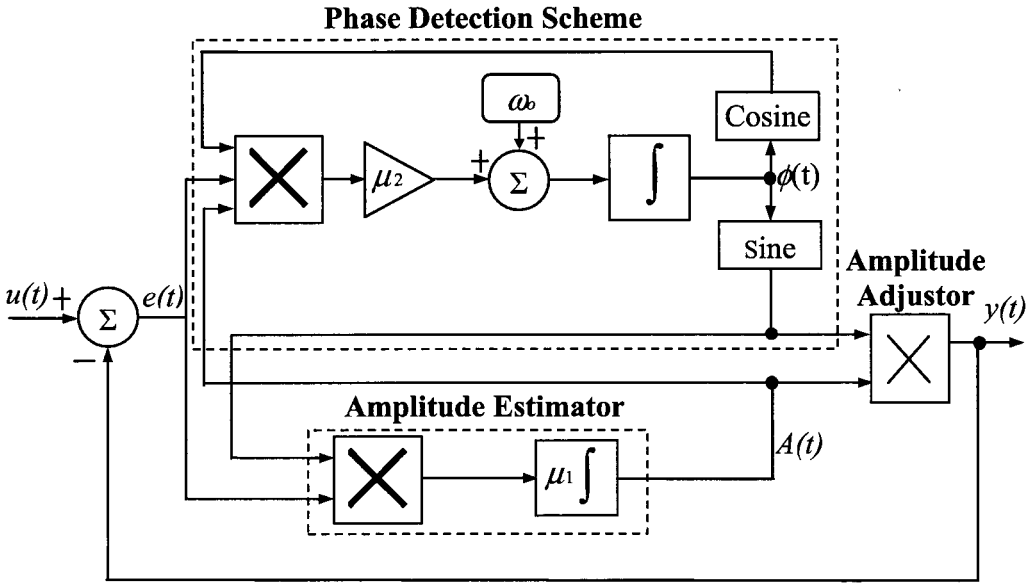

Figure 2.2: Fixed-frequency sinusoid tracking algorithm

The selection of the gain parameters is critically important in defining the engineering performance of the algorithms. These parameters determine the convergence speed versus error compromise and are largely dependent on the application [7]-[9].

2.2.2 *Performance Evaluation of the Algorithm*

The following section deals with some of the basic performance properties of the varying-sinusoid tracking algorithm. The algorithm is implemented in Matlab-Simulink and the results are discussed below. For simulations performed in Sections 2.2.2.1-2.2.2.5, the values for parameters μ_1, μ_2 and μ_3 have been selected as $\mu_1 = 300$, $\mu_2 = 50000$ and $\mu_3 = 0.015$. Section 2.2.2.6 examines the effect of the gain parameters μ_1, μ_2 and μ_3 on the convergence speed versus error compromise of the algorithm.

2.2.2.1 Initial Convergence of the Algorithm

The first experiment illustrates the ability of the algorithm to track and extract a pure sinusoidal input of unity amplitude and frequency 60Hz where the

intial conditions of the algorithm are set to $A_o = 1, f_o = 50\text{Hz}$ and $\delta_o = 0rad.$ Fig. 2.3 shows the input signal to the algorithm, the extracted sinusoid, it's amplitude and frequency. The time required to converge to the input sinusoid is only a few cycles. Once it converges, the steady-state error is zero between the amplitude, frequency and phase of the input and estimated sinusoid. To assist in visualising the convergence of the algorithm, Fig. 2.4 illustrates the convergence to a periodic orbit, at 60Hz, in the frequency domain.

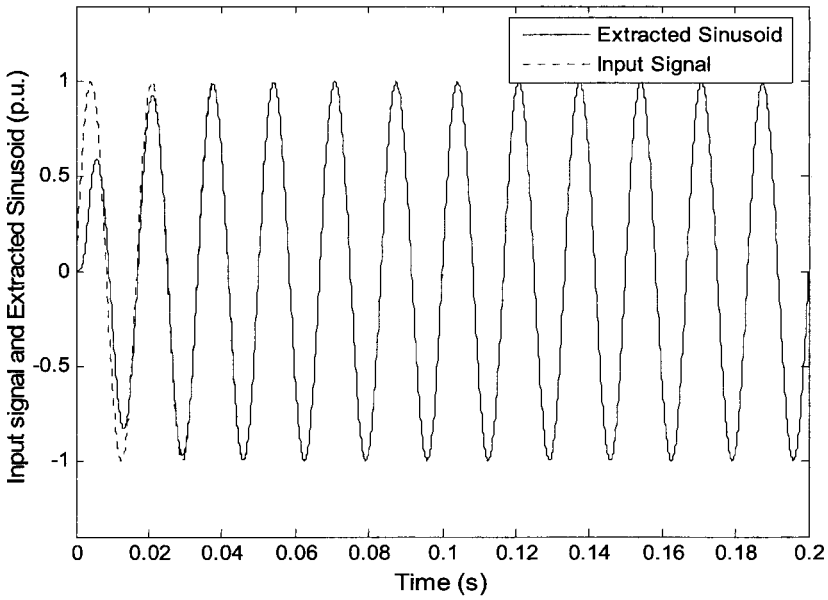

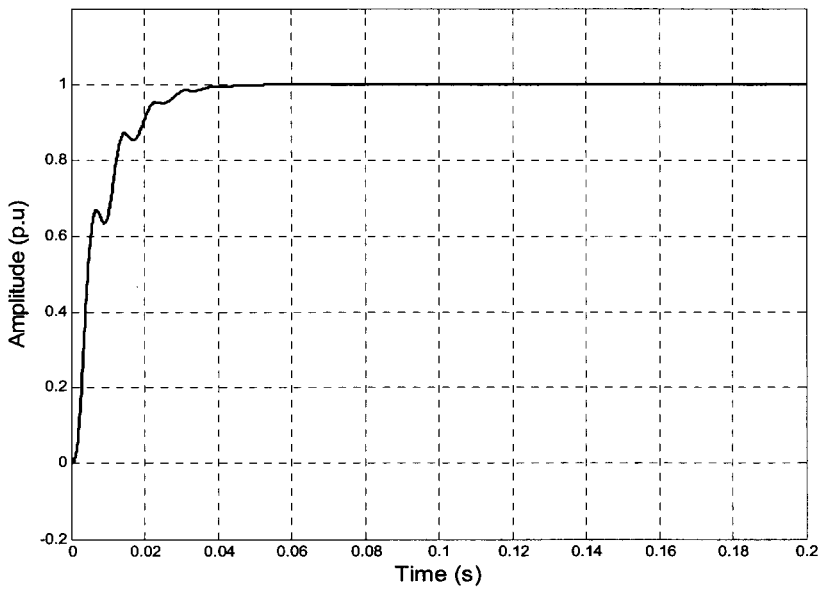

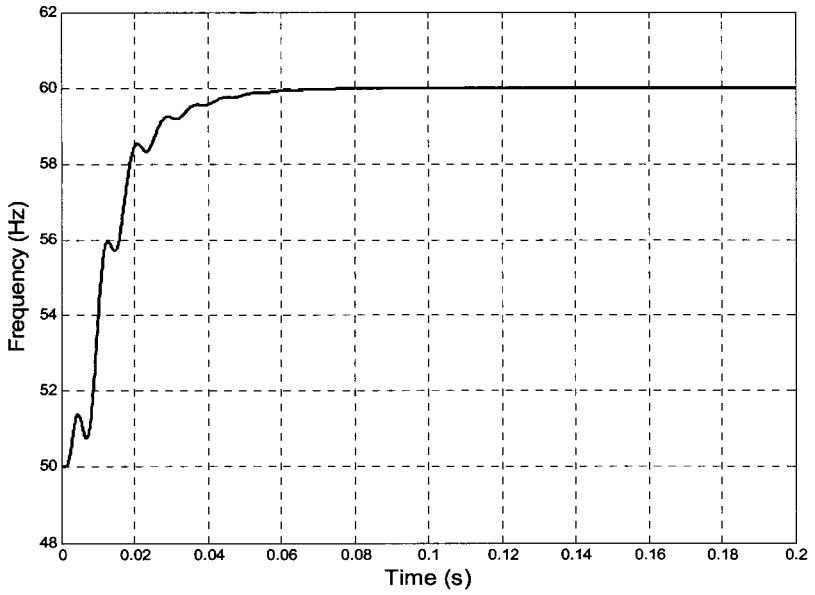

Figure 2.3: Basic initiatory performance of the algorithm extracting a sinusoidal signal

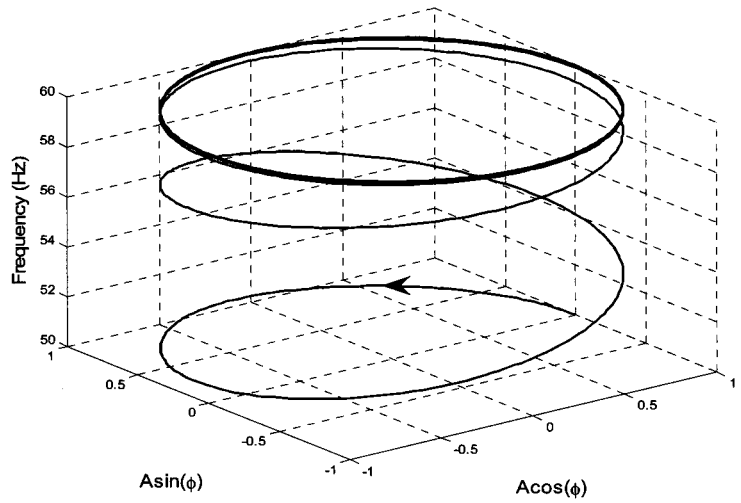

Figure 2.4: Convergence to a periodic orbit (A=1, ω =120π, ϕ = 120πt)

2.2.2.2 Amplitude Tracking

The following simulation illustrates the algorithms amplitude locking ability. The amplitude of the input signal is stepped from unity to 0.9p.u. at 0.05 seconds, while the frequency is maintained at 60Hz. Fig. 2.5 shows the extracted sinusoid, its amplitude and frequency. The algorithm is able to lock

onto the step in amplitude within a few cycles, while converging to the frequency and phase of the input sinusoid.

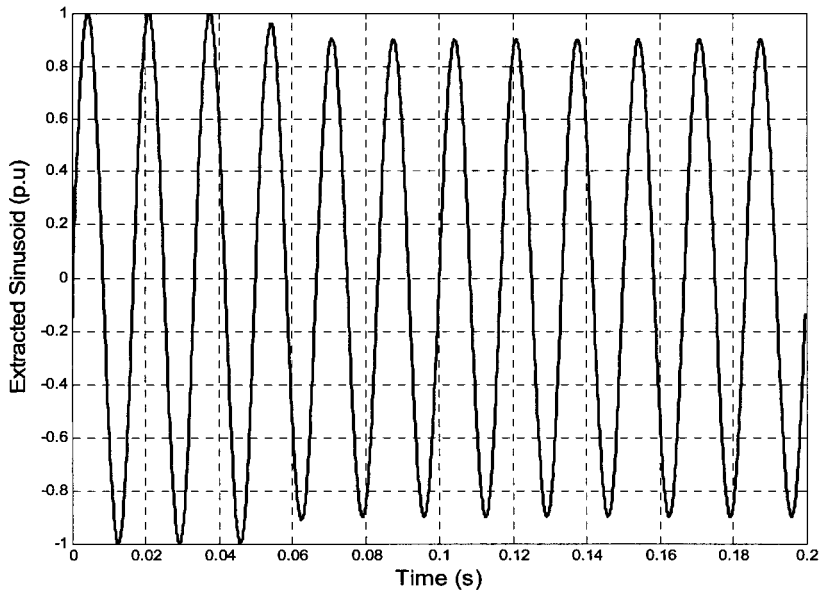

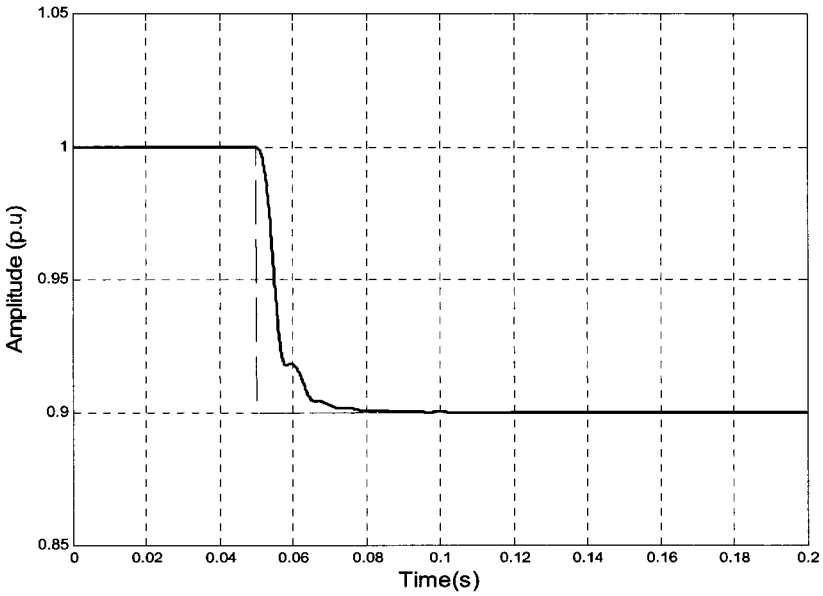

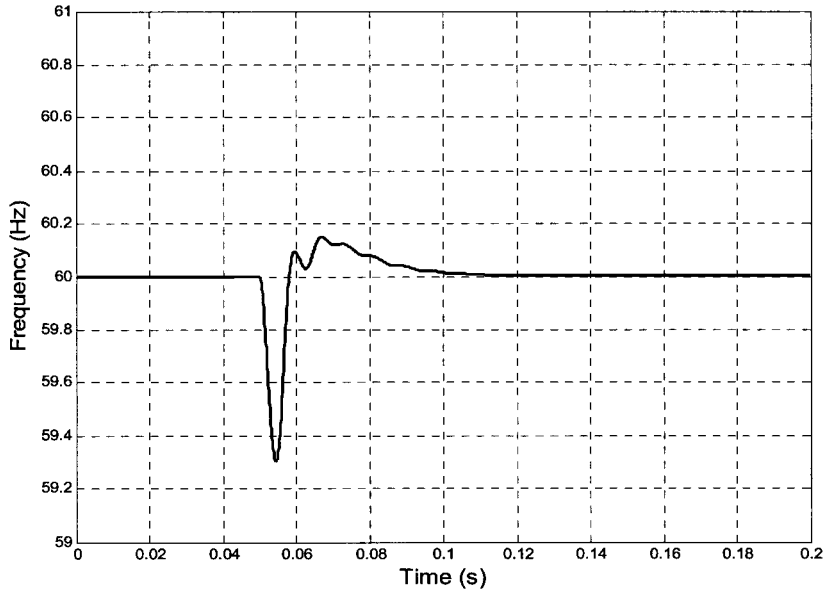

Figure 2.5: Amplitude-locking property of the algorithm

2.2.2.3 Frequency Tracking

To examine its frequency tracking capability, the input sinusoidal frequency is stepped at 0.05 seconds from 60Hz to 40Hz. Fig. 2.6 shows how rapidly the algorithm converges to the change in frequency.

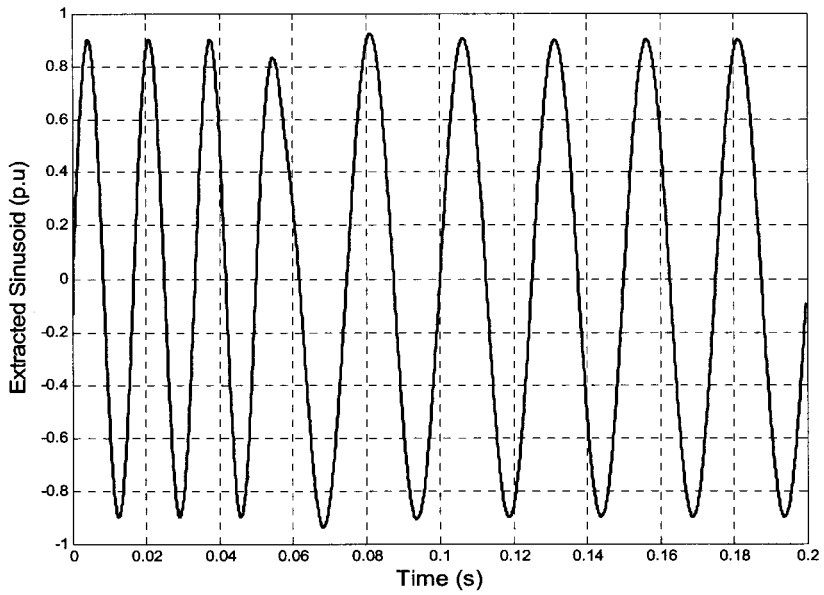

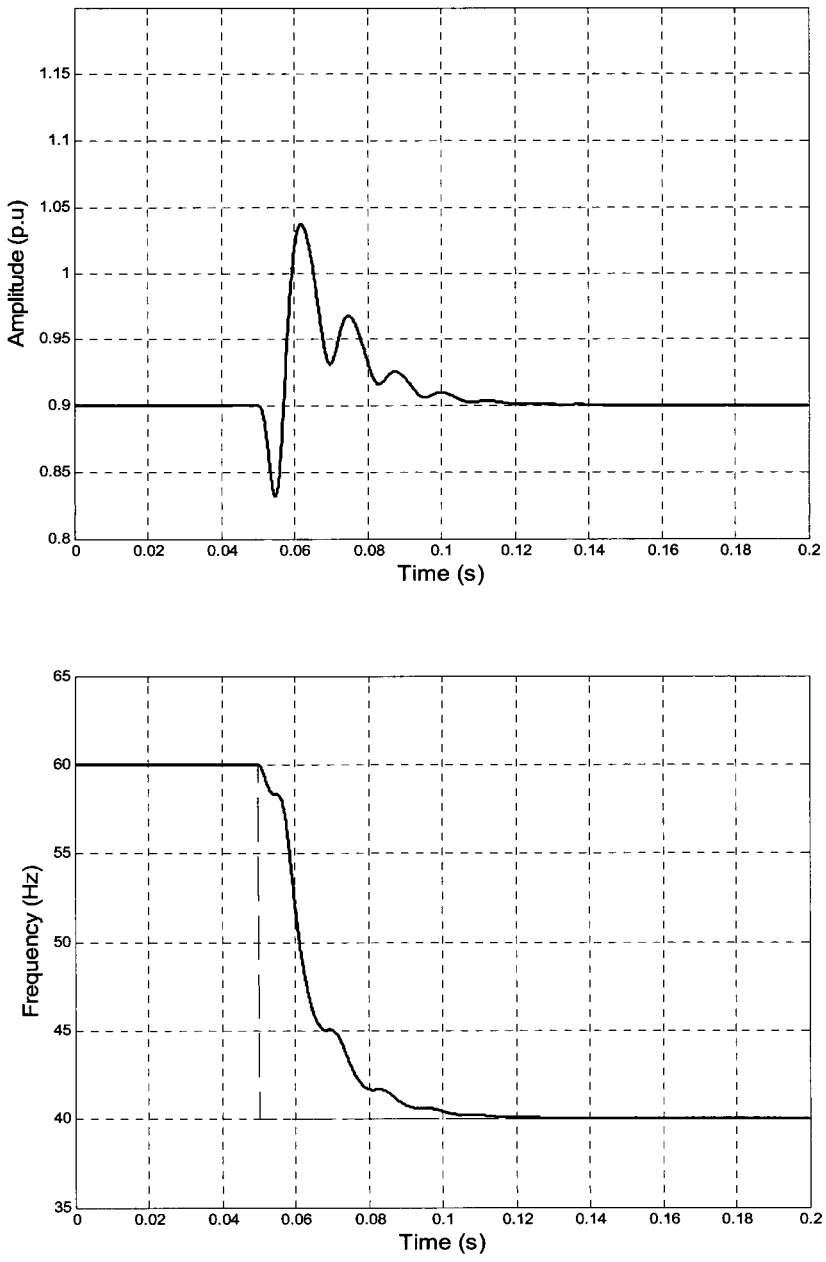

Figure 2.6: Frequency-locking property of the algorithm

2.2.2.4 Phase-Locking

Fig. 2.7 illustrates the phase-locking feature of the algorithm. A 45° phase shift is imposed on the input signal at 0.1 seconds, and within 2 cycles of the phase shift, the algorithm latches onto the input signal.

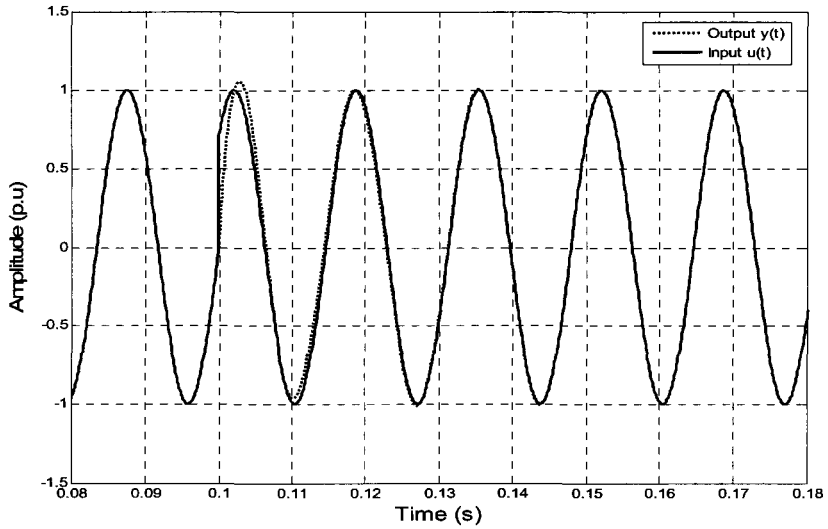

Figure 2.7: Phase-locking property of the algorithm

2.2.2.5 Noise Immunity

This section investigates the noise immunity properties of the algorithm. A pure sinusoid of unity amplitude and frequency 60Hz is added with Gaussian white noise of zero mean and variance 0.025. The noise is effectively filtered out as shown in Fig. 2.8. Fig. 2.9 shows the noise component which is filtered by the algorithm.

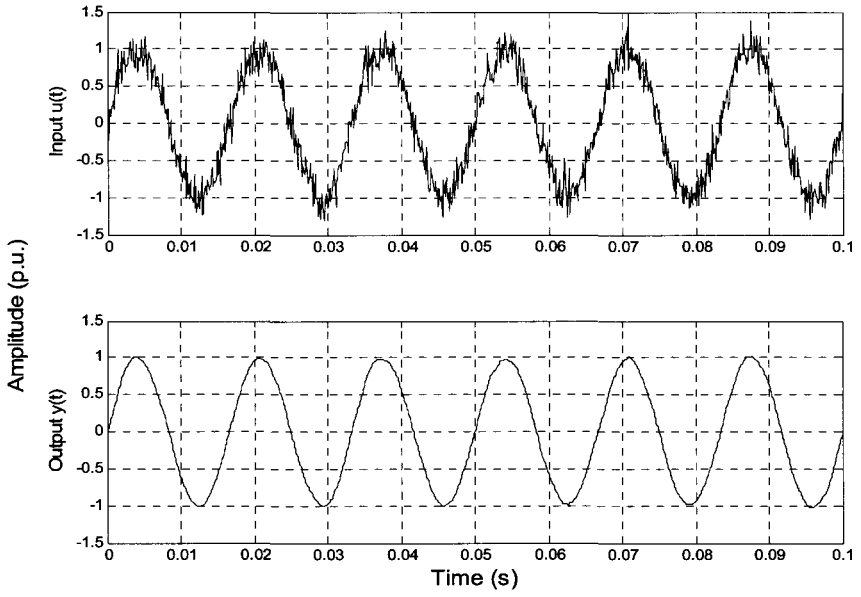

Figure 2.8: Noise immunity feature of the algorithm

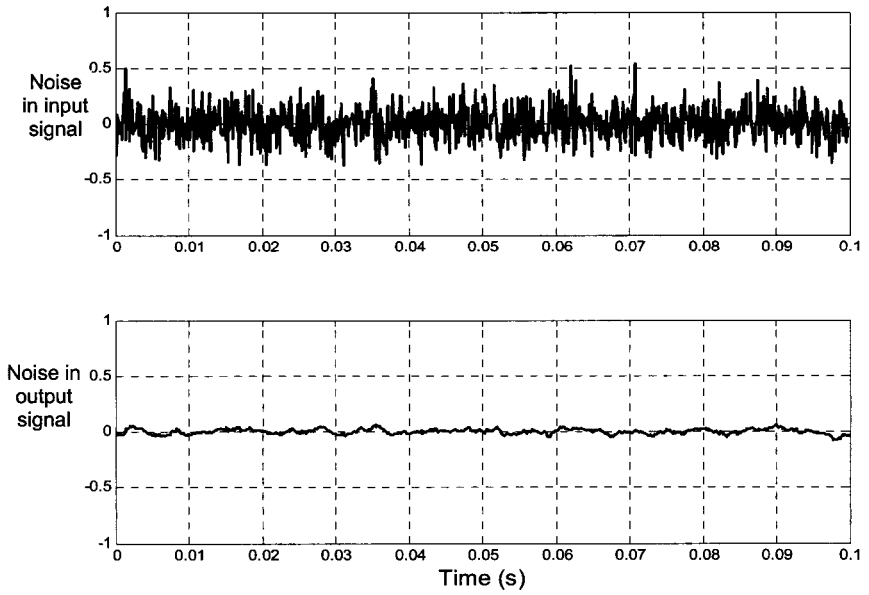

Figure 2.9: Filtering ability of the algorithm in removing noise

2.2.2.6 Effect of Gain Parameters on Performance

The selection of the gain parameters determines the convergence speed versus the steady state error. This section examines the effect of the gain parameters on the amplitude, frequency and phase tracking ability of the algorithm. Specifically, parameter μ_1 controls the speed of the transient response of the algorithm with respect to variations in the amplitude of the interfering signal. Parameters μ_2 and μ_3 mutually control the speed of the transient response of the algorithm with respect to variations in the frequency and phase of the interfering signal. The results shown in Fig. 2.10 indicate the impact of the gain parameter μ_1 on the convergence speed of the amplitude for the simulation test performed in Section 2.2.2.2, whereby only the amplitude of the input sinusoid is stepped from 1p.u. to 0.9p.u. at 0.05 seconds while the frequency is maintained at 60Hz. It is evident from the figure that the convergence speed increases as μ_1 increases, however overshoot is evident at larger gain values. The selection of μ_1 should be guided by the desired convergence time for maximum amplitude deviation of the input signal. In this case, μ_1 =300 seems to provide a good trade-off.

Fig. 2.11 shows the impact of μ_2 and μ_3 on the convergence of the frequency for the test performed in Section 2.2.2.3, whereby the frequency is stepped from 60Hz to 40Hz at 0.05 seconds while the amplitude is maintained at 1p.u. In this case, increasing the gain parameters μ_2 and μ_3, decreases the rate of frequency convergence and overshoot is experienced at the lower gains. These parameters seem to have the opposite effect on frequency convergence compared to the effect μ_1 has on the amplitude convergence.

Fig. 2.12 shows the impact of μ_2 and μ_3 on the convergence of the phase for the test performed in Section 2.2.2.4, whereby a 45° phase shift is imposed on the input signal at 0.1 seconds while the amplitude is maintained at 1p.u and frequency is maintained at 40Hz. It is evident that the higher gains result in faster convergence. Therefore, when selecting μ_2 and μ_3, there should be a trade off between frequency convergence and phase convergence.

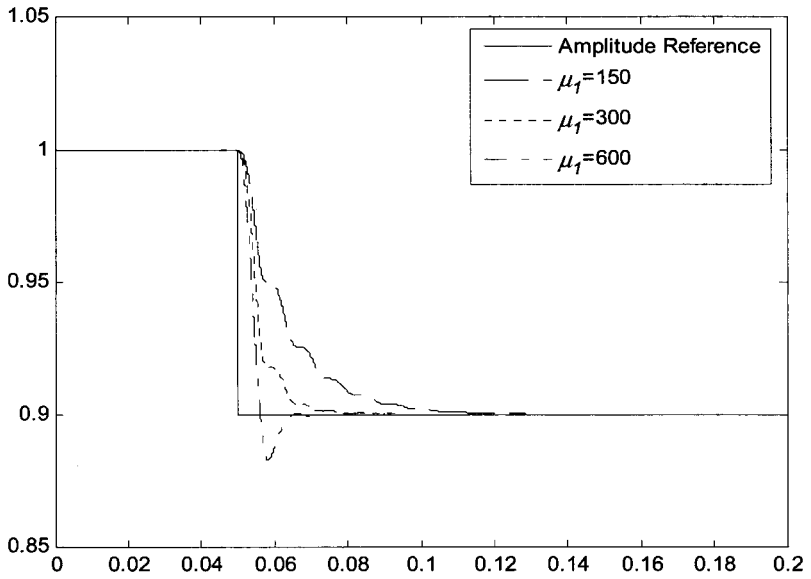

Figure 2.10: Amplitude convergence of the core algorithm under different μ_1 parameters

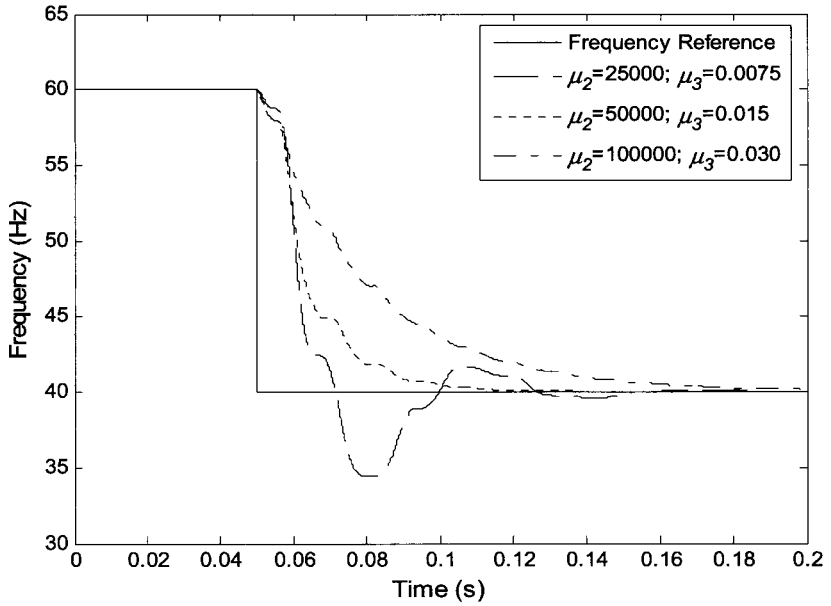

Figure 2.11: Frequency convergence of the core algorithm under different μ_2 and μ_3 parameters

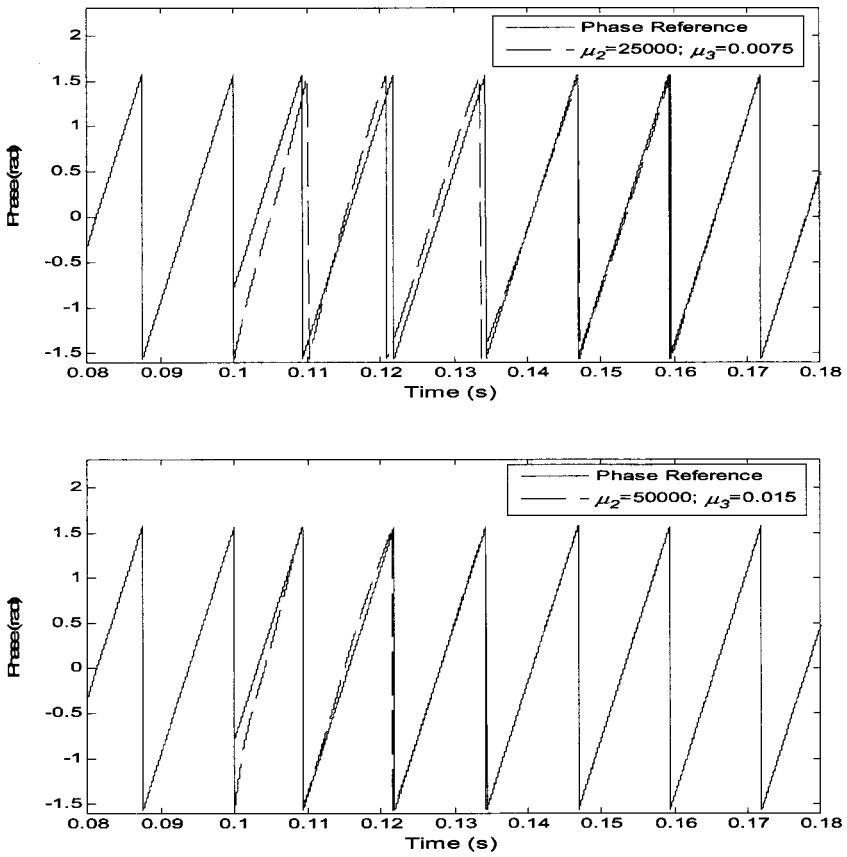

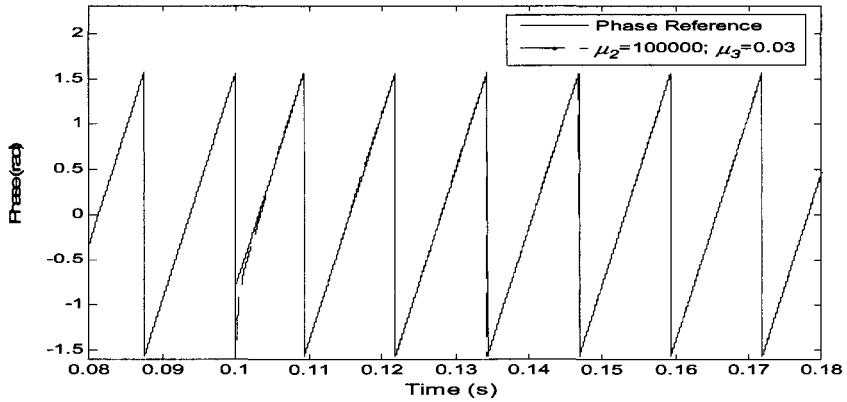

Figure 2.12: Phase convergence of the core algorithm under different μ_2 and μ_3 parameters

2.3 The Wavelet Transform

Transforms are a means of representing a signal in an alternative way without altering its information content. The Wavelet Transform provides a time-frequency representation of a signal. It was introduced as an alternative to the Short Time Fourier Transform (STFT). Although both provide a time-frequency representation of a signal, the Wavelet Transform is able to overcome some of the resolution related difficulties faced by the STFT, i.e. the STFT gives a fixed resolution at all times as indicated in Fig. 2.13(a), whereas the Wavelet Transform provides a variable resolution as shown in Fig. 2.13(b) [16].

The fundamental concept behind Wavelet analysis is to analyze according to scale. It uses a fully scalable modulated window which solves the signal-cutting problem, allowing for variable resolution. The fundamental principle of operation is as follows. A specific sized window is chosen and shifted along the signal, calculating the spectrum as it covers the length of the signal. This process is repeated for different scaled windows, until a time-frequency representation of the signal is attained with different resolutions. However, with wavelets, instead of referring to the frequency, the scale parameter is defined as the inverted frequency.

The ability of the Wavelet Transform to attain variable resolution is critically important since higher frequencies are better resolved in time, and lower frequencies are better resolved in frequency, as underlined by the Heisenberg uncertainty principle. A more mathematical approach to wavelets will now be discussed.

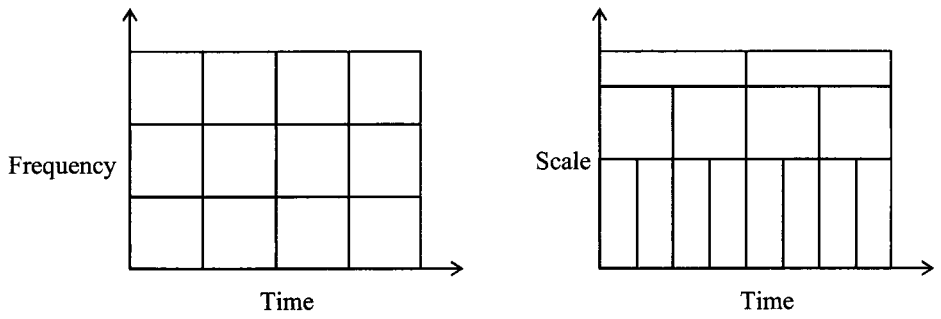

(a) **(b)**

Fig. 2.13: A scalogram showing the (a) fixed resolution as used in the STFT and the (b) variable resolution as used in Wavelet analysis

2.3.1 Fundamental Wavelet Concepts

Certain fundamental concepts will be revisited before the Wavelet Transform is introduced. The first concept is that of a basis for a vector space. A basis of a vector space V is defined as a set of linearly independent vectors, such that any vector in V can be expressed as a linear combination of those basis vectors. The number of vectors in a basis for a vector space is known as the dimension. The second concept is based on the orthogonality of vectors and is defined as follows. Two vectors are said to be orthogonal if their inner product equals zero. Vectors satisfying both conditions discussed above are known as orthogonal basis vectors [17].

The above concepts can easily be extended to sets of functions. This is critically important since the underlying structure in any decomposition algorithm (e.g. Fourier analysis) is a set of basis functions. The basis functions for Fourier analysis are a family of sine and cosine functions, which are

orthogonal on the interval $(-\pi,\pi)$. Similarly for Wavelet analysis, the basis functions are families of scaling functions, $\phi(t)$, and associated wavelet, $\psi(t)$. The scaling function is represented as follows [18],

$$\phi_{j,k}(t)=\sum_{k} P_k \phi\left(2^j t-k\right) \tag{2.24}$$

where,

P_k represents the coefficients of the scaling function

k represents a translation

j represents the scale

The associated wavelet can be formulated using the same coefficients as the scaling function, as shown below, and is referred to as the mother wavelet.

$$\psi_{j,k}(t)=\sum_{k}(-1)^k P_{1-k}\phi\left(2^j t-k\right) \tag{2.25}$$

The scaling functions are orthogonal to each other as well as to the wavelet function as shown below.

$$\int_{-\infty}^{\infty}\phi(2t-k)\phi(2t-l)dt=0 \tag{2.26}$$

for all $k \neq l$.

$$\int_{-\infty}^{\infty}\psi(t)\phi(t)dt=0 \tag{2.27}$$

In Wavelet analysis, there are a number of different wavelets which may be selected, resulting in different coefficients. This is unlike Fourier analysis where it always produces the same coefficients for a signal, because the basis functions are fixed sinusoids. The more common wavelets which are used include the Haar, Daubechies, Morlet, Mexican Hat, Gaussian and Meyer wavelets.

2.3.2 *The Continuous Wavelet Transform*

The Continuous Wavelet Transform (CWT) was designed as an alternative to the STFT, to combat the resolution difficulties as mentioned earlier. CWT measures the degree of similarity between the signal and the transforming function. The CWT of a signal $f(t)$ is defined as follows [16];

$$W_{gf}(a,b)=\frac{1}{\sqrt{a}}\int f(t)\psi^{*}\left(\frac{t-b}{a}\right)dt \tag{2.28}$$

where * denotes the complex conjugate.

$$W_{gf}(a,b)=\frac{1}{\sqrt{a}}\int f(t)\cdot\psi^{*}_{a,b}(t)\,dt \tag{2.29}$$

As shown by the above equation, the transformed signal is a function of two variables, the scale parameter a and translation parameter b. The scaling parameter is defined as (1/frequency) and corresponds to frequency information. It is responsible for dilating or compressing a signal. Large scales correspond to dilated signals, which provide global information about the signal and small scales correspond to compressed signals, which provide detailed information about the signal. The translation parameter represents the shifting or translation of the transforming function $\psi(t)$, which provides the time-localization information of the original signal. $\frac{1}{\sqrt{a}}$ is for energy normalization across the scales [16].

Examples of different wavelets are further examined and discussed below. The Haar family of scaling and wavelet functions form the basis for the simplest of wavelet analysis. The scaling and wavelet function is shown in Figures 2.14(a) and 2.14(b) respectively. A disadvantage of the Haar wavelet is that these wavelets are discontinuous and therefore, do not approximate continuous signals very well [17].

The Haar scaling and wavelet functions are defined mathematically as follows

$$\phi(t)=\begin{cases}1, & \text{if } 0\le t<1\\ 0, & \text{elsewhere}\end{cases} \tag{2.30}$$

$$\psi(t)=\begin{cases}1, & \text{if } 0\le t<1/2\\ -1, & \text{if } 1/2\le t<1\\ 0, & \text{elsewhere}\end{cases} \tag{2.31}$$

The Daubieches wavelet was introduced to overcome some of the drawbacks experienced by the earlier wavelets, i.e. Haar, Shannon and Linear Spline. The simplest of the Daubechies wavelets is the Haar wavelet, however the

hierarchy of the Daubechies wavelets are compactly supported and continuous. In fact, moving further up the hierarchy, results in an increasingly smoother wavelet. The Daubechies2 scaling function and wavelet function is shown in Figures 2.15(a) and 2.15(b) respectively. The Daubechies6 scaling function and wavelet function is illustrated in Figures 2.16(a) and 2.16(b), whereby a smoother waveform is clearly evident. The mathematical derivations for the Daubechies wavelets are illustrated in [17]. The Meyer scaling and wavelet function is another family of wavelets, as shown in Figures 2.17(a) and 2.17(b).

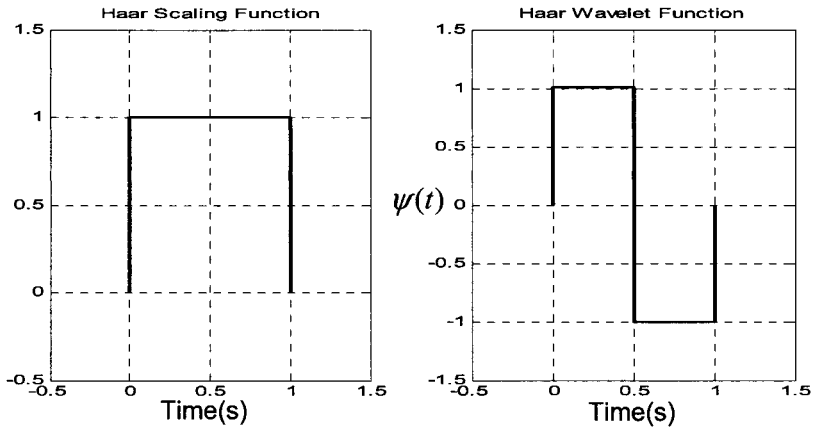

Fig. 2.14: Haar scaling and wavelet function

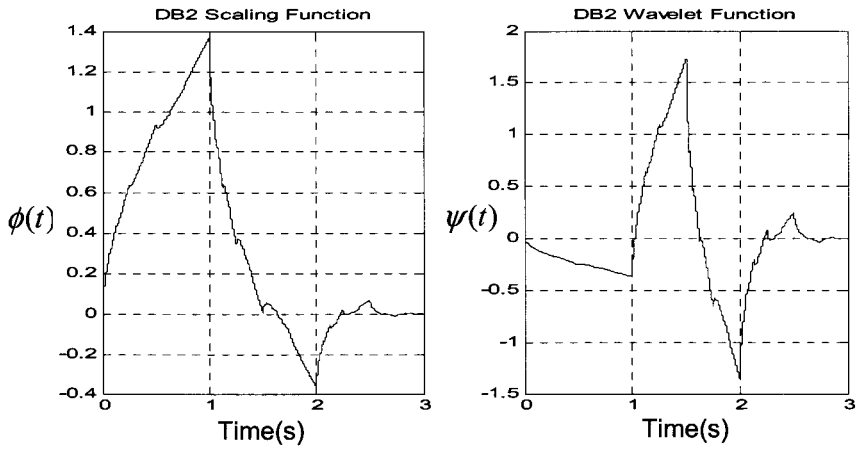

Fig. 2.15: Daubechies2 scaling and wavelet function

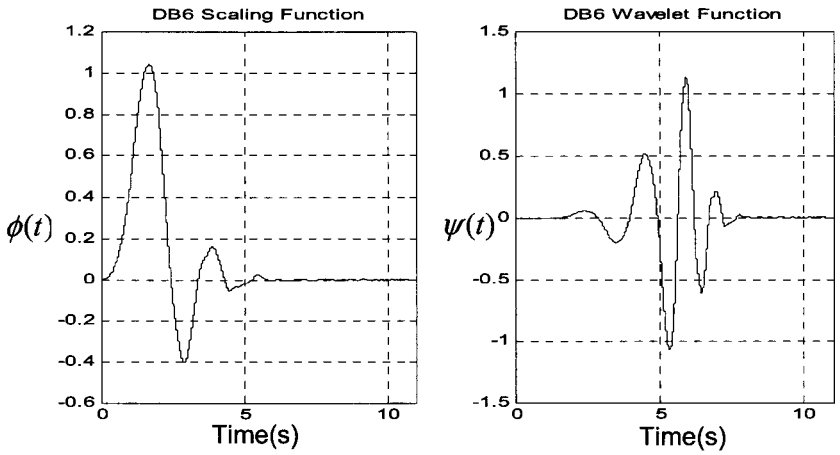

Fig. 2.16: Daubechies6 scaling and wavelet function

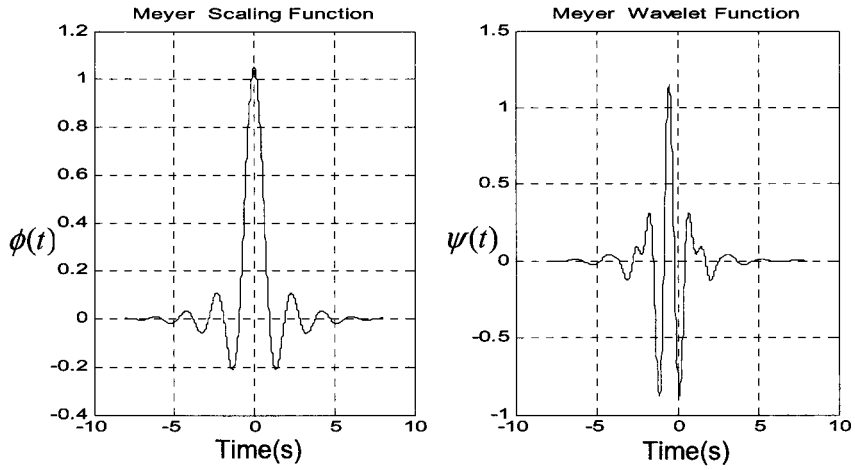

Fig. 2.17: Meyer scaling and wavelet function

The following example shows the Continuous Wavelet Transform of the non-stationary signal as illustrated in Fig. 2.18. The non-stationary signal has four different frequency components, each occurring for time intervals of 0.04 seconds. The Continuous Wavelet Transform of the signal is shown in Fig. 2.19.

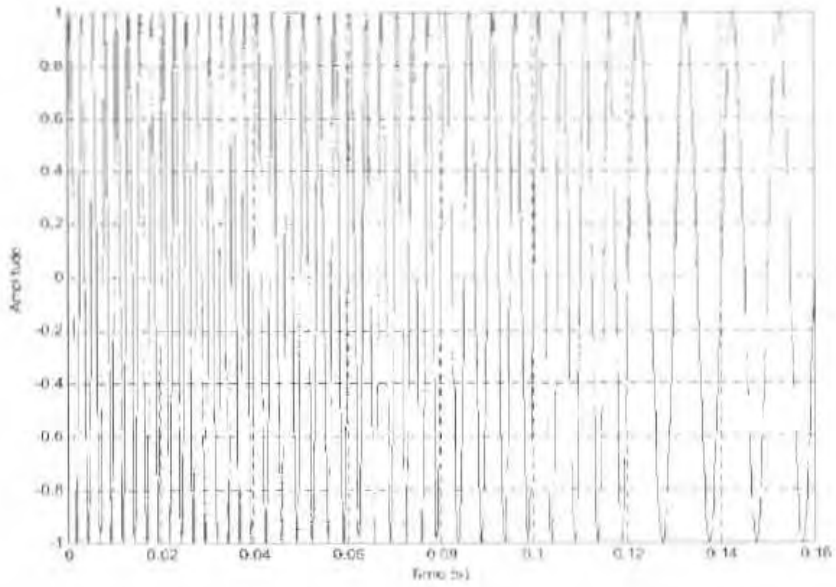

Figure 2.18: A time representation of a non-stationary signal

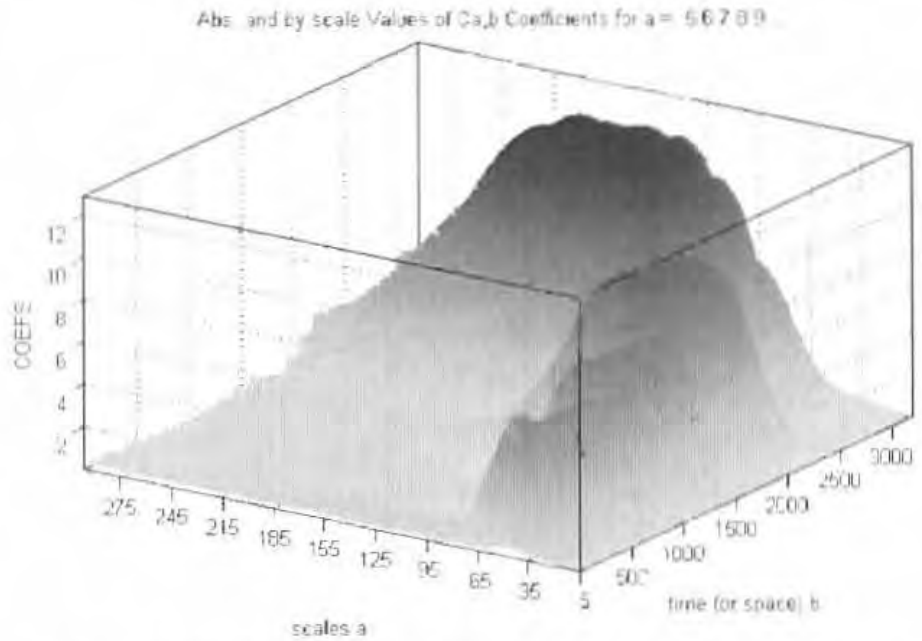

Figure 2.19: Continuous wavelet transform of the non-stationary signal

2.3.3 *The Discrete Wavelet Transform*

The Wavelet Series was introduced as a sampled version of the CWT for implementation on a computer, however it required a considerable amount of computational time and resources. It also suffered from redundancy when attempting to reconstruct a signal. The Discrete Wavelet Transform (DWT) was introduced to overcome the shortcomings faced by the Wavelet Series. The DWT is considerably easier to implement and reduces the computational time. It is implemented through a combination of filters and downsampling operations [18], [19].

As mentioned earlier, in Wavelet analysis, a function may be decomposed into a series of orthogonal basis functions, i.e. the scaling function $\phi_{j,k}(t)$ and the wavelet function $\psi_{j,k}(t)$. The scaling function produces a coarse (approximate) component and the wavelet function produces a refined (detail) component. The first coarse component is then decomposed into a second approximate and detail component. This process may be repeated to produce a structure of orthogonal vector spaces, as illustrated by the following example.

Let $f(t)$ represent a function and $f_j(t)$ represent an approximation of $f(t)$. f_0 represents the original signal. As j increases, the approximation of the signal becomes coarser.

$$f(t) \rightarrow f_0(t) \rightarrow \ldots \rightarrow f_{j-1}(t) \rightarrow f_j(t) \rightarrow \ldots \qquad (2.30)$$

$$(f_{-\infty} = 0)$$

Let $g(t)$ represent the detail in the signal. It can be formulated by taking the difference between two successive approximations.

$$g_j(t) = f_{j-1}(t) - f_j(t) \qquad (2.31)$$

$$g_{j-1}(t) = f_{j-2}(t) - f_{j-1}(t) \qquad (2.32)$$

$$g_0(t) = f_{-1}(t) - f_0(t) \qquad (2.33)$$

The original signal can therefore be reconstructed by summing up the detail components as shown in equation (2.34).

$$f(t)=\sum_{j=-\infty}^{\infty} g_j(t) \tag{2.34}$$

The approximate coefficients, $a_{j,k}$, may be calculated by the inner product of the scaling function and the original signal, [18].

$$a_{j,k}=\int_{-\infty}^{\infty} f_j(t)\cdot\phi_{j,k}(t)dt \tag{2.35}$$

$$\phi_{j,k}(t)=2^{\frac{-j}{2}}\phi\left(2^{-j}t-k\right) \tag{2.36}$$

The original signal at scale j may be reconstructed by summing the product of the scaling function and the discrete approximate coefficients.

$$f_j(t)=\sum_{j=-\infty}^{\infty} a_{j,k}(t)\cdot\phi_{j,k}(t) \tag{2.37}$$

The detail coefficients, $d_{j,k}$, may be calculated by the inner product of the complex conjugate of the wavelet function and the original signal.

$$d_{j,k}=\int_{-\infty}^{\infty} f_j(t)\cdot\psi^{*}{}_{j,k}(t)\,dt \tag{2.38}$$

$$\psi_{j,k}(t)=2^{\frac{-j}{2}}\psi\left(2^{-j}t-k\right) \tag{2.39}$$

The detail of the original signal at scale j can be approximated by summing the product of the detail coefficients and the wavelet function.

$$g_j(t)=\sum_{k=-\infty}^{\infty} d_{j,k}\cdot\psi_{j,k}(t) \tag{2.40}$$

Substituting equation (2.40) into equation (2.34), the original signal can be reconstructed by a double series of the detail coefficients.

$$f(t)=\sum_{j=-\infty}^{\infty}\sum_{k=-\infty}^{\infty} d_{j,k}\cdot\psi_{j,k}(t) \tag{2.41}$$

$$f(t)=\sum_{k=-\infty}^{\infty} a_{j0,k}\cdot\phi_{j0,k}+\sum_{j=-\infty}^{j0}\sum_{k=-\infty}^{\infty} d_{j,k}\cdot\psi_{j,k}(t) \tag{2.42}$$

A discretized signal, $f[n]$, is represented in equation (2.43).

$$f[n]=\sum_{k=0}^{N-1} a_{j,k}\phi_{j,k}(t) \tag{2.43}$$

$$f[n]=\sum_{k=0}^{N-1} a_{(j+1),k}\phi_{(j+1)}(t)_{,k}+\sum_{k=0}^{N-1} d_{(j+1),k}\psi_{(j+1),k}(t) \tag{2.44}$$

The coefficients of the next decomposition level, *(j+1)*, can be expressed as [18]

$$a_{(j+1),k} = \sum_{k=0}^{N} a_{j,k} \int \phi_{j,k}(t) \cdot \phi_{(j+1),k}(t) dt \tag{2.45}$$

$$d_{(j+1),k} = \sum_{k=0}^{N} a_{j,k} \int \phi_{j,k}(t) \cdot \psi_{(j+1),k}(t) dt \tag{2.46}$$

$$a_{(j+1),k} = \sum_{k} a_{j,k} \cdot g[k] \qquad d_{(j+1),k} = \sum_{k} a_{j,k} \cdot h[k] \tag{2.47}$$

$$a_{(j+1),k} = \sum_{m} a_{j,m} g[2k-m] \qquad d_{(j+1),k} = \sum_{m} a_{j,m} h[2k-m] \tag{2.48}$$

Equation (2.48) resembles the structure of a filter [7], i.e.

$$y[n] = x[n] * h[n] = h[n] * x[n] \tag{2.49}$$

$$y[n] = \sum_{k=1}^{N} x[k] \cdot h[n-k] \tag{2.50}$$

$$y[n] = \sum_{k=1}^{N} h[k] \cdot x[n-k] \tag{2.51}$$

The decomposition algorithm of the DWT is implemented using successive levels of the single filter bank structure shown in Fig. 2.20. The signal is denoted by x[n], where n is an integer. The signal is then passed through a half band high pass and low pass filter. The half band low pass filter is denoted by g[n] and the half band high pass filters are denoted by h[n]. The frequency response of the high pass and low pass filters is shown in Fig. 2.21. The output of the filters are then downsampled by 2, which will be discussed in greater depth later. As mentioned earlier, at each level the high pass filter produces detail information d[n] and the low pass filter produce coarse approximations a[n]. Once the signal has been filtered, the bandwidth of the signal is effectively halved, however the scale remains unchanged [16], [20].

The downsampling of the signal however has an impact on the scale. If the signal has a highest frequency of π, then by satisfying the Nyquist Criteria, the minimum sampling frequency should be 2π. However, by passing the signal through the low pass filter, the bandwidth is halved and the highest frequency becomes $\pi/2$. In accordance with the Nyquist rule, the number of samples may now be halved by discarding every other sample without loss in information,

since the highest frequency is halved. Subsampling by 2 makes half the number of samples redundant, thus doubling the scale, [16], [21] and [22].

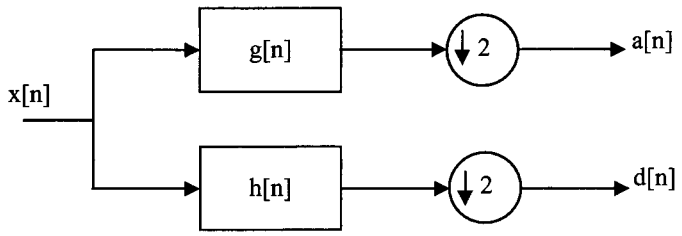

Figure 2.20: A single level of the filter bank structure used by the decomposition algorithm of the DWT

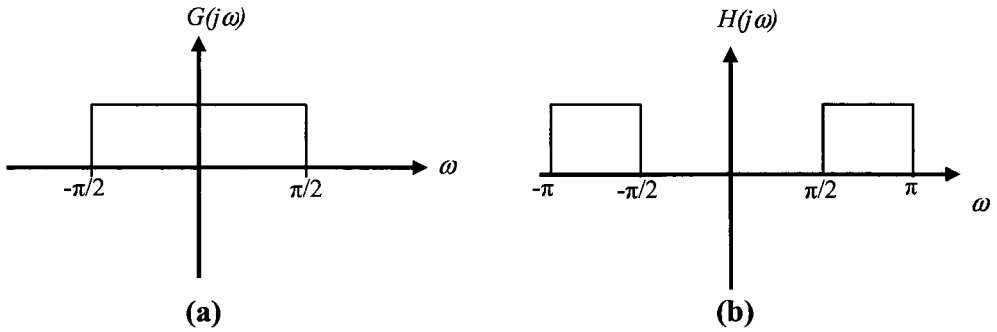

Figure 2.21: The frequency response of the (a) half band low pass filter and the (b) half band high pass filter

The above process is repeated for further decomposition. At each level, the filtering and subsampling will result in half the frequency band and half the number of samples.

In summary, at each decomposition level, the filtering and subsampling will result in half the number of samples (and hence half the time resolution) and half the frequency band spanned (and hence double the frequency resolution). The DWT successive filtering process is shown in Fig. 2.22 and is known as the Mallat-tree decomposition, [18]. Although the diagram only indicates a 3-level decomposition tree, the maximum number of levels is dependent on the number of samples in the signal. The original signal may be reconstructed using the known approximate and detail coefficients as shown in Fig. 2.23. This indicates a 3-level reconstruction of the signal x[n].

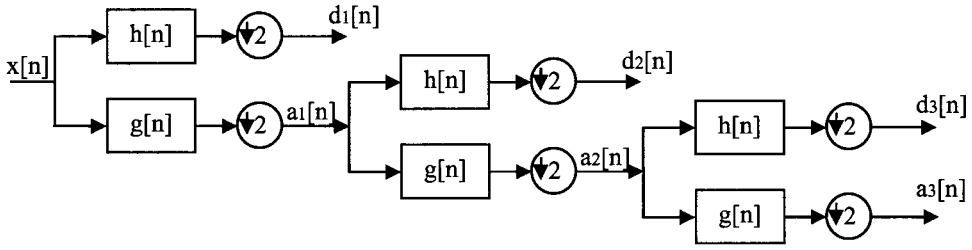

Figure 2.22: A three-level decomposition of the signal x[n]

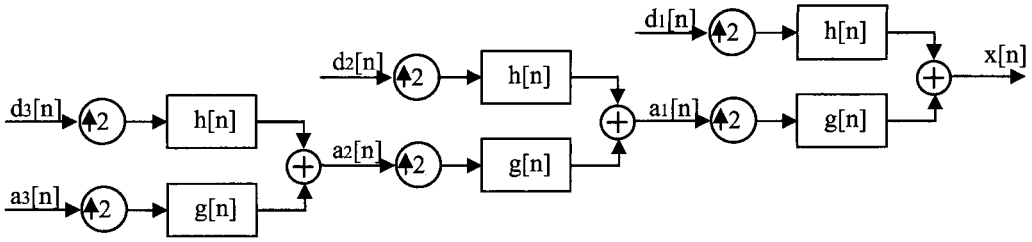

Figure 2.23: A three-level reconstruction of the signal x[n]

The following diagrams show a three level decomposition and reconstruction of a signal, x[n], consisting of 2 sinusoids with different frequencies, as shown in Fig. 2.24. The higher frequency sinusoid has a frequency four times greater than the lower frequency sinusoid. Gaussian white noise of zero mean and variance 0.02 is added to the signal.

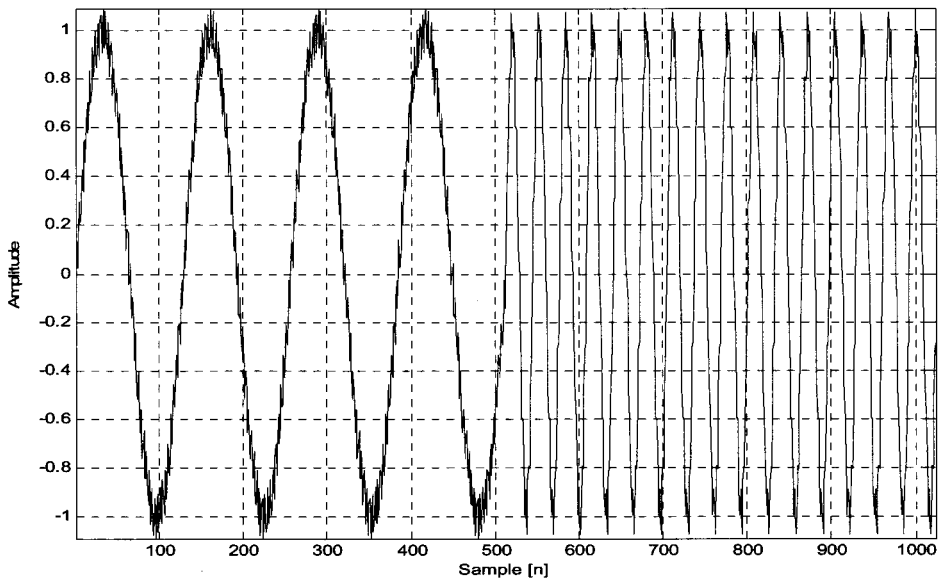

Figure 2.24: Non-stationary sinusoid with Gaussian white noise

Figures 2.25(a) and 2.25(b) show the detail and approximate coefficients for the first level decomposition of the signal, x[n]. The detail and approximate coefficients for the second level of decomposition is illustrated in Figures 2.26(a) and 2.26(b), respectively. The third level decomposition of x[n] is shown in Figures 2.27(a) and 2.27(b).

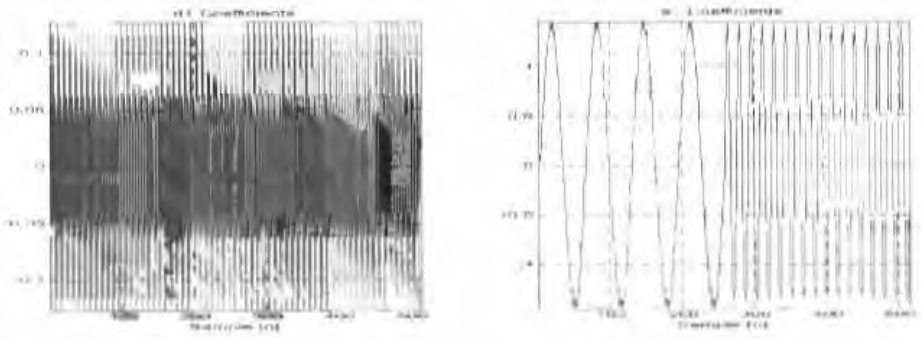

(a) (b)

Figure 2.25: First level decomposition of signal x[n]: (a) detail coefficients and (b) approximate coefficients

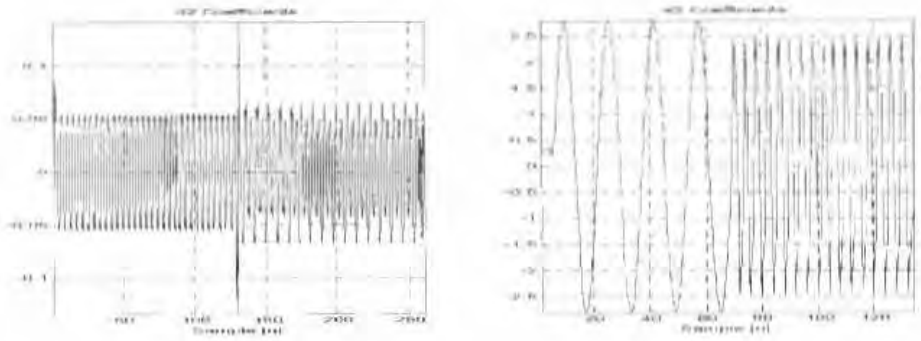

(a) (b)

Figure 2.26: Second level decomposition of signal x[n]: (a) detail coefficients and (b) approximate coefficients

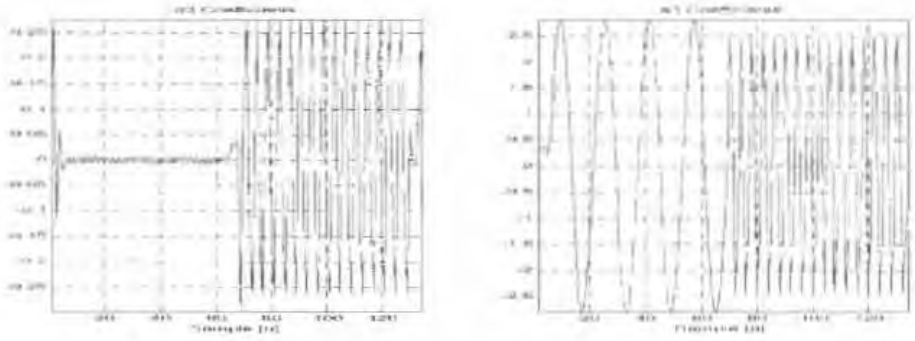

(a) (b)

Figure 2.27: Third level decomposition of signal x[n]: (a) detail coefficients and (b) approximate coefficients

Fig. 2.28 shows the reconstruction of the original signal using the detail and approximate coefficients, which are also shown in the figure. These coefficients are specifically required to reconstruct the original signal, as illustrated in Fig. 2.28.

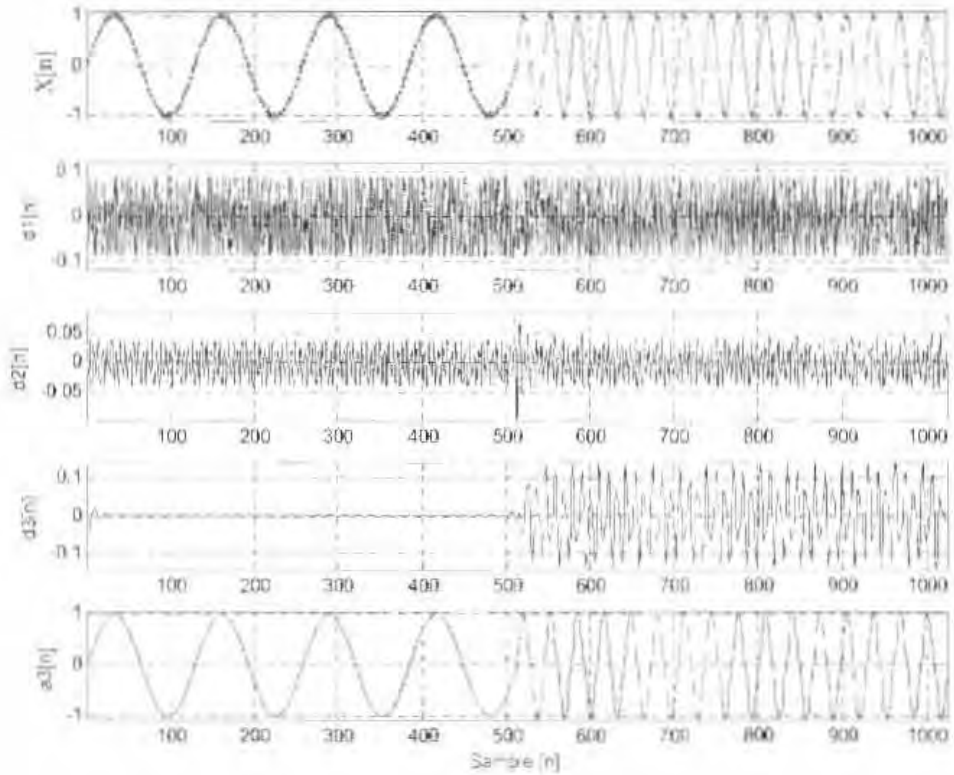

Figure 2.28: The reconstructed signal, X[n], and the necessary approximate and detail coefficients required to reconstruct the input signal, X[n]=a3+d3+d2+d1

2.4 Conclusions

The mathematical derivation and performance evaluation of the non-linear adaptive algorithm are presented. Two versions of the non-stationary adaptive algorithm are described. The first is the varying-frequency algorithm which extracts the dominant sinusoidal component from the input signal. The second is the fixed-frequency algorithm which extracts a sinusoidal component for a specified frequency. Some of the algorithm's key adaptive features are highlighted in the performance evaluation of the algorithm. These include the ability to track changes in amplitude, frequency and phase, while also offering immunity to noise. The gains which need to be defined within the algorithm, provide a trade-off between speed of response versus steady-state error.

The second time-frequency signal processing technique presented is Wavelet analysis. The Wavelet Transform has overcome the resolution related problems faced by the earlier time-frequency based technique, i.e. STFT. Unlike the STFT, the resolution is varied through the use of a fully scalable modulated window. This satisfies the criterion that higher frequencies are better resolved in time and lower frequencies are better resolved in frequency. The Continuous Wavelet Transform produces a surface in the time and scale (1/frequency) domain. The Discrete Wavelet Transform was introduced to overcome the computing and redundancy problems faced by the wavelet series, which served as a sampled version of the Continuous Wavelet Transform. The transform is implemented through a series of filter bank structures and downsampling/upsampling operations.

2.5 References

[1] A. K. Ziarani, "Extraction of Nonstationary Sinusoids," Ph.D. dissertation, University of Toronto, Toronto, Canada, 2002.

[2] D. M. McNamara, A. K. Ziarani, T. H. Ortmeyer, "A New Technique of Measurement of Nonstationary Harmonics," IEEE Trans. on Power Delivery, vol. 22, no. 1, pp 387 – 395, Jan 2007.

[3] A. K. Ziarani, A. Konrad, "A Nonlinear Adaptive Method of Elimination of Power Line Interference in ECG Signals," IEEE Trans. on Biomed. Eng, vol. 49, no. 6, pp 540 – 547, June 2002.

[4] A. K. Ziarani, M. Karimi-Ghartemani, "On the Equivalence of Three Indepenently Developed Phase-Locked Loops," IEEE Trans. on Automatic Control, Vol.50, No.12, December 2005.

[5] A. K. Ziarani, A. Konrad, A. N. Sinclair, "A Novel Time-Domain Method of Analysis of Pulsed Sine Wave Signals," IEEE Trans. on Instrumentation and Measurement, vol. 52, no. 3, pp 809 – 814, June 2003.

[6] A. K. Ziarani, M. Karimi-Ghartemani, "A Nonlinear Time-Frequency Analysis Method," IEEE Trans. on Signal Processing, vol. 52, no. 6, pp 1585 – 1595, June 2004.

[7] B. Wu, M. Bodson, "A Magnitude/Phase-Locked Loop Approach to Parameter Estimation of Periodic Signals," IEEE Trans. on Automatic Control, vol. 48, no. 4, pp 612 – 618, April 2003.

[8] M. Karimi-Ghartemani, M. R. Iravani, "Measurement of Harmonics/Inter-Harmonics of Time-Varying Frequencies," IEEE Trans. On Power Delivery, vol. 20, no.1, January 2005.

[9] M. Karimi-Ghartemani, H. Karimi, M. R. Iravani, "A Magnitude/Phase-Locked Loop System Based on Estimation of Frequency and In-Phase/Quadrature-Phase Ampplitudes," IEEE Trans. On Industrial Electronics, vol. 51, no. 2, April 2004.

[10] H. Douglas, P. Pillay, A. K. Ziarani, "Broken Rotor Bar Detection in Induction Machines with Transient Operating Speeds," IEEE Trans. on Energy Conversion, vol. 20, no. 1, March 2005.

[11] [H. Douglas, P. Pillay, A. K. Ziarani, "A New Algorithm for Transient Motor Current Signature Analysis using Wavelets," IEEE Trans. on Industry Appl., vol. 40, no. 5, 30 Sept/ Oct 2004.

[12] H. Douglas, P. Pillay, A. K. Ziarani, "The Impact of Wavelet Selection on Transient Motor Current Signature Analysis," IEEE-International Conference on Electrical Machines and Drives IEMDC, 2005, pp 80-85.

[13] Faliang Niu, Jin Huang, "Rotor Broken Bars Fault Diagnosis for Induction Machines based on Wavelet Ridge Energy Spectrum,"

Proceedings of the Eighth International Conference on Electrical Machines and Systems ICEMS 2005, vol. 3, pp 2274-2277, Sept. 2005.

[14] T. W. S. Chow, Shi Hai, "Induction Machine Fault Diagnostic Analysis with Wavelet Technique," IEEE Trans. on Industrial Electronics, vol. 51, Issue 3, pp 558-565, June 2004.

[15] J. A. Antonino-Daviu, M. Riera-Guasp, J. R. Folch, M.P.M. Palomares, "Validation of a New Method for the Diagnosis of Rotor Bar Failures via Wavelet Transform in Industrial Induction Machines," IEEE Trans. on Industry Applications, vol. 42, no. 4, pp: 990-996, July-Aug. 2006.

[16] Robi Polikar, "The Engineer's Ultimate Guide to Wavelet Analysis: The Wavelet Tutorial", Rowan University, 2001, unpublished. Available by HTTP at http://users.rowan.edu/~polikar/WAVELETS/WTtutorial.html.

[17] A. Boggess, F. J. Narcowich, "A First Course in Wavelets with Fourier Analysis," Prentice Hall, 1st Edition, 2001.

[18] H. Douglas, "The Application of Wavelets to the Condition Monitoring of Energy Conversion Devices," Ph.D. dissertation, Clarkson University, Potsdam, New York, US, 2005.

[19] A. Mertins, "Signal Analysis: Wavelets, Filter Banks, Time-Frequency Transforms and Applications," John Wiley & Sons Ltd, 1999.

[20] V. K. Madisetti, D. B. Williams, "Digital Signal Processing Handbook," Chapman & Hall/CRCnetBASE, 1999.

[21] G. Kaiser, "A Friendly Guide to Wavelets," Birkhauser, Boston, 1994, pp 44-45.

[22] I. Daubechies, "Ten Lectures on Wavelets," 2nd Edition, Philadelphia: SIAM, 1992. CBMS-NSF Regional Conference Series in Applied Mathematics.

Chapter 3

3. THE DETECTION OF FAULTS IN INVERTER-FED PERMANENT MAGNET MACHINES

3.1 Introduction

This chapter describes a new adaptive algorithm for fault detection of inverter-fed permanent magnet (PM) machines during non-stationary conditions using the stator currents. The algorithm discussed in Section 2.2, forms the basis for development of the proposed fault detection algorithm. The machine faults examined include permanent magnet damage, inter-coil shorts and static eccentricity. The chapter begins by describing the experimental setup and fault arrangements. It then leads on to investigating the use of the more common stationary fault detection technique, Motor Current Signature Analysis (MCSA), to attempt to identify the faults during steady-state and transient conditions. The new non-stationary fault detection algorithm is then described and attempts to identify the faults during non-stationary conditions are examined and discussed.

3.2 A Description of the Overall System

A surface-mounted PM machine is at the heart of the implementation of the system. This specific PM machine is a low voltage-high current device and a drive matching its capabilities is designed and implemented from fundamental principles. Field Orientated Control is chosen as the preferred control strategy, since it equates the control of the 3-phase AC machine to that of an equivalent DC machine [1], [2]. Fig. 3.1 represents a schematic of the vector control strategy implemented for the low voltage-high current drive. It also illustrates the implementation of a typical fault detection strategy. The system is limited to operation below base speed. Since the reluctance paths along the *d*- and *q*-axes are identical for the surface mounted PM machine, the only component contributing to the electromagnetic torque is the field alignment torque and therefore the electromagnetic torque may be expressed as follows

$$T_e = \frac{3}{2} p \lambda_{pm} i_q \tag{3.1}$$

T_e is the electromagnetic torque, p is the pole pairs, λ_{pm} is the flux linking the d-axis coil due to the permanent magnets, i_q is the q-axis current.

The proportional and integral gains for the speed PI controller are attained experimentally and from the literature. The speed controller for T=0.055s is as follows

$$k(z) = 0.1521\left(\frac{z-9724}{z-1}\right) \tag{3.2}$$

The equivalent circuit parameters of the PM machine may be estimated experimentally as described in [3]-[5]. The approach approximates the equivalent circuit parameters through the step response test for certain circuit and rotor configurations of the machine. This method simplifies the relationship between the phase and dq-axes quantities in an attempt to determine the equivalent d and q-axes reactances. The equivalent circuit parameters for the PM machine were found to be $r_s = 26.74m\Omega$, $L_d = 36.1\mu H$ and $L_q = 36.8\mu H$, which were used for simulation purposes.

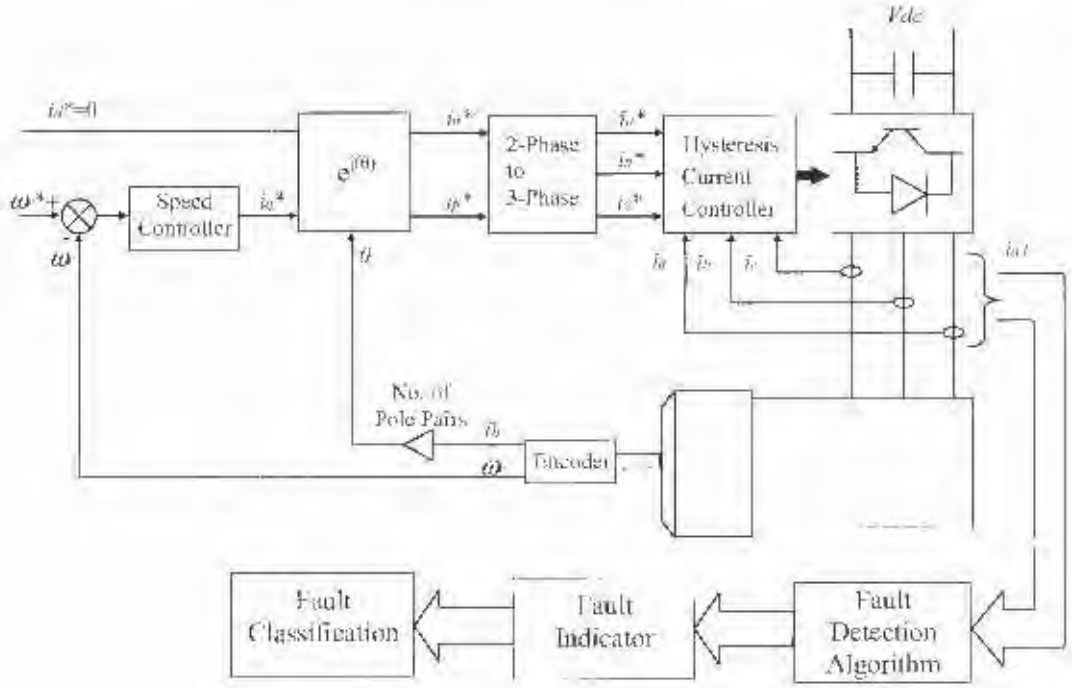

Figure 3.1: Schematic of the low voltage-high current drive and fault detection strategy

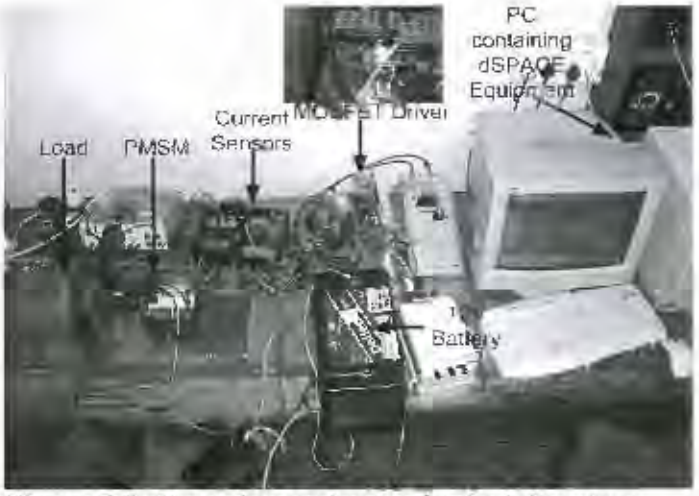

Figure 3.2: Experimental setup in the laboratory

Fig. 3.2 illustrates the experimental implementation of the system. The PM machine used is a 72A, 6-pole machine. A 12V battery is used to supply the DC voltage to the inverter while 100A mosfets are used for the switching of the inverter. A DS1104 R&D Controller Card is used to perform the computational and control tasks for the inverter. Some of the more important

features of the card include the main processor, which is a MPC 8420, PowerPC 603e core with a 250MHz clock frequency. It also consists of 8ADC channels, 20-bit digital I/O ports and a slave DSP subsystem from Texas Instruments (i.e. DSP TMS 320F240). The controller card forms part of the Advanced Control Educational Kit. It is fully programmable from the Matlab-Simulink block diagram environment, provided that the real-time interface software, supplied by dSPACE, is installed. This software transfates the simulink model into equivalent C-code for processing by the board. This allows for rapid testing of control prototypes.

3.3 Practical Implementation of Faults

Four PM machines, as described in the experimental setup, are used in the experimental tests. One of the machines is kept in its original, unfaulted condition while faults are applied to the other three machines. This provides a comparative study into the effect of the different faults. The faults implemented are an inter-coil short, damaged permanent magnet and static eccentricity. Fig. 3.3 shows the inter-coil short which is implemented on one of the machines. This fault occurs when two or more coils of a particular phase are shorted. The fault is implemented by removing the insulation on sections of the stranded conductors of the respective coils and then shorting them by placing a conductive material (solder in this case) between the exposed copper.

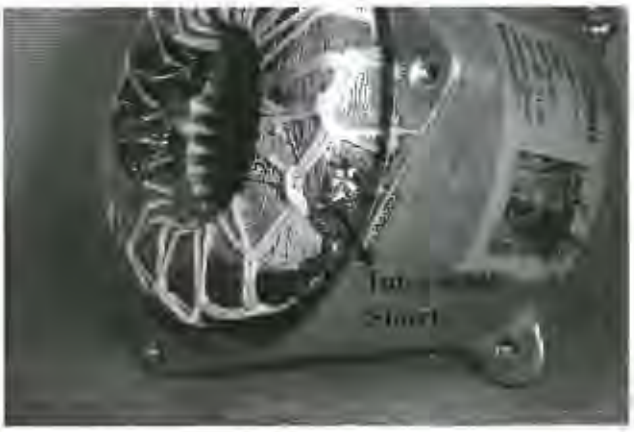

Figure 3.3: Implementation of the inter-coil short

Fig. 3.4 shows the next fault which is damage to the permanent magnet. Half the magnet of a particular pole is removed as shown in the figure.

Figure 3.4: Implementation of the damaged PM fault

The third fault is the static eccentricity. There are two types of eccentricity faults, static and dynamic eccentricity [6], however only the static eccentricity is implemented. With static eccentricity, the rotor is shifted from the stator bore center but is still running on its own axis, as shown in Fig. 3.5. To implement the static eccentricity, the stator housing bore is increased by machining. A bushing is then placed within the bore. A bore is machined within the bush to match the size of the bearing, however the center of the bore is offset by 0.25mm from the bush's center, as shown in the figure. This causes the rotor to be offset from the stator bore center, but still allowing it to run on its own axis.

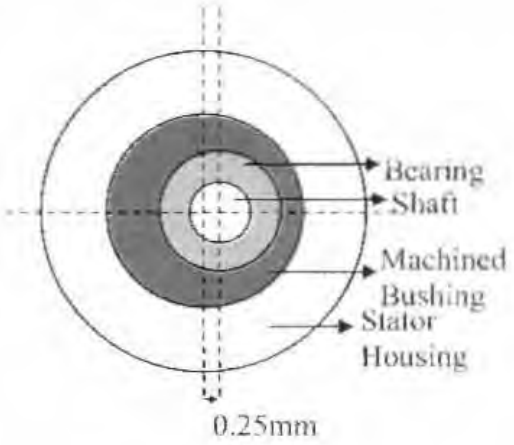

Figure 3.5: Implementation of the static eccentricity fault

3.4 Motor Current Signature Analysis (MCSA)

3.4.1 Theoretical Principles

In the static eccentricity case, the position of minimum air-gap is static in relation to the stator, which manifests in differences between phase inductances. This creates negative sequence components of harmonic components that are already present in the normal machine (multiples of the harmonic number 1/p). In the damaged permanent magnet case, there is a flux disturbance due to the missing magnet piece. This would manifest a step change in the flux density curve around the rotor which creates frequency components at multiples of the rotating frequency; i.e. (multiples of the harmonic number 1/p) [7], [8], [9].

Therefore, a number of frequency components are changed in the currents due to the presence of rotor faults. These appear at frequencies of the rotor speed and multiples thereof. This is given by equation (3.3).

$$f_{rf} = \frac{nf_s}{p} \tag{3.3}$$

f_{rf} are the frequency components associated with rotor faults, $n = 1,2,3,\ldots$, f_s is the stator fundamental frequency, p is the pole pairs.

It is shown in [10] and [11] that the third harmonic is naturally present in the normal machine. However, the modelling of the inter-turn fault in [10] indicates that the positive sequence components are developed at the third harmonic as a result of an inter-turn short. Therefore, the fault harmonics to be monitored for shorts within the stator winding of brushless synchronous machines should be located at

$$f_{short} = 3f_s \tag{3.4}$$

where f_{short} is the frequency component associated with inter-coil shorts within the stator winding, f_s is the stator fundamental frequency.

As shown by equations (3.3) and (3.4), the frequency components associated with rotor faults and inter-coil shorts are dependent on the supply frequency. Therefore during changes in speed, the location of these components change and attempting to identify them using steady-state techniques becomes difficult. Using the Fast Fourier Transform, a frequency spectrum of the stator currents is shown and examined in the following section, for the various health conditions mentioned in Section 3.3.

3.4.2 Analysis and Discussion of Results

In this section, the three fault conditions will be analysed using MCSA. Numerous tests were performed in assessing MCSA, however only the results highlighting its key aspects will be presented and discussed.

Fig. 3.6 shows the current spectrum for the normal and the damaged permanent magnet machines. Since the fault is located on the rotor, it is classified as a rotor fault condition and therefore identified by locating the fault harmonics given by equation (3.3). The machines are operating at 500rpm under no load conditions. It is noted that for all tests performed for this fault condition, the most dominant of the fault components given by equation (3.3), is located at $\frac{2f_s}{3}$, i.e. n=2. For steady-state operation at 500rpm, the fundamental frequency is 25Hz, therefore the more dominant fault component should be evident at 16.67Hz, which is shown in Fig. 3.6.

Fig. 3.7 then shows the current spectrum of the machines for a ramp up in speed from 500rpm to 800rpm over 0.75s. The fundamental shifts from 25Hz to 40Hz. However attempting to locate the fault harmonic is considerably difficult, since the fault harmonic shifts from 16.67Hz to 26.67Hz during the ramp up in speed. Adding to the difficulty in locating the fault harmonic during the shift is the overshadowing of the fault component by the fundamental component.

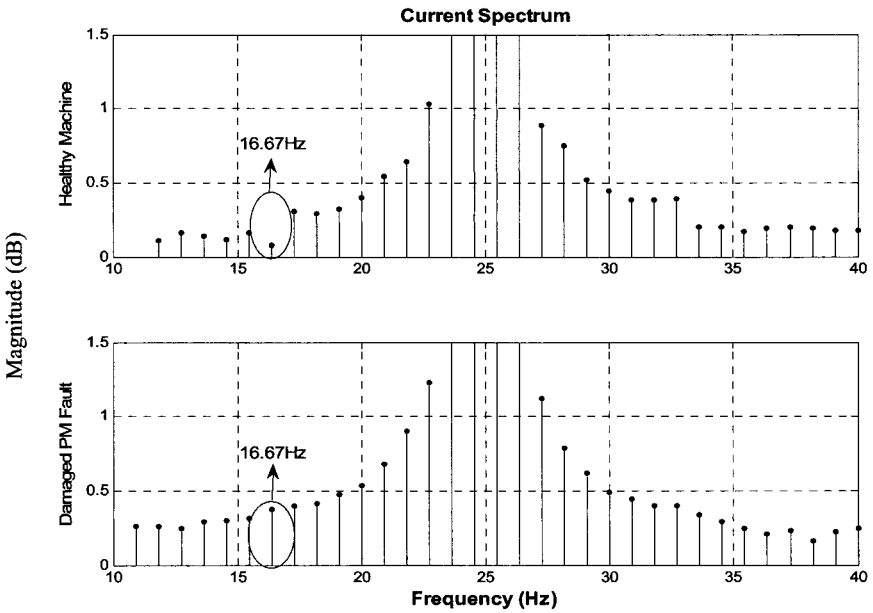

Figure 3.6: Current spectrum for the normal and damaged PM case (500rpm)

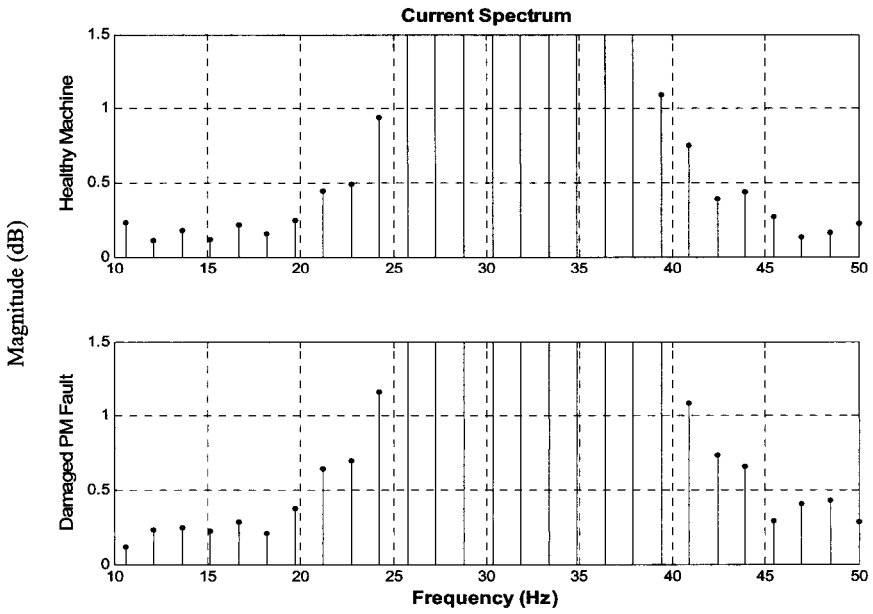

Figure 3.7: Current spectrum for the normal and damaged PM case (ramp up in speed from 500rpm to 800rpm)

Fig. 3.8 shows the steady-state operation of the normal machine, as well as the machine with the static eccentricity fault for no load operation at a rotor speed of 500rpm. This fault condition is also classified as a rotor fault. For the various tests performed, the fault component which appeared to be more dominant than the rest, appeared at $\frac{4f_s}{3}$, i.e. n=4, which is different to the dominant fault component for the damaged PM case. Operating at 500rpm, the fault harmonic is located at 33.33Hz, as indicated by Fig. 3.8. Fig. 3.9 illustrates the current spectrum of the two machines, for a ramp up in speed from 500rpm to 800rpm over a 0.75s period. The fault harmonic shifts from 33.33Hz to 53.33Hz and identical problems are encountered as mentioned in the damaged permanent magnet machine case during the transient test.

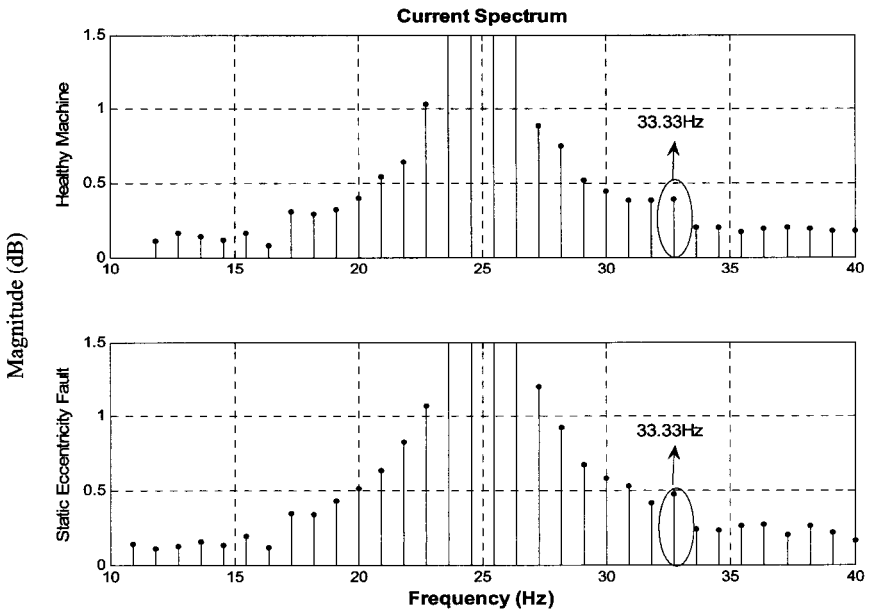

Figure 3.8: Current spectrum for the normal and static eccentricity case (500rpm)

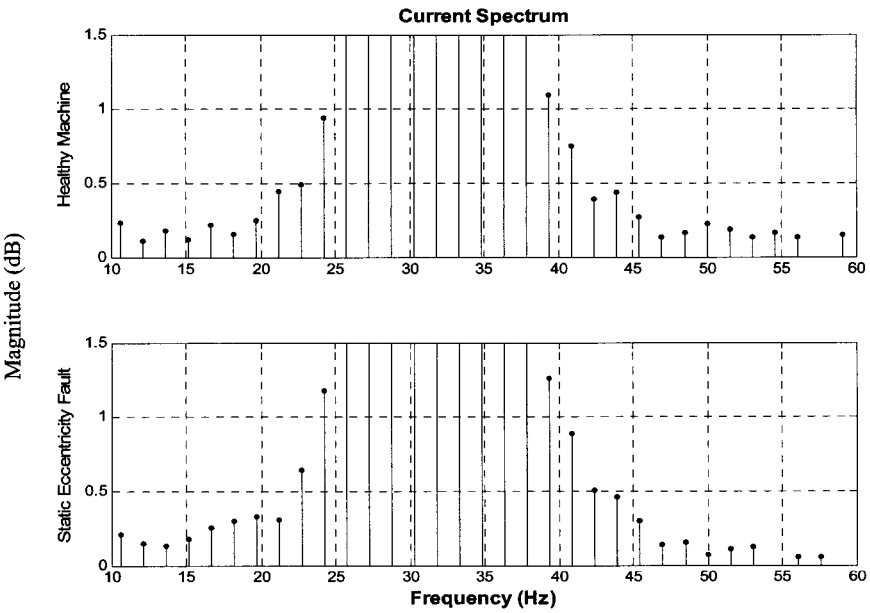

Figure 3.9: Current spectrum for the normal and static eccentricity case (ramp up in speed from 500rpm to 800rpm)

Fig. 3.10 displays the current spectrum for the steady-state operation of the healthy machine and the machine with an inter-coil short. The two machines are operated at 500rpm under no load conditions. Here the fault harmonic is clearly evident at 75Hz. Fig. 3.11 shows the current spectrum for the machines during a ramp up in speed from 500rpm to 800rpm. The fault harmonic is located at a considerable distance from the fundamental, and therefore for this transient test, it is not overshadowed by the fundamental. However, locating the fault harmonic during the speed change still proves to be very difficult, since a band of frequency components are affected and not only a single component. The band of fault components could overlap with other fault components, resulting in the incorrect diagnosis of machine failure.

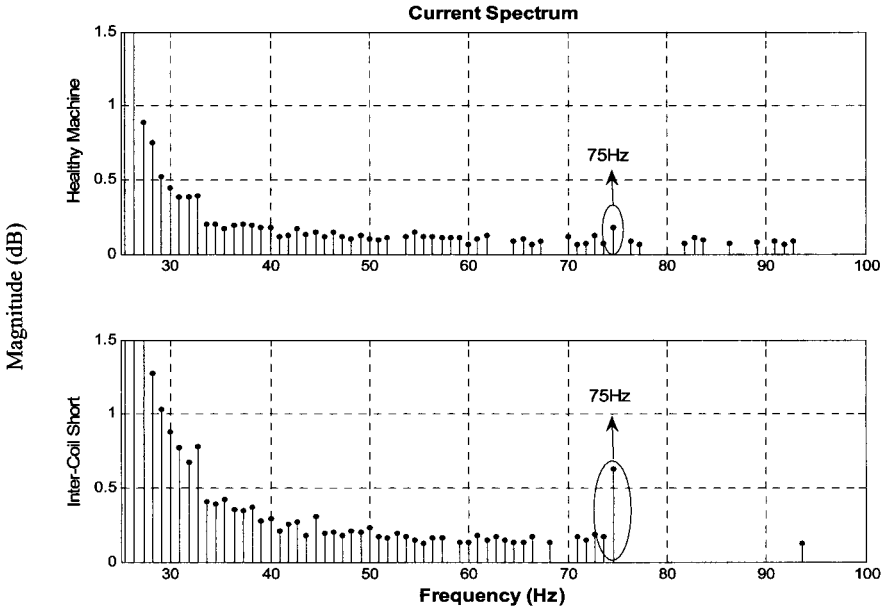

Figure 3.10: Current spectrum for the normal and inter-coil shorted case (500rpm)

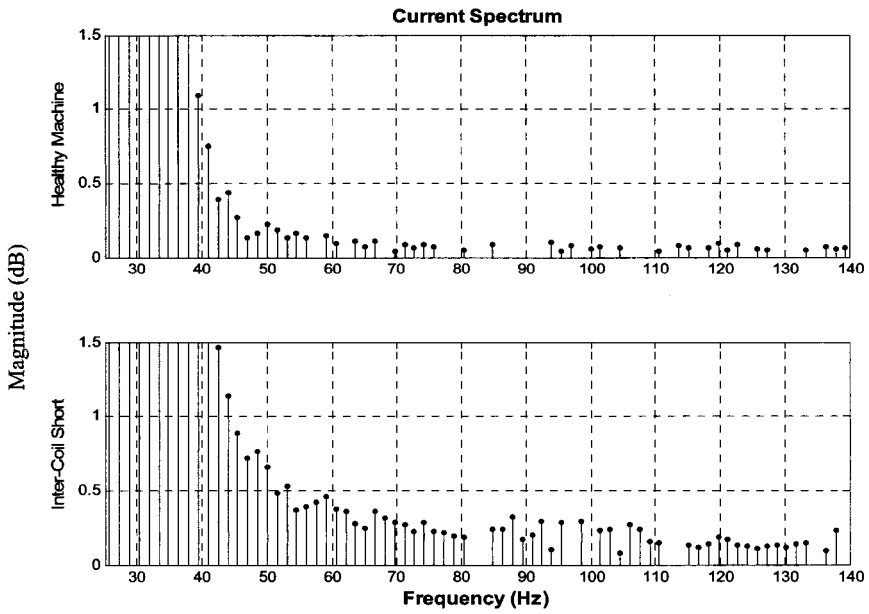

Figure 3.11: Current spectrum for the normal and inter-coil shorted case (ramp up in speed from 500rpm to 800rpm)

From the above results, the following can be concluded. MCSA performs acceptably under steady-state operation. However, under transient conditions, trying to identify fault harmonics becomes very difficult since the location of the fault harmonics is constantly changing due to its dependence on the supply frequency. Also fault harmonics situated close to the fundamental, suffer the risk of being overshadowed by the fundamental component during transients. In essence, the FFT used in MCSA operates most effectively under complete steady-state conditions and any changes in the signal would diminish its accuracy.

3.5 A Novel Method of Extracting Fault Associated Sinusoids

This section discusses a novel technique of extracting fault information from the stator currents of inverter-fed PM machines during non-stationary conditions. The technique combines the fault equations used in MCSA with the adaptive property of the non-stationary algorithms discussed in Section

2.2. It will be shown that by cascading these algorithms, various faults may be monitored.

3.5.1 Theoretical Principles

The MCSA equations provide the location of the frequency components which are characteristic of a specific fault. If the fault frequency, as specified by MCSA, were to serve as the frequency-input and the current signal as the signal-input to the fixed-frequency algorithm presented in Section 2.2, the extracted output would be the respective fault associated sinusoid. This concept serves as the basis for the fault detection scheme, although there are certain adjustments which are made to enhance the technique [12].

The first adjustment made is to ensure that the algorithm dynamically adjusts to changes in the location of the fault frequency. This is achieved as follows. The fault frequencies are solely dependent on the fundamental frequency for PM machines, as shown by the equations in MCSA. By dynamically monitoring the location of the fundamental frequency and by incorporating the MCSA fault equation, the relevant fault frequency can be dynamically monitored. The dynamic monitoring of the fundamental frequency is achieved through the use of the varying-frequency algorithm, as discussed in Section 2.2.

The second adjustment made is to incorporate the error signal from the varying-frequency algorithm. This serves as the signal-input to the fixed-frequency algorithm instead of the actual current signal. This is significant since the error signal contains the residual current components after the fundamental has been removed from the original signal, since the fundamental tends to mask other components.

Fig. 3.12 illustrates the final non-stationary fault detection algorithm for a specific fault. The cascading of the varying-frequency algorithm and the fixed-frequency algorithm is evident. The fundamental frequency which is monitored by the varying-frequency algorithm, is incorporated with the MCSA equation. This serves as the frequency-input to the fixed-frequency

algorithm. To improve the extraction capabilities of the algorithm, the error signal of the varying-frequency algorithm, forms the input to the fixed-frequency algorithm. The parameters in Fig. 3.12 are as follows,

$i(t)$ denotes the input current signal comprising of a sinusoidal component and some undesired components, $e(t)$ is the error signal, $I(t)$ is the amplitude of the fundamental component, $\omega(t)$ is the frequency of the fundamental component, $\phi(t)$ is the phase of the fundamental component, $i_{fund}(t)$ is the extracted fundamental sinusoid, $\omega_{fault}(t)$ is the location of the fault component, $I_f(t)$ is the estimated amplitude of the fault associated sinusoid, $\omega_f(t)$ is the estimated frequency of the fault associated sinusoid, $\phi_f(t)$ is the estimated phase of the fault associated sinusoid, $i_f(t)$ denotes the extracted fault associated sinusoid.

The principle of operation is as follows:

1) The varying-frequency algorithm removes the fundamental from the input current signal,
2) The remaining error signal, which contains the fault harmonics and the other unwanted signals, would now serve as the input to fixed-frequency algorithm whereby the fault associated sinusoid would be extracted,
3) To extract the desired fault component, the fault frequency is to be specified in the fixed-frequency algorithm. This is achieved dynamically by incorporating the relevant fault equation from MCSA and by dynamically monitoring the fundamental frequency, which is achieved by the varying-frequency algorithm,
4) The output of the fixed-frequency algorithm would therefore represent the fault associated sinusoid

Fig. 3.13 shows how the varying-frequency algorithm can be cascaded into a network of fixed-frequency algorithms, whereby various fault components could be monitored.

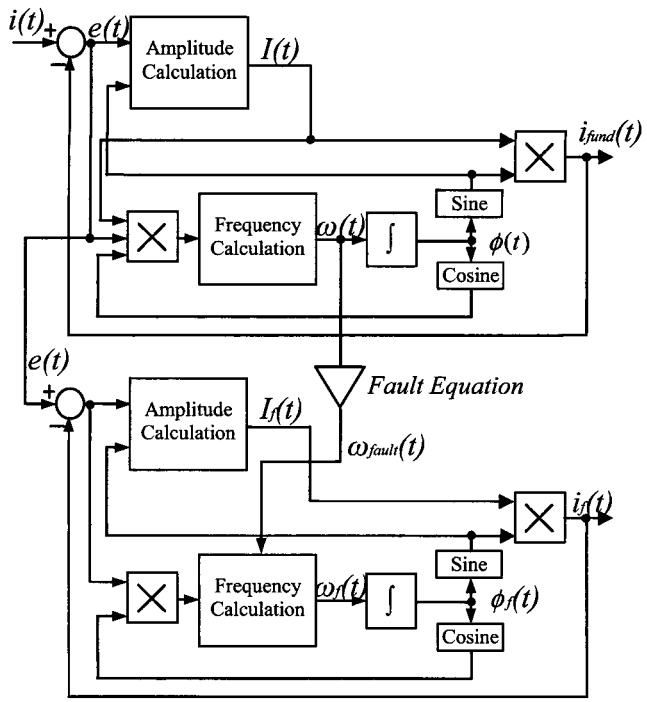

Figure 3.12: Block diagram representing the proposed fault detection algorithm

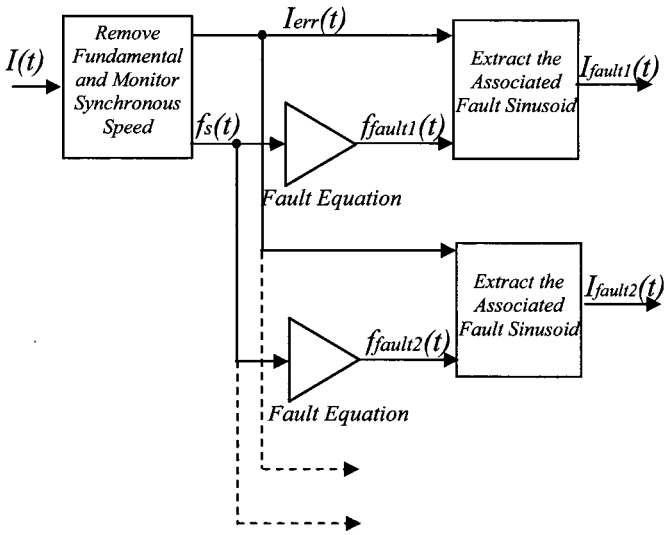

Figure 3.13: Network of the fault detection algorithms

3.5.2 *Analysis and Discussion of Results*

Numerous tests are performed to test the validity of the approach discussed above. The first set of results explain the process in which the algorithm is implemented to extract the fault associated sinusoid, as described in the Section 3.5.1. The case of the damaged permanent magnet fault is chosen to explain the process. The results show the test for the normal and faulted machine during a ramp up in speed from 400rpm to 600rpm over 0.75s under no load conditions. Fig. 3.14 represents the speed response for the machines and Fig. 3.15 represents the transient response of the current as the speed is ramped. The measured line current is then fed into the first stage of the algorithm whereby the fundamental is removed and the fundamental frequency is tracked. Fig. 3.16 shows the extracted current fundamental. Once the fundamental is removed, the remaining signal (shown in Fig.3.17) serves as the input to the fixed-frequency algorithm. The dynamically monitored fundamental frequency is incorporated with the relevant MCSA fault equation, $\frac{2fs}{3}$,to produce the dynamic fault frequency which is to be extracted by the fixed-frequency algorithm. The algorithm then extracts the associated fault sinusoid, as shown in Fig. 3.18, from which the RMS value of the sinusoid is calculated. It is clear from the figure that there is a considerable difference in magnitude of the RMS values between the normal and faulted condition of the machine. This serves as an indicator for the fault condition.

The results shown indicate good performance by the algorithm to track amplitude and frequency changes for this particular system. However, the gain parameters (μ_1, μ_2 and μ_3) need to be chosen so as to optimize the ability of the algorithm to track these changes for a particular system. These parameters need to be chosen based on the maximum deviations of the amplitude and frequency for the system. Guidelines for choosing these parameters are further highlighted in [13]. The values chosen for gain parameters of the fundamental tracking algorithm are μ_1=50, μ_2=100 and μ_3=0.02. This seemed to offer a good trade-off between the convergence speed and steady-state error. The gain parameters selected for the fixed-frequency algorithm were μ_1=20, μ_2=50 for

the rotor fault cases and μ_1=20, μ_2=100 for the inter-turn fault. The frequency tracking gain for the latter case is increased since the algorithm is required to track a larger variance in frequency compared to the rotor fault cases.

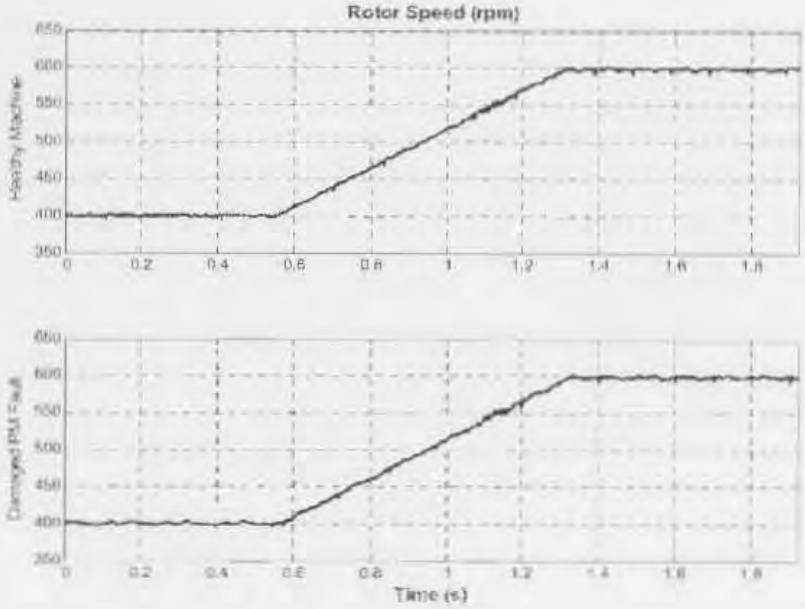

Figure 3.14: Speed Response for a ramp up in speed from 400rpm to 600rpm for the normal and damaged PM case

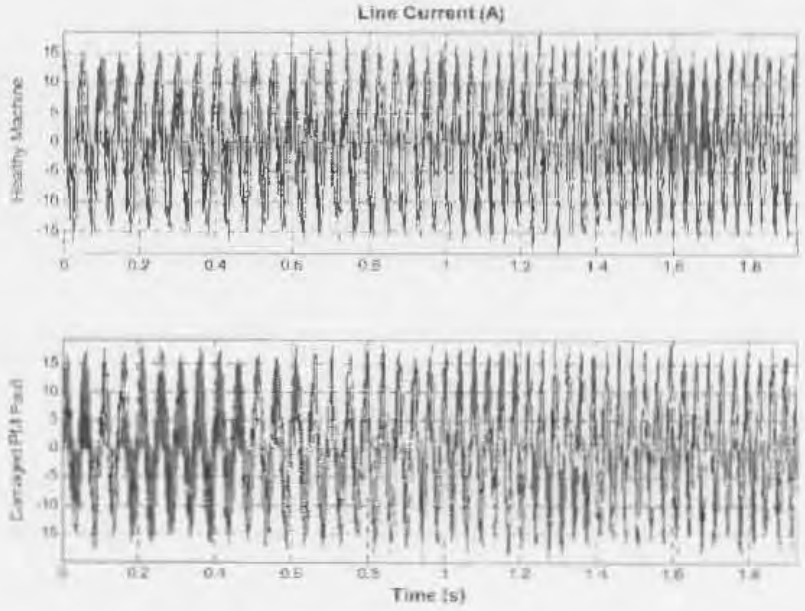

Figure 3.15: Current Response for a ramp up in speed from 400rpm to 600rpm for the normal and damaged PM case

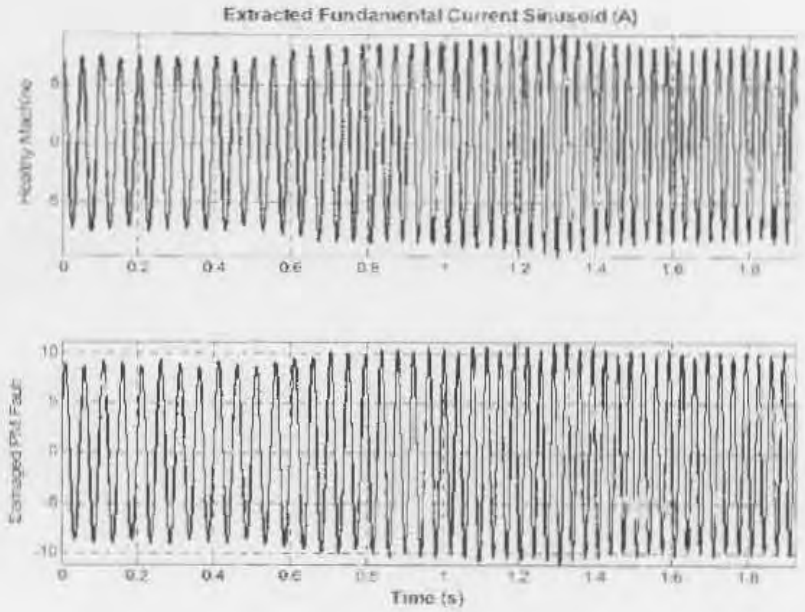

Figure 3.16: Extracted fundamental sinusoids for the normal and damaged PM case

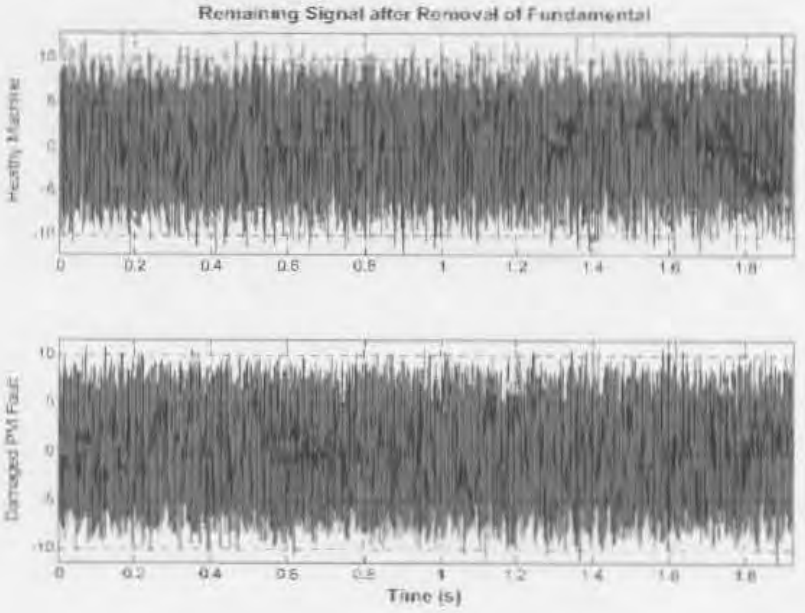

Figure 3.17: Remaining signal after the fundamental is removed for the normal and damaged PM case

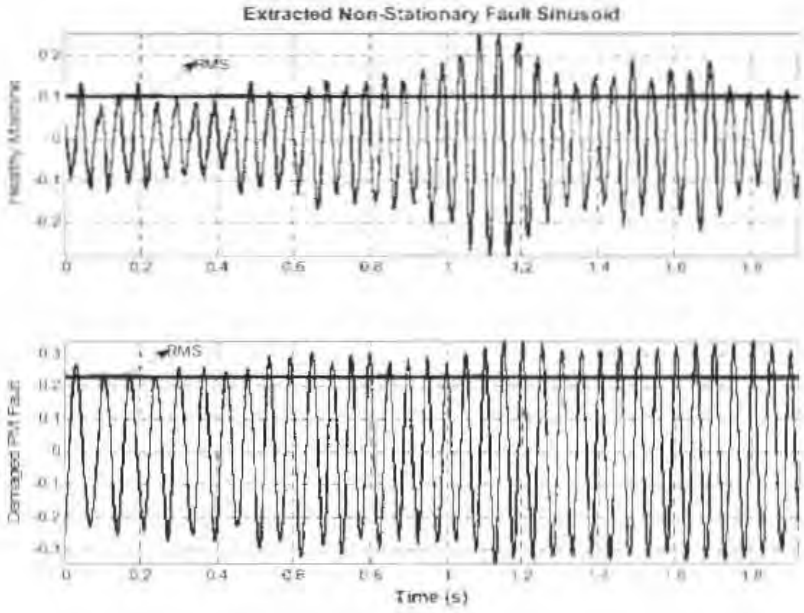

Figure 3.18: Extracted non-stationary fault sinusoid for the normal and damaged PM case

The following set of results indicates the rms values of the extracted fault sinusoids for different operating conditions. It should be mentioned again that the fault equations used in the algorithm were based on the most noticeable fault frequency component, as shown in the MCSA section. The table below lists the abbreviations for the different operating conditions. In all of the operating conditions, the speed is ramped up from 400rpm to 600rpm, however the load and the acceleration is varied. The load in the table refers to the loading of the machine, once the desired steady-state speed has been reached after accelerating.

Table 3.1: Abbreviation for the different operating conditions

Abbreviation	Load	Acceleration (m/s^2)
NL-0.75s	No Load	266.7
L-0.75s	50% Load	266.7
NL-1.5s	No Load	133.3
L-1.5s	50% Load	133.3

Fig. 3.19 indicates the RMS value of the extracted non-stationary fault sinusoid associated with the damaged PM fault, for different operating conditions mentioned above. There is clear difference in amplitude between the normal and the damaged PM case. There does appear to be a slight decrease in magnitude for the loaded conditions compared to the unloaded conditions, however the difference is considerably small.

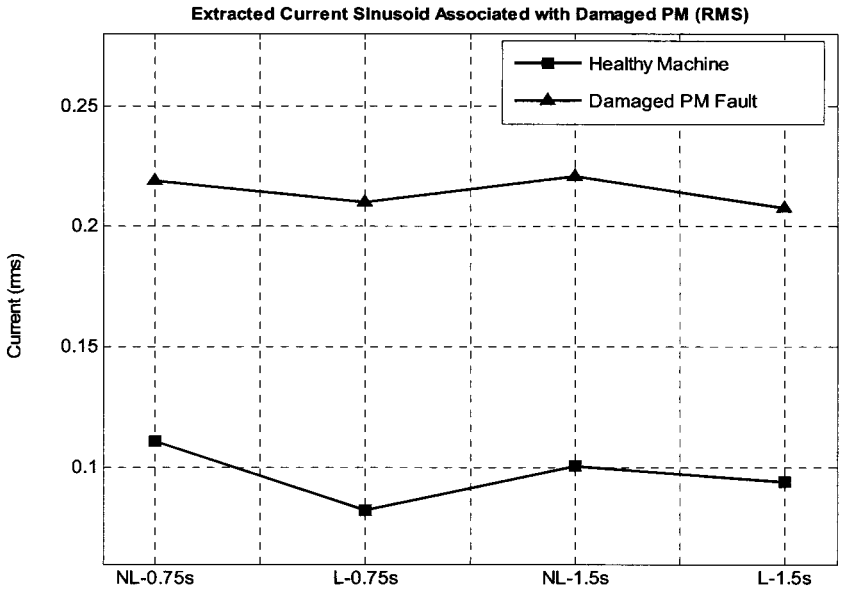

Figure 3.19: RMS value of the extracted non-stationary fault sinusoid under different operating conditions for the normal and damaged PM case

Fig. 3.20 shows the RMS value of the extracted non-stationary fault sinusoid associated with the static eccentricity fault, for the different operating conditions. The magnitude for the faulted case is larger than the normal case, however the difference isn't as large as the damaged PM case.

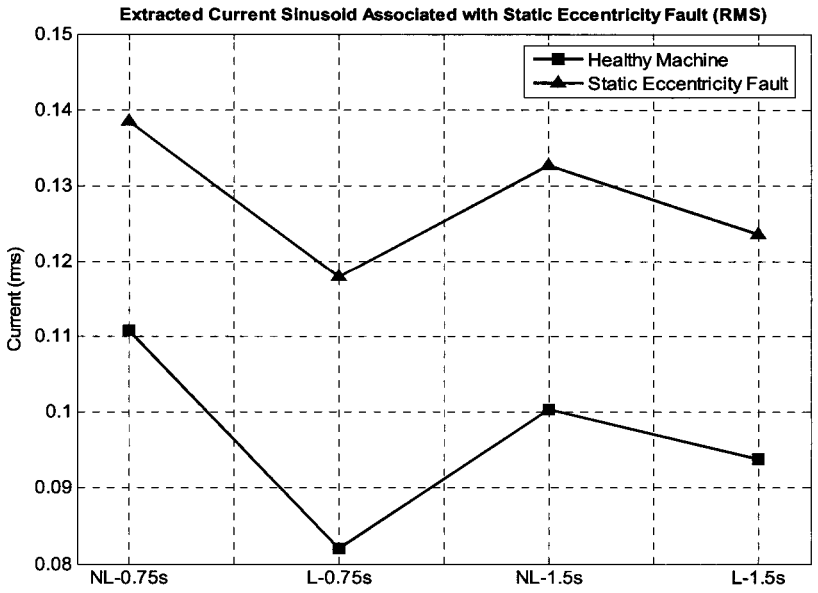

Figure 3.20: RMS value of the extracted non-stationary fault sinusoid under different operating conditions for the normal and static eccentricity case

Fig. 3.21 shows the RMS value of the extracted non-stationary fault sinusoid associated with the inter-coil short, for the different operating conditions. For this case the magnitude difference between the normal and the faulted case is significant and easily detectable. The magnitude for the faulted machine increases drastically during loaded conditions, unlike the fault components for the previous fault conditions.

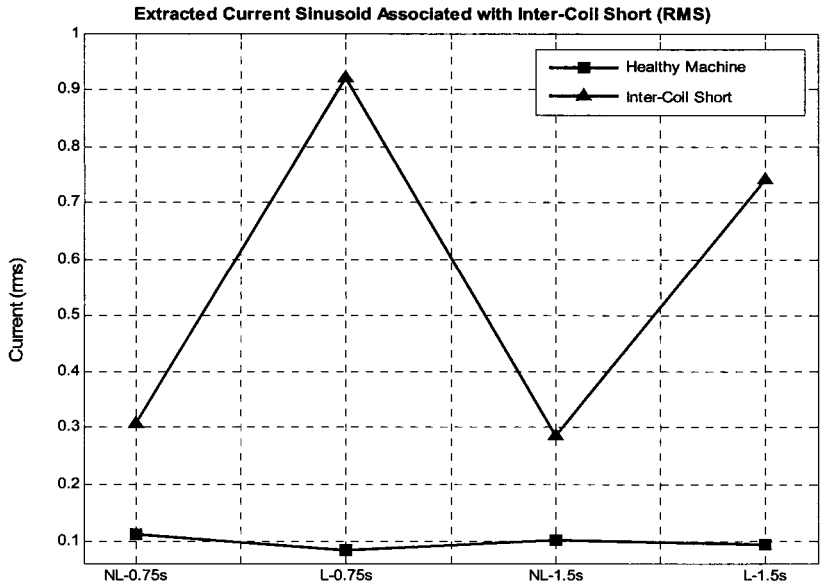

Figure 3.21: RMS value of the extracted non-stationary fault sinusoid under different operating conditions for the normal and inter-coil short case

From the above results, the following is evident. The results for the machine with the inter-coil short seems far more distinctive than for the other two damaged cases. This is attributed to the increase in magnitude of the inter-turn fault component as a result of the implemented fault, as shown in Section 3.4.2, indicating that the component is considerably sensitive to this fault. The cascaded algorithm also provides a far more accurate prediction of the more dominant principle components, as discussed in [14]. Therefore faults which directly impact on the principle frequency components, would be more accurately assessed. Although other components are less accurately predicted, the results still indicate that the technique is capable of providing sufficient information to assess the health of the machine.

3.6 Conclusions

The details for implementation of a low-voltage high-current PM drive for fault analysis has been described. Three of the more common faults in PM

Machines (i.e. damaged PM, static eccentricity and inter-coil short) have been described and implemented on the machines.

A new algorithm for fault detection of inverter-fed PM machines operating under non-stationary conditions has been proposed. The detection technique is based on an adaptive algorithm which has been cascaded to extract fault associated sinusoids using the current signals. The results show the algorithm's capability of tracking fault sinusoids under speed and load changes of the machine. It is shown that the case of the inter-coil short produced more promising results than the other two cases, however this is attributed to the sensitivity of the inter-turn fault frequency component and the accuracy of the algorithm to tracking the principal/dominant fault components. However the results still indicate that the algorithm's predictive capability is sufficiently accurate in identifying the faults under non-stationary conditions. The proposed fault detection algorithm proves to be extremely successful in its ability to identify different faults under non-stationary operating conditions.

3.7 References

[1] I. Boldea, S.A. Nasar, "Electric Drives," CRC Press, New York, 1999.

[2] T.J.E. Miller, "Brushless Permanent-Magnet and Reluctance Motor Drives," Oxford University Press, New York, 1989.

[3] J.F. Gieras, E. Santini, M. Wing, "Calculation of Synchronous Reactances of Small Permanent-Magnet Alternating-Current Motors: Comparison of Analytical Approach and Finite Element Method with Measurements," IEEE Trans. on Magnetics, vol. 34, no.5, pp 322-328, Sept. 1998.

[4] F.P. de Mello, L.N. Hannett, "Determination of Synchronous Machine Electrical Characteristics by Tests," IEEE Trans. on Power Apparatus and Systems, vol. PAS-102, no. 12, pp 3810-3815, Dec. 1983.

[5] S. Weisgerber, A. Proca, A. Keyhani, "Estimation of Permanent Magnet Rotor Parameters," Proc. IEEE Ind. Appl. Soc. (IAS'97), New Orleans, pp. 29-34, Oct.1997.

[6] M. Hajiaghajani, Hao Lei, S.M. Madani, H.A. Toliyat, "A Method For Detection Of Eccentricity In Permanent Magnet," Proc. IEEE Ind. Appl.

Soc. (IAS'03), Salt Lake City, UT, vol. 3, pp 1833-1838, 12-16 Oct. 2003.

[7] W. Le Roux, R.G. Harley and T.G. Habetler, "Detecting Rotor Faults in Permanent Magnet Synchronous Machines," IEEE SDEMPED, pp 198-203, 24-26 Aug. 2003.

[8] W. Le Roux, R.G. Harley and T.G. Habetler, "Detecting Rotor Faults in Low Power Permanent Magnet Synchronous Machines," IEEE Trans. on Power Electronics, vol. 22, no.1, pp 322-328, Jan. 2007.

[9] W. le Roux, R. G. Harley, and T. G. Habetler, "Converter Control Effects on Condition Monitoring of Rotor Faults in Permanent Magnet Synchronous Machines," Proc. IEEE Ind. Appl. Soc. (IAS'03), Salt Lake City, UT, pp. 1389–1396, Oct. 12–16, 2003.

[10] J. Sottile, F.C. Trutt and A.W. Leedy, "Condition Monitoring of Brushless Three-Phase Synchronous Generators with Stator Winding or Rotor Circuit Deterioration," Proc. IEEE Ind. Appl. Soc. (IAS'01), Chicago, vol. 3, pp 1587-1594, 30 Sept.-4 Oct. 2001.

[11] C. Gerada, K. Bradley, M. Sumner , "Winding Turn-To-Turn Faults In Permanent Magnet Synchronous Machine Drives," Proc. IEEE Ind. Appl. Soc. (IAS'05), Hong Kong, vol. 2, pp 1029-1036, 2-6 Oct. 2005.

[12] A.K. Ziarani, "Extraction of Nonstationary Sinusoids," Ph.D. dissertation, University of Toronto, Toronto, Canada, 2002.

[13] A. K. Ziarani, A. Konrad, "A Nonlinear Adaptive Method Of Elimination Of Power Line Interference In ECG Signals," IEEE Trans. on Biomed. Eng, vol. 49, no. 6, pp 540 – 547, June 2002.

[14] M. Karimi-Ghartemani, M. R. Iravani, "A Nonlinear Adaptive Filter for Online Signal Analysis in Power Systems: Applications," IEEE Trans. On Power Delivery, vol. 17, no. 2, pp 617-622, April 2002.

Chapter 4

4. THE DETECTION OF MECHANICAL IMBALANCES IN INVERTER-FED INDUCTION MACHINES

4.1 Introduction

This chapter examines the use of non-stationary signal processing techniques in its application to identifying mechanical imbalances in inverter-fed induction machines. One of the key problems faced when attempting to identify fault frequency components of induction machines under non-stationary conditions (i.e. changes in speed and/or load) is the dependence of the fault components not only on the supply frequency, but also slip [1]. Unfortunately, this dependence on two variables poses a considerable challenge for the predictive capability of the cascaded adaptive algorithms. This is discussed in Chapter 3 for the permanent magnet machines, and an alternate approach needs to be investigated. Thus far, the second non-stationary signal processing technique has not been required (i.e. wavelets). However since the detection of mechanical imbalances in the induction machine does pose a considerable challenge for the isolated use of the adaptive algorithms, the use of wavelets will need to be examined. Although the chapter focuses on the use of wavelets, the results will show that the adaptive algorithm still forms a critical part of the detection scheme and therefore cannot be excluded from the final detection algorithm. Work has been done using wavelets to detect faults in induction machines during direct-online startup. For this specific case, the slip is large at startup, which separates the fault component from the fundamental, making it considerably easy to detect using wavelets as shown in [2], [3]. By incorporating a drive, the fault component is a lot harder to detect due to the drive's ability to slowly ramp up in speed, thus limiting the slip. Therefore certain conditions need to be met, which will be discussed in this chapter.

Mechanical imbalances may also be detected by monitoring the electromagnetic flux, which is measured by coils which sense the axial

leakage flux. The drawback of the technique is the required installation of the coils in the stator slots [4], [5]. Vibration analysis is one of the more effective methods of detecting mechanical faults in induction machines, since these faults induce mechanical forces which translate to vibration [6]. Although there are effective alternatives to monitoring mechanical faults, electrical signals provide a more complete monitoring solution, since these signals are more susceptible to a wider variety of faults.

The chapter is organized as follows. Section 4.2 discusses the use of MCSA when detecting mechanical imbalances in induction machines. The proposed detection scheme is discussed in Section 4.3. The experimental results are presented and discussed in Section 4.4. Conclusions are drawn in Section 4.5.

4.2 Motor Current Signature Analysis

A mechanical imbalance in an induction machine can be identified by monitoring the spectral components located at [7]-[11]

$$f_u = f_1 \pm m f_r \tag{4.1}$$

f_u are the frequency components associated with the mechanical imbalance, m = 1,2,3,..., f_1 is the stator fundamental frequency, f_r is the mechanical rotor speed in Hertz.

Fig. 4.1 shows the current spectrum of a fully loaded 2-pole induction machine without any imbalance operating under steady-state conditions. Fig. 4.2 shows a fully loaded 2-pole induction machine with a mechanical imbalance operating under steady-state conditions. Although, the fault harmonics are immersed by noise caused by the inverter, with a high enough sampling frequency and acquisition time, the lower order harmonics which are associated with the imbalanced fault can be identified as shown in Fig. 4.2. A sampling frequency of 40kHz was used with an acquisition of 3.28 seconds, providing a frequency resolution of 0.3Hz. According to MCSA, the dominant imbalanced fault component should be located at the lower frequency range (0-8Hz). This component is clearly visible in Fig. 4.2, as indicated. The ability

to detect this fault using MCSA is largely governed by the loading and steady-state operation of the machine, as mentioned previously. Fig. 4.3 shows the current spectrum of the healthy machine at 30% loading. Fig. 4.4 shows the spectrum of the damaged machine at 30% loading, whereby the fault component is no longer evident.

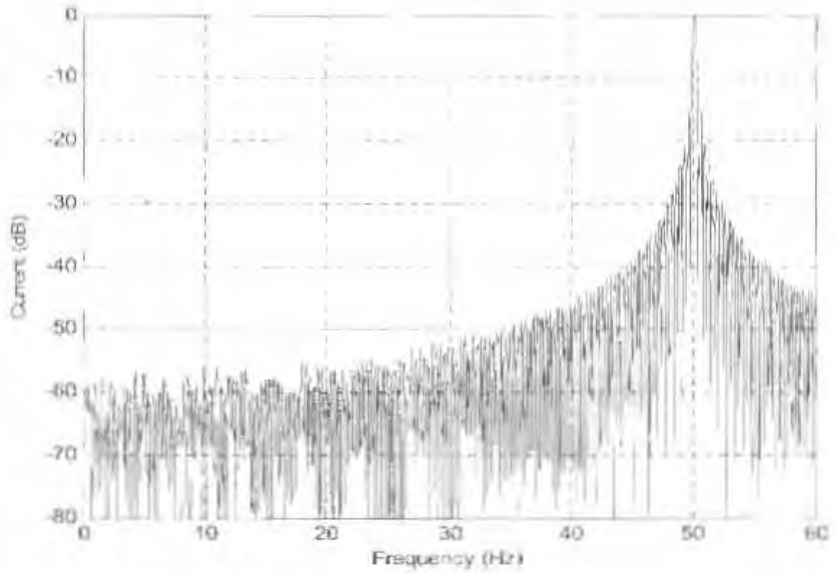

Figure 4.1: Current spectrum of a healthy induction motor under full load

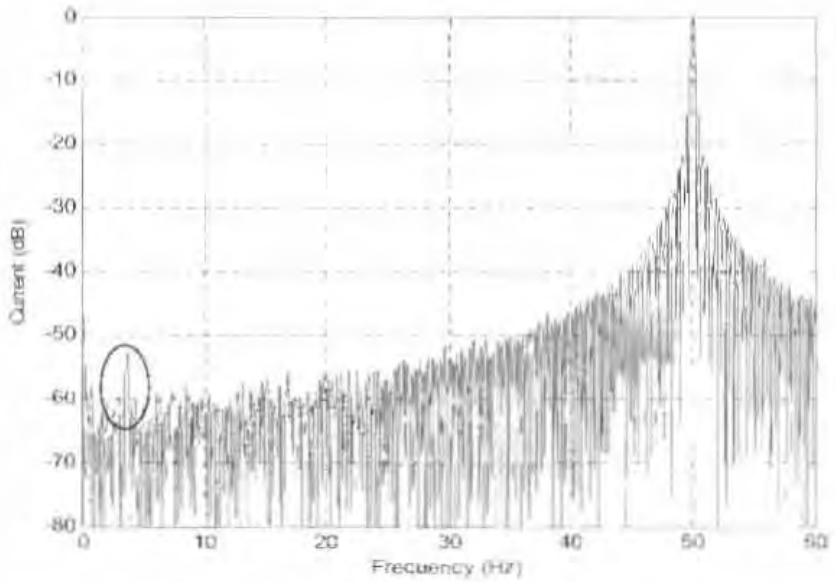

Figure 4.2: Current spectrum of an induction motor with a mechanical imbalance under full load

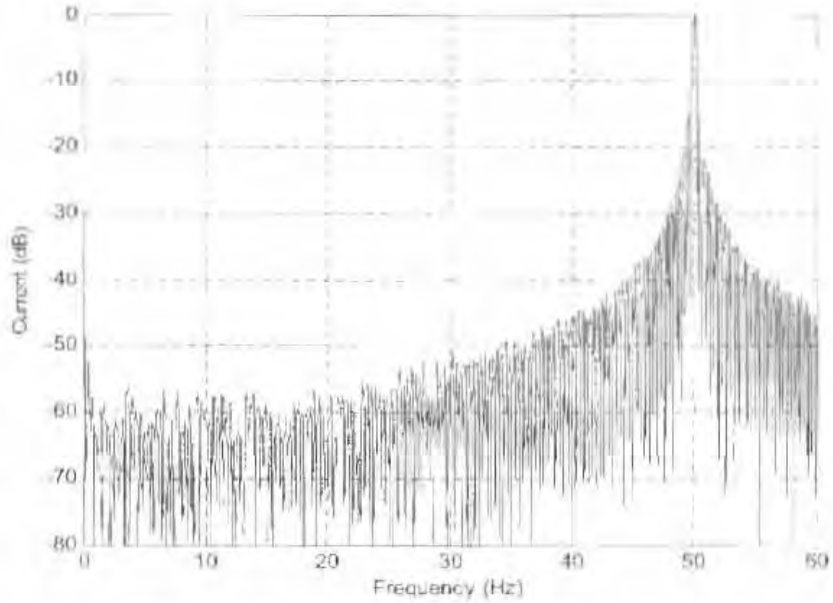

Figure 4.3: Current spectrum of a healthy induction motor under 30% load

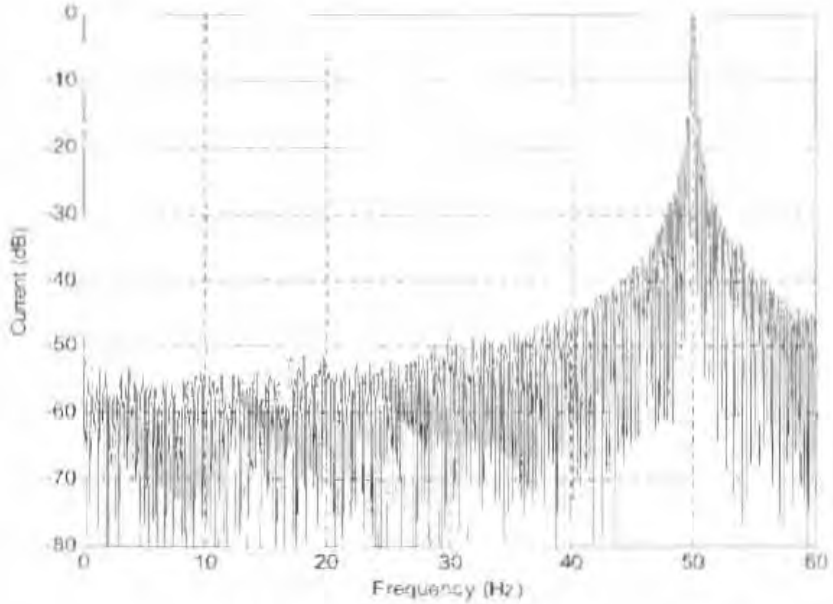

Figure 4.4: Current spectrum of an induction motor with a mechanical imbalance under 30% load

4.3 Proposed Detection Scheme

As mentioned in the previous chapter, the disadvantage of using MCSA and other steady-state analysis techniques are that many applications exist where the electrical machine is not able to operate under complete steady-state conditions. Changes in speed pose a considerable problem when attempting to analyze the currents, since the dominating fundamental tends to mask all fault related frequency components. It is therefore critical to remove the fundamental before any form of analysis may be performed. The non-stationary varying-frequency adaptive algorithm is used to extract the non-stationary fundamental. Wavelets are then used to analyze the residual currents. The results are shown and discussed in greater detail in the following section.

4.4 Experimental Results

The experiments were conducted using a 1kW, 2-pole squirrel-cage induction machine. To perform the various ramps in speed, a 5kW drive is connected to the machine. The drive uses volts/hertz control to vary the speed of the machine. The same rotor is used to conduct the comparative investigation, thus ensuring that any differences in the results could only be attributed to the inflicted fault. The initial condition of the rotor is referred to as the healthy motor, after which the mechanical imbalance is placed on the rotor. It is then referred to as the faulted or imbalanced machine. The imbalance is achieved by removing 12mg of material from the rotor. Fig. 4.5 indicates the location of mass which is removed. The design of the rotor allowed material to be removed without affecting the rotor bars, end rings or laminations.

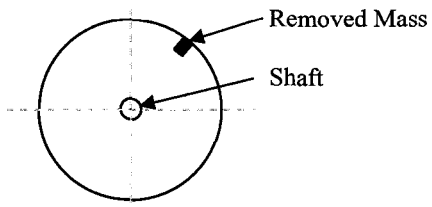

Figure 4.5: Load imbalance caused by removal of mass on the rotor

The extraction algorithm takes a few cycles to converge to the amplitude and frequency of the fundamental, for starting conditions. Therefore, only once convergence of the algorithm is reached should the estimated signal be used for any further analysis. The parameters chosen for the gains of the algorithm are μ_1=100, μ_2=10000 and μ_3=0.02. They proved to provide a good trade-off between rate of convergence and steady-state error [12], [13]. Based on these parameters, the algorithm converges after 0.3 sec. The estimated fundamental is subtracted from the original signal and the residual signal is decomposed using the discrete wavelet transform. The Daubechies 8 wavelet is selected to perform the decomposition as this proved to indicate the greatest variation in results between the healthy motor and the motor with the mechanical imbalance.

Fig. 4.6 shows the stator current for startup of the machine under full load. The machine linearly ramps up to a synchronous frequency of 60Hz. The amplitude, frequency and phase of the fundamental is estimated and removed using the extraction algorithm. The residual current, as shown in Fig. 4.7, has information relating to the health of the machine.

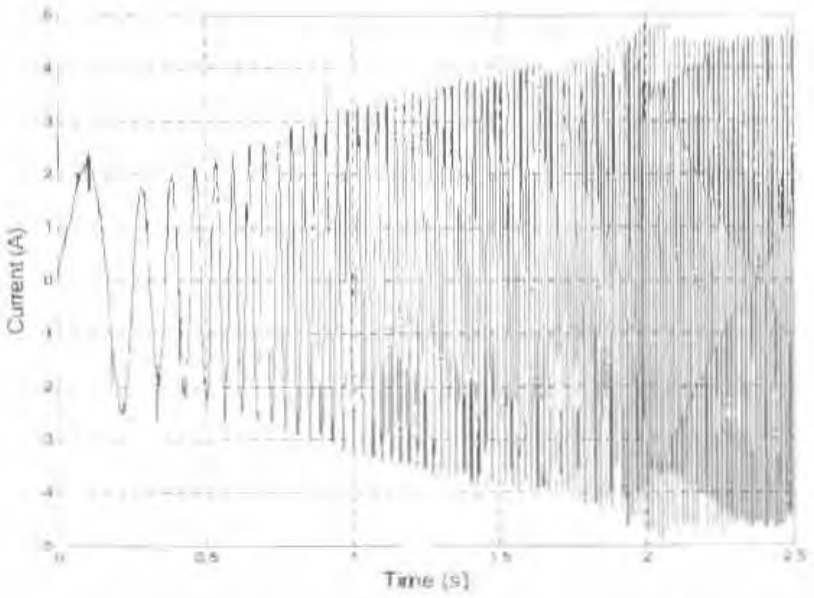

Figure 4.6: Time-domain representation of the stator current during startup

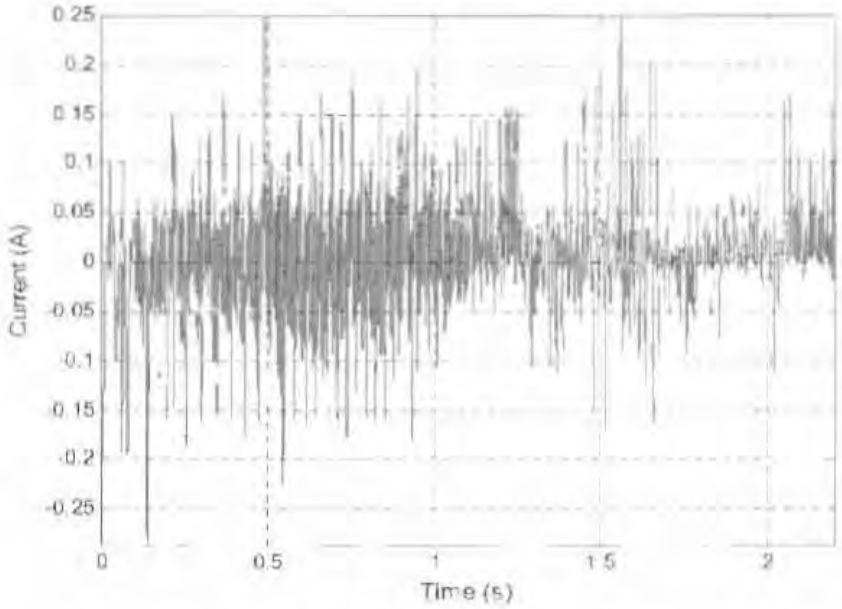

Figure 4.7: Residual current after removing the fundamental

The resulting waveform is then decomposed using the discrete wavelet transform. By examining the first 9 detail levels it is evident that there appear to be differences between the healthy motor and the imbalanced motor. These however, are neither significant nor consistent with other results. When examining levels 10-12 of the healthy machine, Fig. 4.8, and comparing it to the faulted machine, Fig. 4.9, there appears to be a distinct difference in the wavelet coefficients at detail level 11, as shown in Fig. 4.10. The location of the fault harmonic in the higher order detail level is expected, since the fault harmonic is located within the range of 0-8Hz, which is dependant on loading, and the detail level 11, corresponds with the frequency range 5-10Hz.

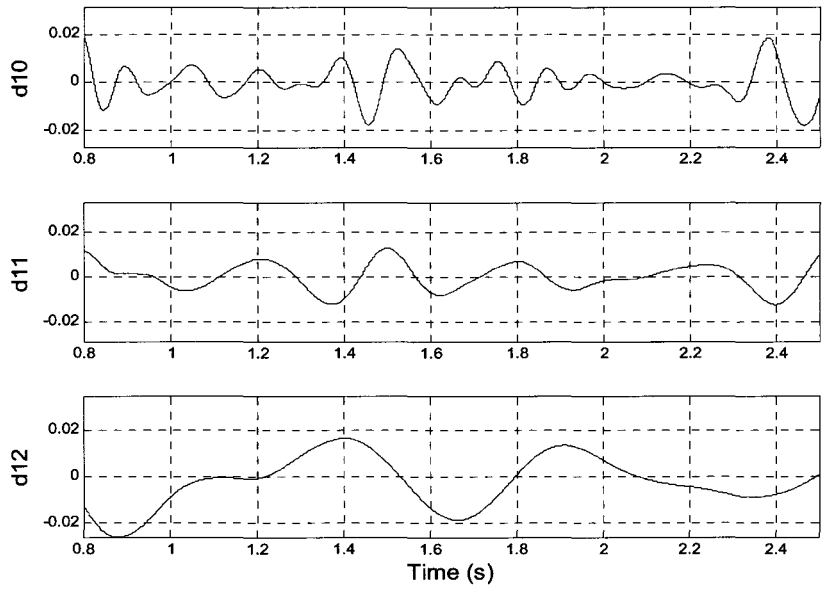

Figure 4.8: Detail levels 10-12 for the healthy machine under full load

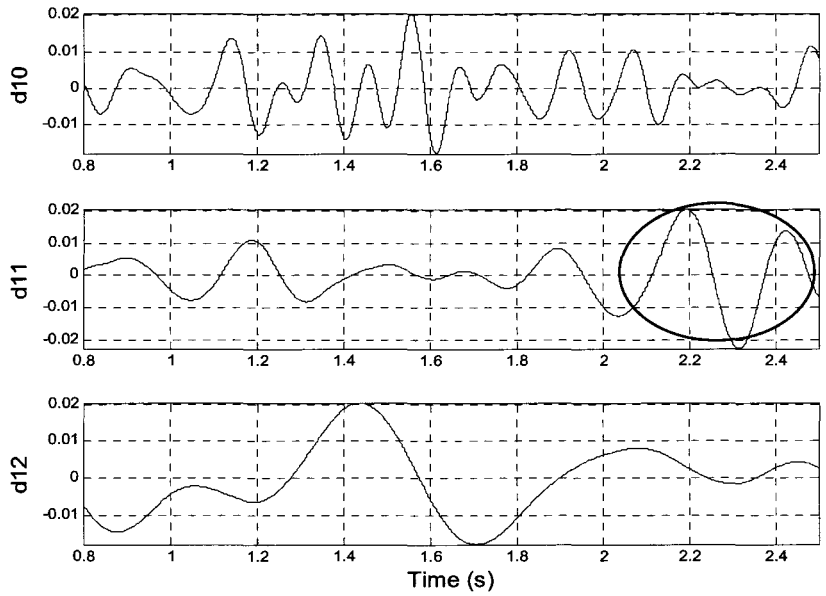

Figure 4.9: Detail levels 10-12 for the imbalanced machine under full load

To investigate the effect of loading on the detection algorithm, the machine is loaded between full load and no load using the above starting condition. Fig. 4.10 shows the results for 30% loading of the healthy and imbalanced

machines. Again the feature appears at detail level 11 for the imbalanced case, however it appears sooner and is less distinctive than for the fully loaded case. It is observed from all other results that this is the lowest loading condition required to detect the significant feature common to the machine with the imbalanced fault.

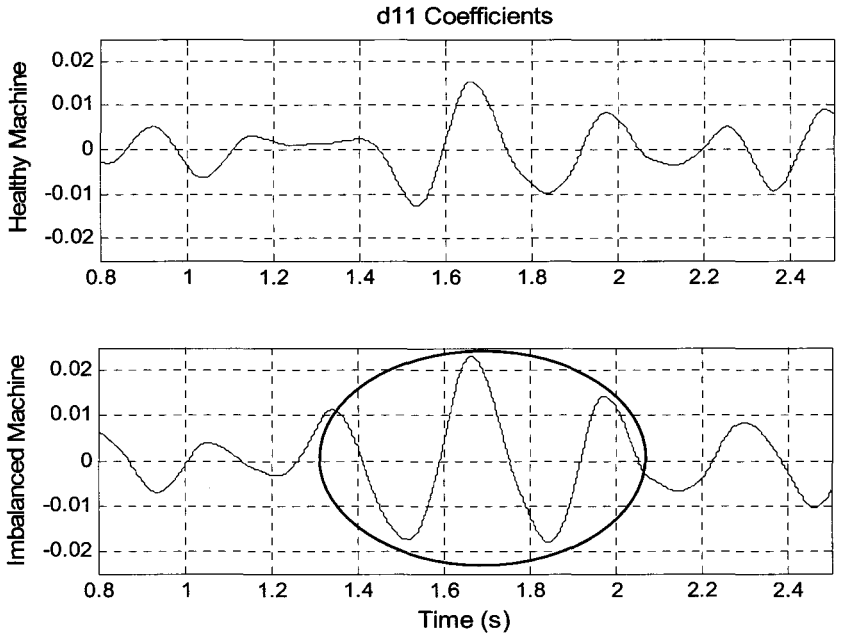

Figure 4.10: Detail level 11 for the healthy and imbalanced machines under 30% load

The starting tests were repeated with the machine ramping up to 50Hz and 35Hz under the various loading conditions mentioned above. The stator current for the 50Hz condition is shown in Fig. 4.11. Fig. 4.12 shows the wavelet decomposition at detail level 11 under full load, whereby the feature is clearly evident for the imbalanced machine. Fig. 4.13 shows the d11 coefficients for the machines under 30% load. As with the 60Hz case, the feature appears earlier than for the fully loaded imbalanced machine.

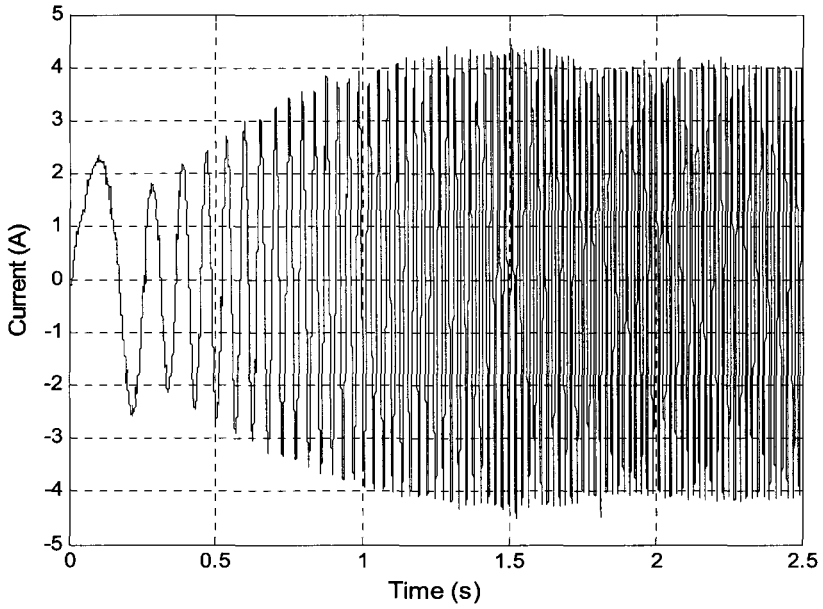

Figure 4.11: Time-domain representation of the current during startup

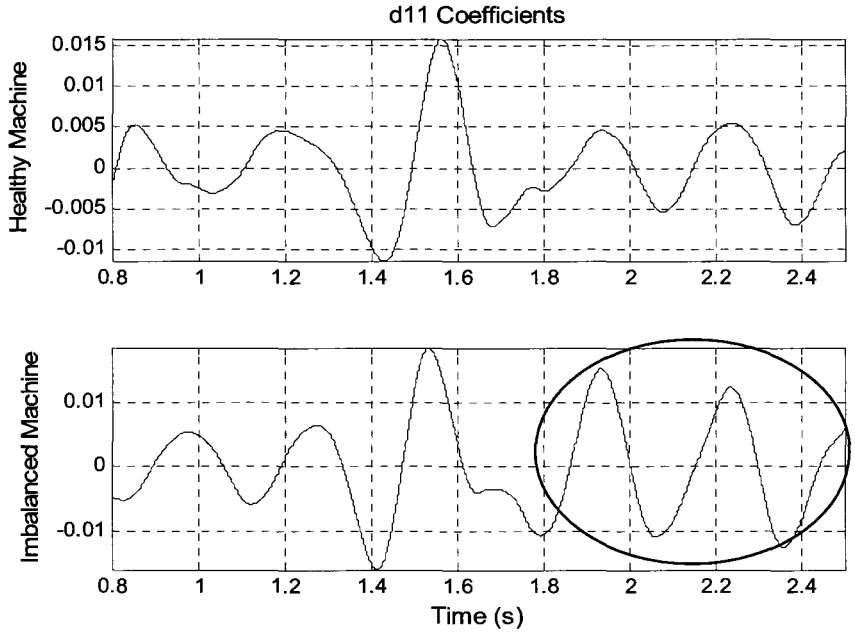

Figure 4.12: Detail level 11 for the healthy and imbalanced machines under full load

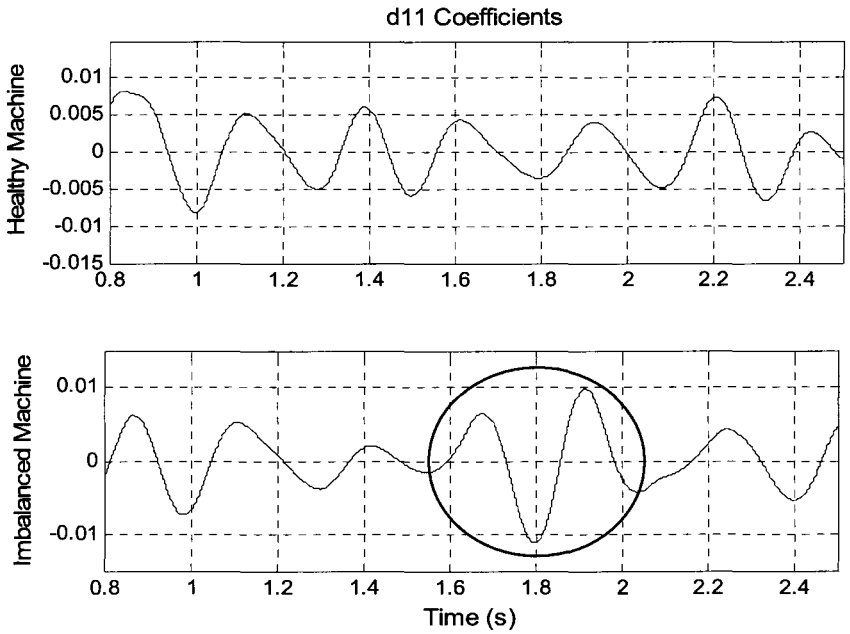

Figure 4.13: Detail level 11 for the healthy and imbalanced machines under 30% load

Fig. 4.14 shows the startup current of the fully loaded healthy machine, as it ramps up to a synchronous frequency of 35Hz. Figures 4.15 and 4.16 show the wavelet decomposition of the healthy and faulted machines at detail level 11 under 100% and 30% load, respectively. The feature maintains the characteristics observed in the previous two cases.

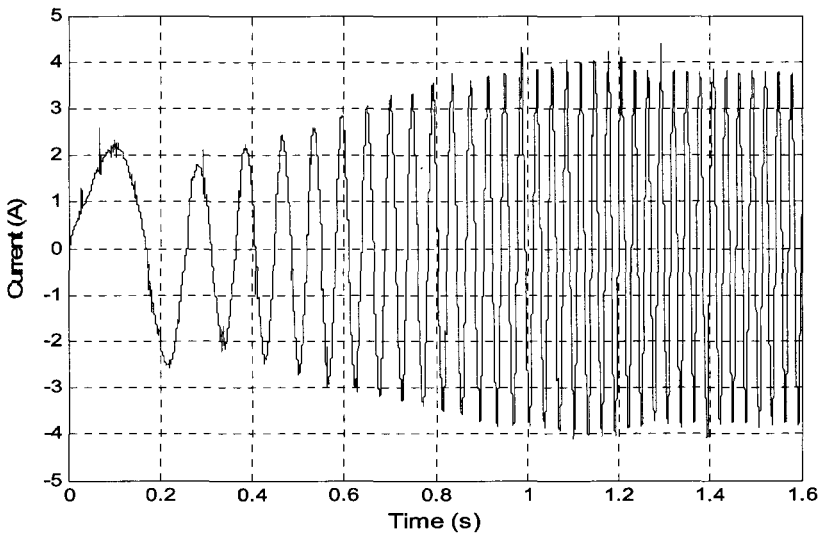

Figure 4.14: Time-domain representation of the current during startup

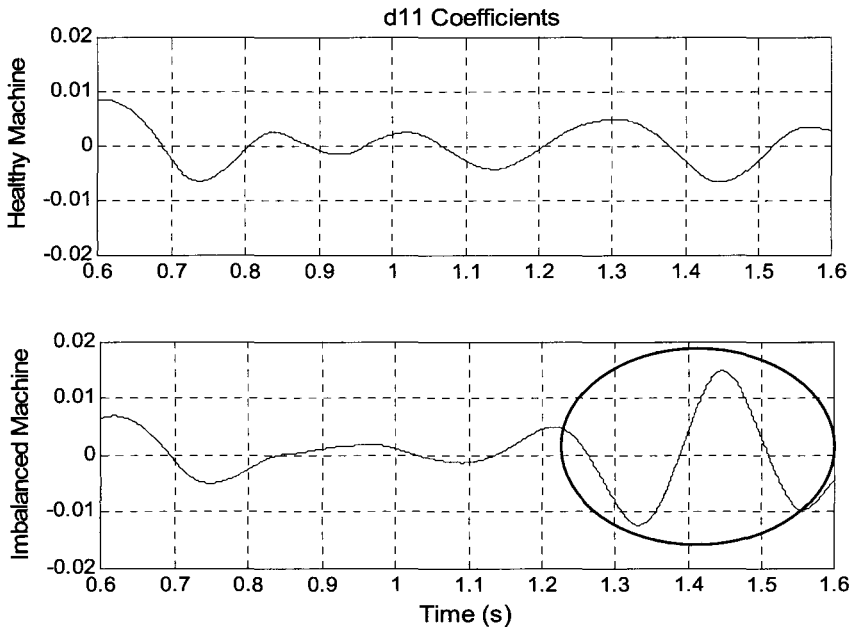

Figure 4.15: Detail level 11 for the healthy and imbalanced machines under full load

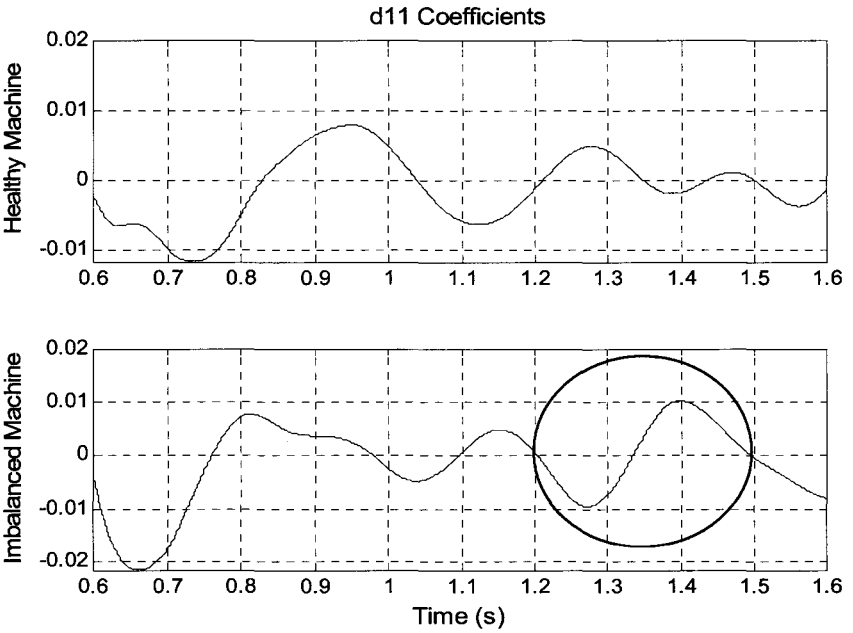

Figure 4.16: Detail level 11 for the healthy and imbalanced machines under 30% load

Fig 4.17 shows the current response for the ramp up in speed from 25Hz to 60Hz, under fully loaded conditions. Figures 4.18 and 4.19 shows the d11 coefficients for the ramp up in speed for the healthy and imbalanced machine, under full and 30% load, respectively. The feature again has similar characteristics to that of the startup conditions whereby it is more distinct under full load and shifts to the left as the load is decreased.

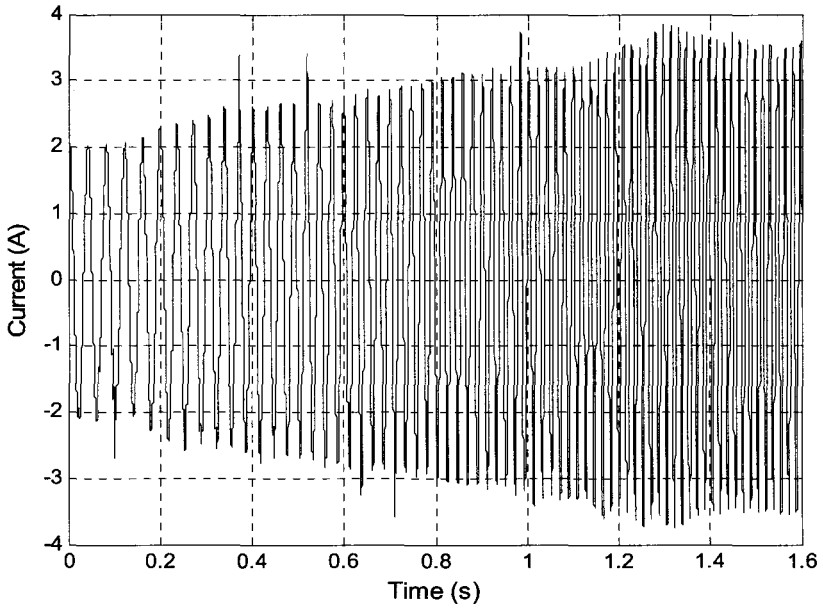

Figure 4.17: Current response for a ramp up in speed from 25Hz to 60Hz under full load

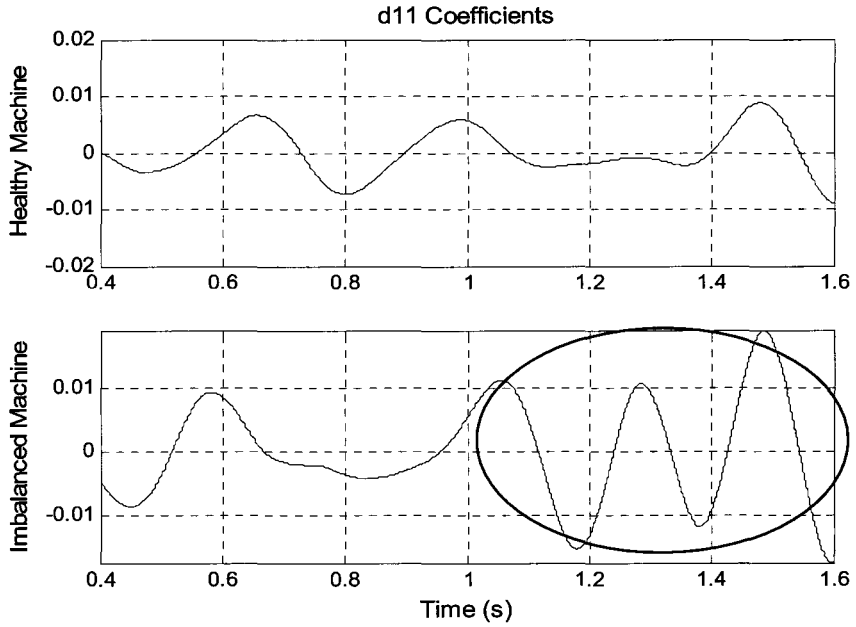

Figure 4.18: Detail level 11 for the healthy and imbalanced machines under full load

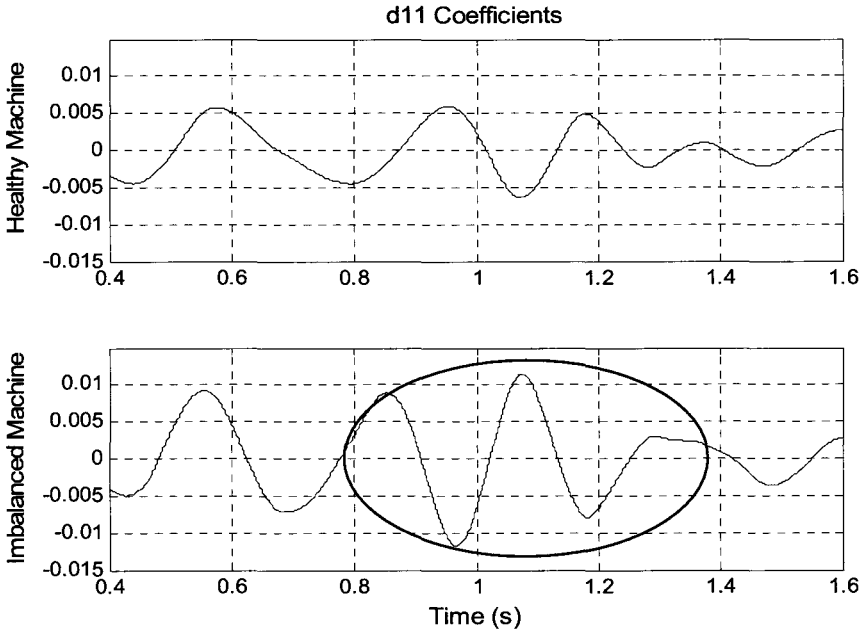

Figure 4.19: Detail level 11 for the healthy and imbalanced machines under 30% load

Fig 4.20 shows the current response for the ramp up in speed from 25Hz to 35Hz, under fully loaded conditions. Figures 4.21 and 4.22 shows the d11 coefficients for the ramp up in speed for the healthy and imbalanced machine,

under full and 30% load, respectively. The feature continues to follow the trend as indicated by previous results.

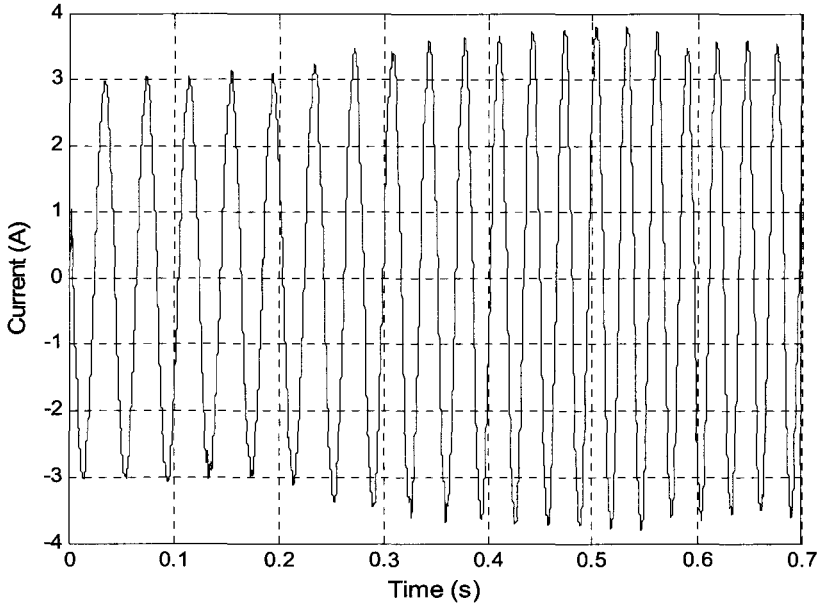

Figure 4.20: Current response for a ramp up in speed from 25Hz to 35Hz under full load

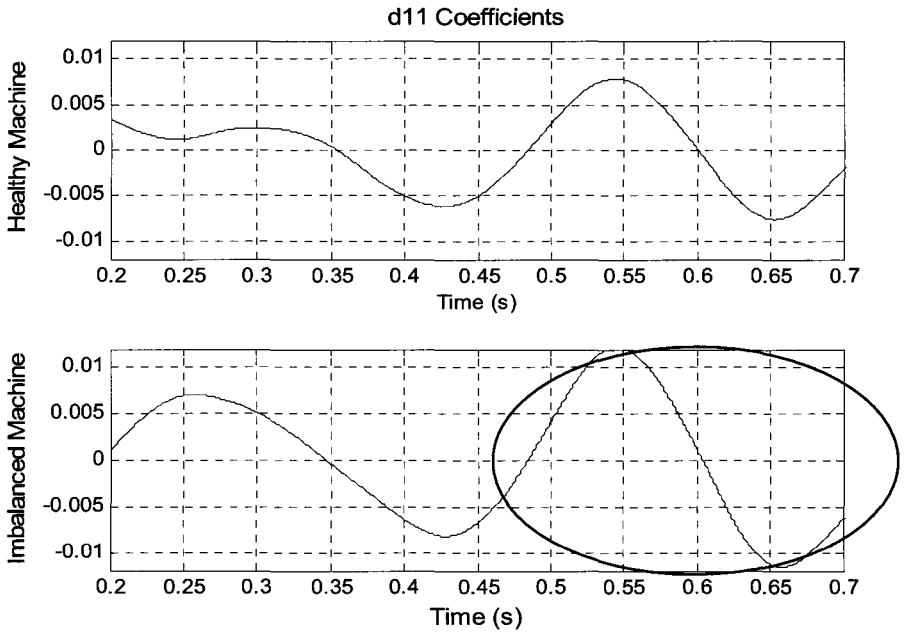

Figure 4.21: Detail level 11 for the healthy and imbalanced machines under full load

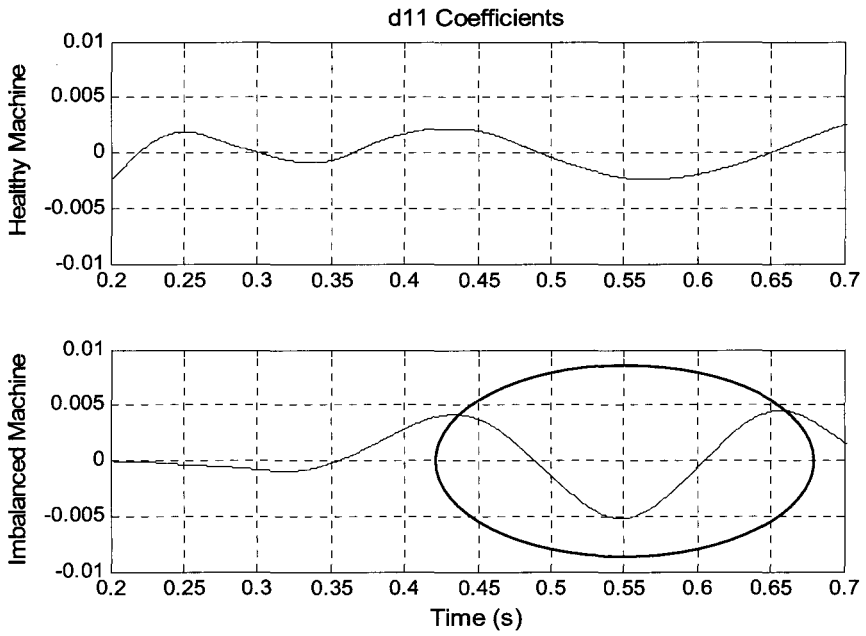

Figure 4.22: Detail level 11 for the healthy and imbalanced machines under 30% load

The lowest loading condition required to detect any significant difference in the d11 coefficients of the imbalanced machine is 30% loading, which holds true for all conditions discussed above. This is a significant improvement from the loading conditions required to detect the fault using MCSA. The significance of locating the defect in the higher order detail level is attributed to the location of the imbalanced fault components in the frequency domain, which is situated at the lower frequency levels, as suggested by MCSA.

4.5 Conclusions

It has been shown that imbalanced faults in inverter-fed induction machines can be identified by decomposing transient inrush currents. This is significant, since most fault detection schemes fail or operate at a diminished level when drives are connected to the machine. The detection algorithm is load dependent, however it only requires a minimum load of approximately 30% at the desired speed. This is a considerable improvement from steady-state

analysis techniques where heavier load conditions are required, particularly in the case of inverter-fed machines.

The methodology employed is the key and further research using this technique (i.e. for different faults and machines), would only serve to extend the knowledge base, so as to establish more complete guidelines on fault detection for machines of different designs and sizes.

4.6 References

[1] C. Kral, T. G. Habetler, R. G. Harley, "Detection of Mechanical Imbalances of Induction Machines without Spectral Analysis of Time-Domain Signals," IEEE Trans. on Industry Applications, vol. 14, pp 1372-1377, Dec. 1999.

[2] H. Douglas, P. Pillay, A. K. Ziarani, "Broken Rotor Bar Detection in Induction Machines with Transient Operating Speeds", IEEE Trans. on Energy Conversion, vol. 20, no. 1, March 2005.

[3] H. Douglas, P. Pillay, A. K. Ziarani,"A New Algorithm for Transient Motor Current Signature Analysis using Wavelets", IEEE Trans. on Industry Appl., vol. 40, no. 5, 30 Sept/ Oct 2004.

[4] M. Cabanas, M. Melero, G. Orajo, F. Rodriguez, J. S. Sariego, " Experimental Application of Axial Leakage Flux to the Detection of Rotor Asymmetries," Mechanical Anomalies, and Interturn Short Circuits in Working Induction Motors," Proc. Int. Conf. Electrical Machines, 1998, pp 420-425.

[5] W. Jarzyna, " Diagnostic Charactersistic sof Axial Flux in an Induction Machines," Proc. 7th Int. Conf. Electrical Machines and Drives, 1995, pp 141-146.

[6] T. W. S. Chow, G. Fei, "Three Phase Induction Machines Asymmetrical Faults Identification Using Bispectrum," IEEE Trans. on Industrial Electronics, vol. 51, no. 3, pp 558-565, June 2004.

[7] M. E. H. Benbouzid, "A Review of Induction Motors Signature Analysis as a Medium for Faults Detection", IEEE Trans. on Industry Electronics, vol. 47, no. 5, Oct 2000.

[8] M. E. H. Benbouzid, G. B Kliman, "What Stator Current Processing-Based Technique to Use for Induction Motor Rotor Faults Diagnosis", IEEE Trans. on Energy Conversion, vol. 18, no. 2, June 2003.

[9] Zhenxing Liu, Xinaggen Yin, Deshu Chen, "Online Rotor Mixed Fault Diagnosis Way Based on Spectrum Analysis of Instantaneous Power in Squirrel Cage Induction Motors," IEEE Trans. on Energy Conversion, vol. 19, no. 3, pp 1101-1106, September 2004.

[10] G. B. Kliman, "Methods of Motor Current Signature Analysis," Elect. Mach. Power Syst., vol. 20, no. 5, pp463-474, Sept. 1992.

[11] W. T. Thomson, D. Rankin, D. G. Dorrell, "On-line Current Monitoring to Diagnose Airgap Eccentricity in Large Induction Motors-Industrial Case Histories to Verify the Predictions," IEEE Trans. on Energy Conversion, vol. 14, pp 1372-1377, Dec. 1999.

[12] A.K. Ziarani, "Extraction of Nonstationary Sinusoids," Ph.D. dissertation, University of Toronto, Toronto, Canada, 2002.

[13] A. K. Ziarani, M. Karimi-Ghartemani, "On the Equivalence of Three Independently Developed Phase-Locked Loops", IEEE Trans. on Automatic Control, vol. 50, no. 12, pp 2021 - 2027, Dec. 2005.

Chapter 5

5. THE DETECTION OF INTER-TURN STATOR FAULTS IN DOUBLY-FED WIND GENERATORS

5.1 Introduction

Due to economical and environmental benefits, Wind Energy Conversion Systems (WECS) have received tremendous growth in the past decade. This has prompted the design and implementation of many WECS's across the globe. The preferred topology that is used for wind generators in the megawatt range is the doubly-fed induction generator (DFIG). The advantages of this topology include high efficiency, good controllability, and most importantly, reduction in the cost of the power electronic converters compared to stator-controlled systems [1]. These generators are designed to support the grid by delivering rated power over a limited speed range.

As a direct consequence of the increase in these generators, comes the need for the reduction of operational and maintenance costs. The most effective way of reducing these costs would be to continuously monitor the condition of these generators. A common induction machine failure is inter-turn shorts within the stator which is caused by deterioration of the stator winding. Presently, many techniques that are based on steady-state analysis are being applied to wind generators. However, the operation of wind generators is predominantly in the transient, therefore prompting the search for non-stationary fault detection techniques.

In this chapter it will be shown that steady-state analysis techniques i.e. Motor Current Signatures Analysis (MCSA) and the Extended Park's Vector Approach (EPVA), is not effective when applied to doubly-fed wind generators since their operation is predominately in the transient. A new non-stationary method of detecting inter-turn stator faults is proposed. The proposed method is a combination of EPVA and the non-stationary adaptive algorithm, presented in Section 2.2. The new method shows that inter-turn

stator faults can unambiguously be identified during non-stationary conditions while also providing insight into the degree of severity of the fault. Previous work has been able to detect inter-turn faults during transients with the use of wavelets [2]. The new technique however has the added advantage of providing insight into the degree of severity of the fault, while also reducing the processing requirements for real-time implementation.

The chapter is organised as follows, Section 5.2 gives a description of the DFIG system and Section 5.3 describes the implementation of the simulated inter-turn fault on the DFIG. Sections 5.4 and 5.5 describe the MCSA and EPVA techniques respectively, and attempts are made to identify the inter-turn fault using these techniques. Section 5.6 describes the new algorithm for detecting inter-turn faults during non-stationary operation and the technique is then applied to the DFIG. The results are analysed and discussed, after which conclusions are drawn.

5.2 Description of the Overall Doubly-Fed Induction Generator System

When both the rotor and stator are capable of delivering power as with the wound rotor induction generator, they are known as doubly-fed induction generators [3]. Fig. 5.1 shows the DFIG in its application to wind generation. The generator uses an AC-AC converter in the rotor circuit while the stator is directly connected to the grid. The rotor circuit is capable of bi-directional power flow and operates in three regions: 1) sub-synchronous operation (speeds below synchronous speed), 2) synchronous operation 3) super-synchronous operation (speeds above synchronous speed).

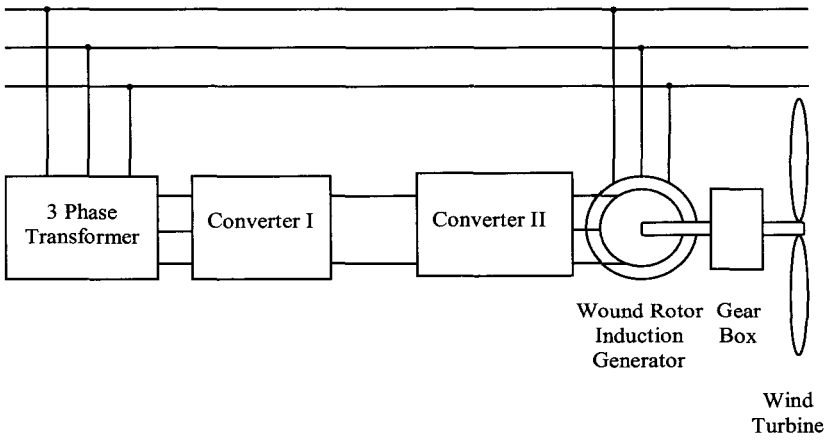

5.1: Principle layout of the variable speed WECS using a wound rotor induction generator

Fig. 5.2 represents a schematic of the vector control strategy used for the DFIG system. Field orientated control (FOC) of the machine is achieved via the rotor-side converter, which allows for independent control of torque and rotor excitation. The supply-side converter is responsible for maintaining a constant DC-link voltage and control of the power factor. A DC drive is used to emulate the wind turbine.

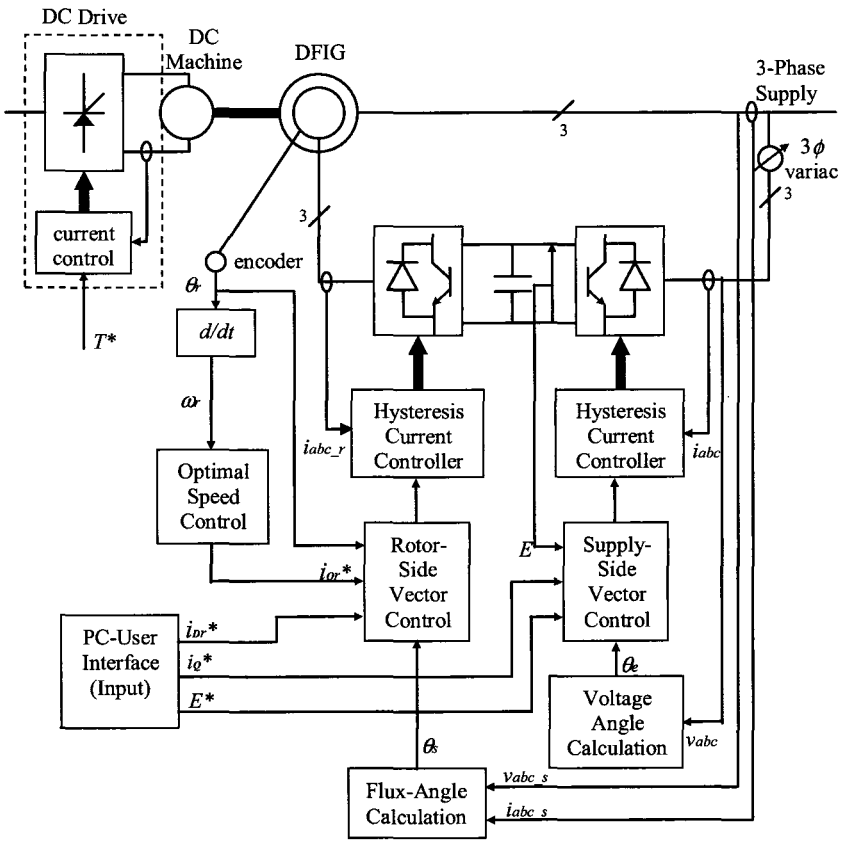

Figure 5.2: Schematic of a vector control system for a doubly-fed induction generator using back-to-back converters

5.2.1 *Control of the Supply-Side Converter*

The supply-side converter is used to maintain a constant DC-link voltage, regardless of the direction of rotor power flow. A vector control approach is used, as shown in Fig. 5.3, whereby independent control of active and reactive power is achieved.

The supply voltage angle calculation is achieved as follows

$$\theta_e = \arctan\left(\frac{v\beta}{v\alpha}\right) \tag{5.1}$$

where θ_e represents the supply voltage vector position[4].

Once the setpoint 3-phase currents have been determined, they are then processed by a hysteresis current controller, which then triggers the switching of the IGBT converter.

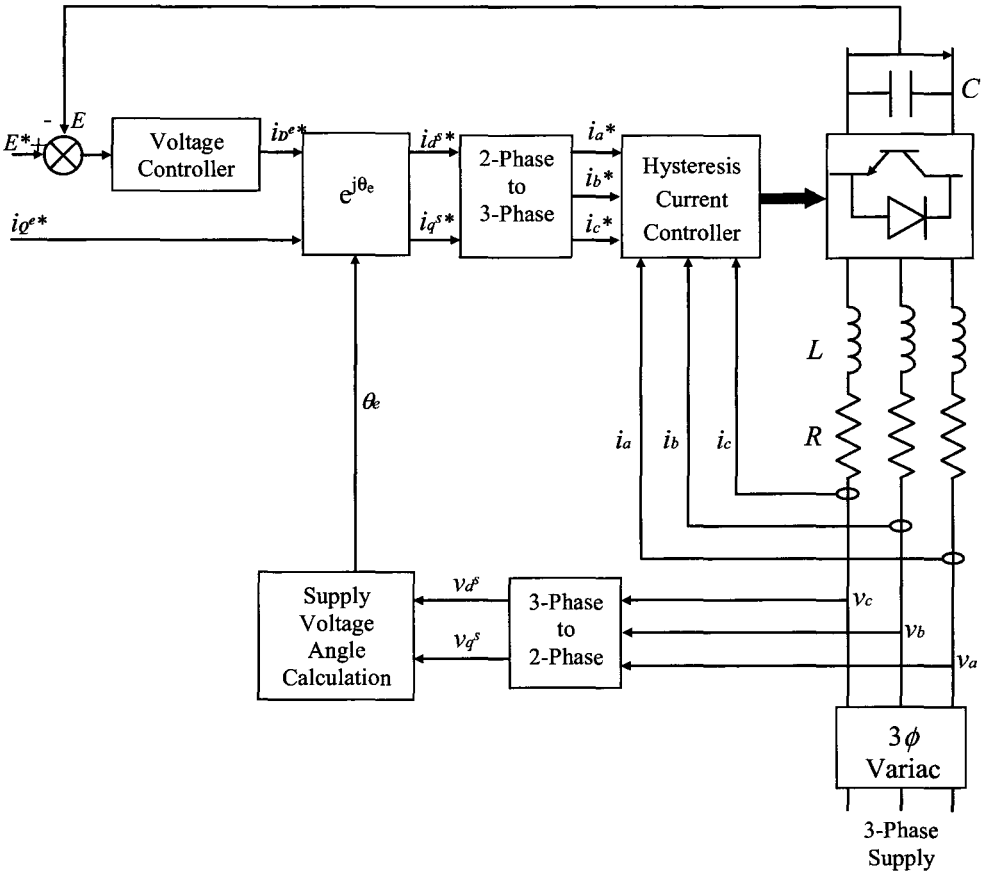

Figure 5.3: Schematic of vector control for the supply-side converter

5.2.2 Control of the Rotor-Side Converter

Field orientated control from the rotor-side is achieved in the synchronously rotating DQ reference frame. The D-axis is aligned with the stator-flux vector position, which sets the Q-axis stator-flux component to zero. In this way, a decoupled control between the electrical torque and the magnetic field is obtained [4], [5].

Once the setpoint 3-phase currents have been determined, they are then processed by a hysteresis current controller, which then triggers the switching of the IGBT converter.

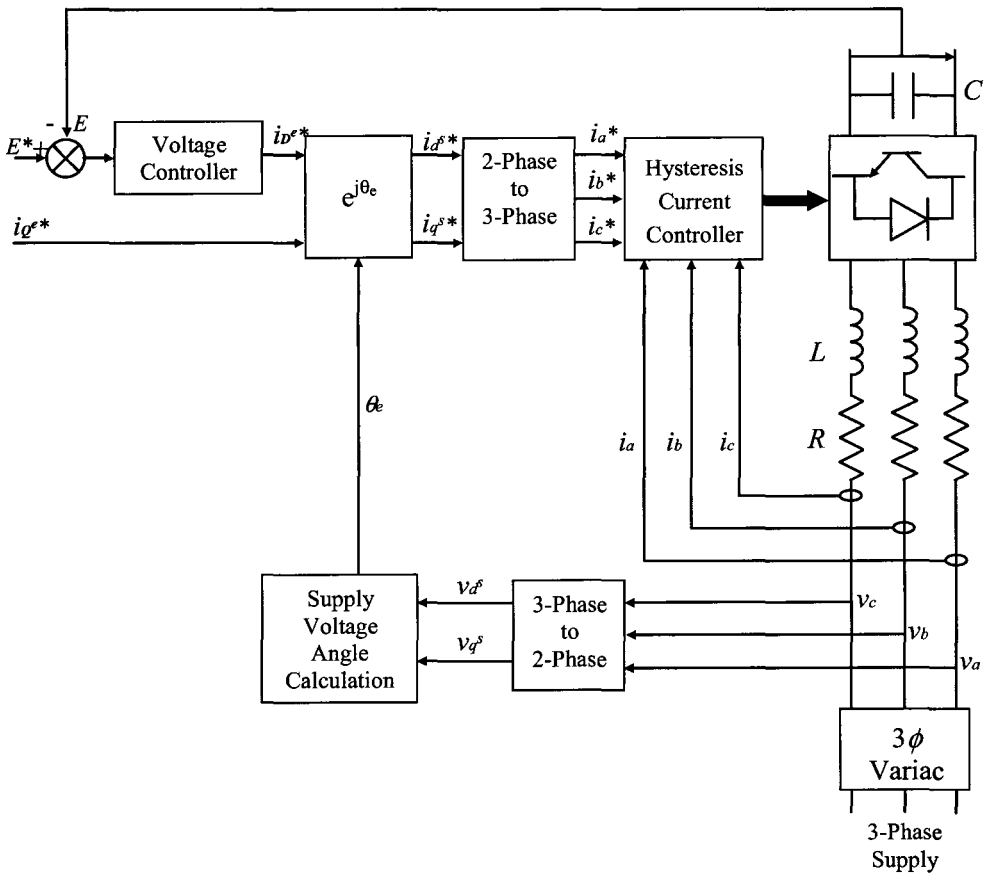

Figure 5.3: Schematic of vector control for the supply-side converter

5.2.2 *Control of the Rotor-Side Converter*

Field orientated control from the rotor-side is achieved in the synchronously rotating DQ reference frame. The D-axis is aligned with the stator-flux vector position, which sets the Q-axis stator-flux component to zero. In this way, a decoupled control between the electrical torque and the magnetic field is obtained [4], [5].

Since

$$\lambda_{QS} = 0 \tag{5.2}$$

the torque is described as follows

$$T = -\frac{P}{3}\frac{L_m}{L_s}\lambda_{DS} i_{Qr} \tag{5.3}$$

Fig. 5.4 illustrates the schematic block diagram for the machine control. i_{Dr}* is used to control the rotor excitation, however assuming that the reactive power to the machine is supplied by the stator, i_{Dr}* may be set to zero [4], [5]. The torque is proportional to i_{Qr}, thus once T* is determined via the speed controller, i_{Qr}* is calculated (using the above torque equation).

The 3-phase current setpoints are then achieved using the correct transformations, and the desired currents into the machine are attained via the use of the hysteresis current controller.

The stator flux is determined as follows

$$\lambda_{\alpha s} = \int (v_{\alpha s} - R s i_{\alpha s})\, dt \tag{5.4}$$

$$\lambda_{\beta s} = \int (v_{\beta s} - R s i_{\beta s})\, dt \tag{5.5}$$

The stator flux angle is calculated as follows

$$\theta_s = \arctan\left(\frac{\lambda_{\beta s}}{\lambda_{\alpha s}}\right) \tag{5.6}$$

where θ_s represents the stator flux position [4], [5].

The ω_r error is processed by a PI controller to give the setpoint torque (T*). The diagram below indicates the complete vector control for the rotor-side converter using the above formulas to calculate the stator flux and stator flux angle.

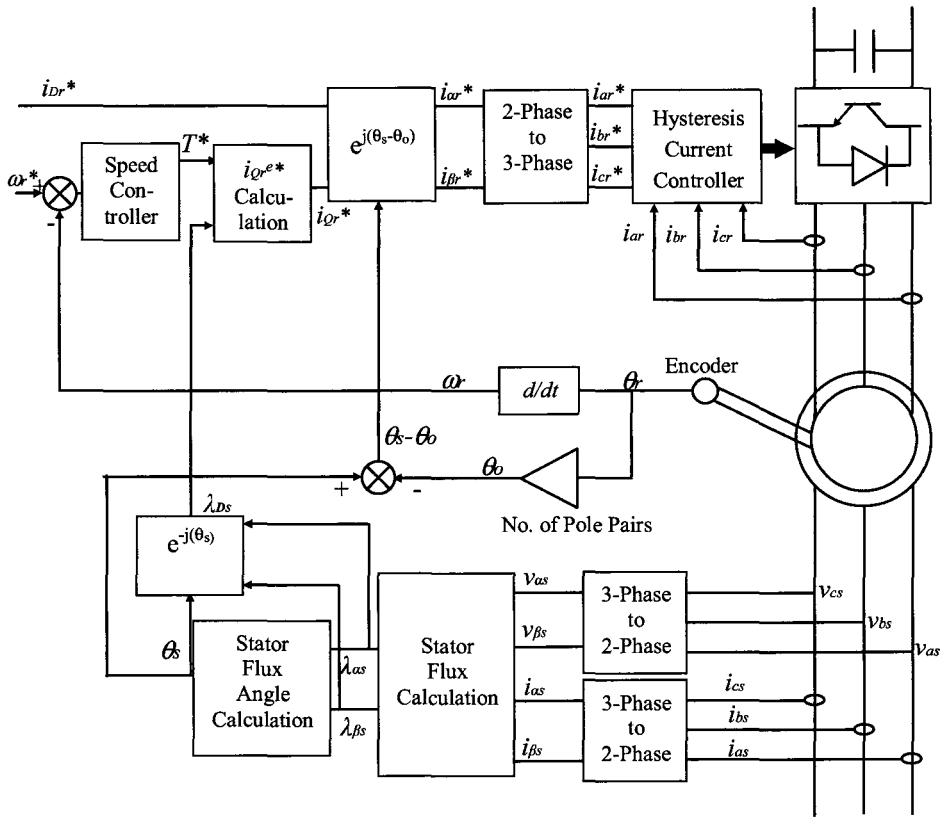

Fig. 5.4: Schematic of vector control for the rotor-side converter

5.2.3 *Experimental Setup*

Fig. 5.5 shows a picture of the overall experimental system. The wound rotor induction machine (WRIM) used is a 2.2kW, 3-Ph, 380V, 50Hz, 4 pole machine. Two hysteresis current controlled converters are placed in the rotor circuit, which provides the supply- and rotor-side control. Extra resistors and chokes are added to the supply-side converter, which are located between the 3-phase variac and the supply-side converter. The extra resistors and inductors added onto the supply-side converter is, R =0.1Ω and L=20mH. The DC-link voltage is maintained at 300V and the supply-side 3-phase voltage is set to 100V (i.e output of the variac). The DC drive used to emulate the wind turbine consists of a 2.2kW DC machine, which is torque controlled by an AC-DC thyristor converter.

The DS1104 R&D Controller Card is used to perform the computational and control tasks for both converters. Some of the key features of the controller package have already been listed in Chapter 3. The converters used are standard 100A commercial IGBT inverters. The inverters are switched at a maximum frequency of 5kHz during the simulated and experimental tests, due to the computational ability of the controller card. However, this switching frequency employed in the prototype confirms that the control techniques can be extended to higher power levels.

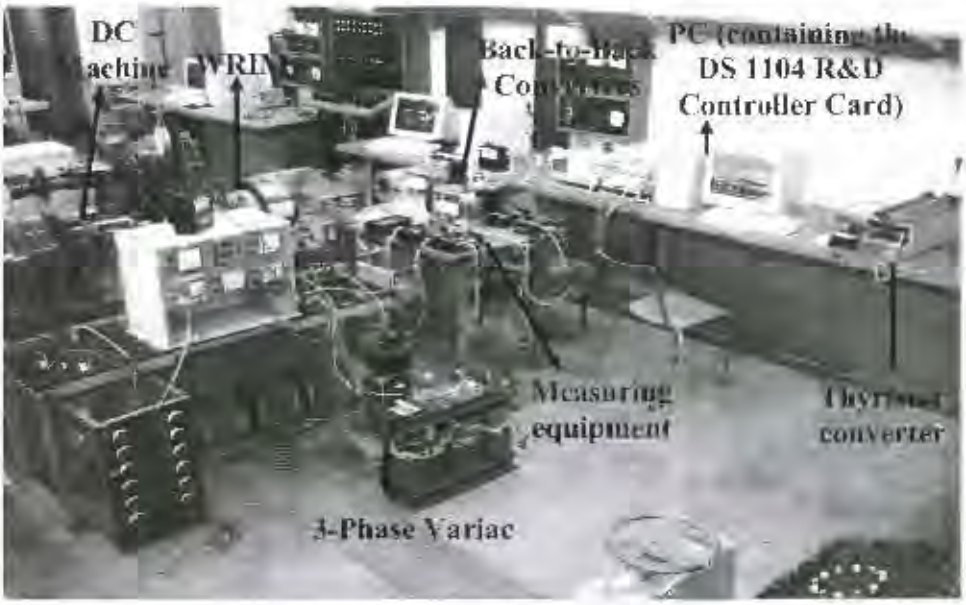

Figure 5.5: Experimental setup in the Laboratory

5.3 Practical Technique to Simulate an Inter-Turn Fault of a Stator Phase Winding

An inter-turn fault of a stator phase winding is a result of the deterioration of insulation between the individual coils. This is in essence a short circuit of the stator phase winding, which changes the symmetrical stator current to one that is asymmetrical. For predicting the electrical behavior from the stator supply due to an inter-turn fault, it would appear that the impedance of the short-circuited stator winding has decreased. The degree to which its impedance has decreased depends on the severity of the fault. To simulate the inter-turn fault on the DFIG, the impedance of the stator phase winding is decreased by

placing a resistor in parallel with the winding, as shown in Fig. 5.6 [6]. Two resistor values are chosen (i.e. 180Ω and 280Ω), to illustrate a change in the severity of the fault. The stator phase winding is connected in star.

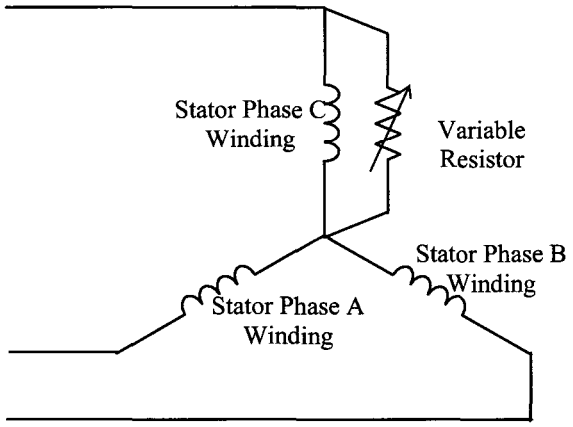

Figure 5.6: Simulated stator turn-to-turn fault

5.4 Motor Current Signature Analysis (MCSA)

5.4.1 *Theoretical Principles*

The equation below gives the frequency components which are characteristic of a shorted stator turn [7].

$$f_{st} = f_1\left[\frac{n}{p}(1-s)\pm k\right] \tag{5.7}$$

f_{st} is the stator frequency components that are a function of shorted turns, f_1 is the supply frequency, n = 1,2,3,..., k = 1,3,5,..., p is the pole-pairs, s is the per unit slip

As shown by equation (5.7), the inter-turn fault frequency components are dependent upon slip and the fundamental frequency. Using the Fast Fourier Transform (FFT), a frequency spectrum of the stator currents is shown and examined, for the DFIG operating at constant speed and a speed change from sub-synchronous to super-synchronous speed.

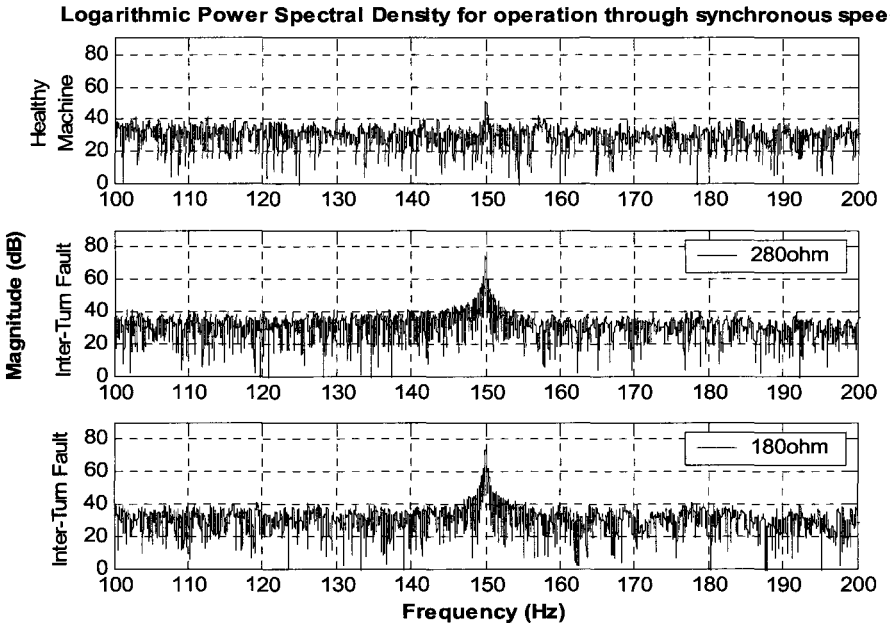

Figure 5.8: Spectrum of stator currents for operation through synchronous operation

From the above results, the following can be concluded. MCSA again shows that it performs acceptably under steady-state operation. However, under transient conditions, trying to identify fault harmonics becomes very difficult since the location of the fault harmonics is constantly changing due to its dependence on slip.

5.5 The Extended Park's Vector Approach (EPVA)

The EPVA is an extension of the Park's Vector Approach, however it has the benefit of providing greater insight into the severity of the fault. It has successfully been applied in the steady-state diagnosis of inter-turn faults, rotor cage damage, unbalanced supply voltage and mechanical load misalignment [6].

5.5.1 *Theoretical Principles*

The Park's Vector representation of the instantaneous stator line currents is attained using the transformation given in equation (5.8). The Park's Vector representation of 3-phase symmetrical currents (i.e. for a healthy machine) follows a perfect circular trajectory, as shown in Fig. 5.9(a). An unbalance in the line currents due to turn faults, results in an elliptical trajectory of the Park's Vector as shown in Fig. 5.9(b). The Park's Vector Approach is based on identifying the shape of the trajectory mapped by the currents of the Park's Vector representation.

In order to provide greater insight into the results attained from the Park's Vector Approach, the Extended Park's Vector Approach was introduced. This technique examines the frequency spectrum of the Park's Vector modulus. The modulus of the Park's Vector for a healthy machine is constant due to the circular trajectory of the Park's Vector, as illustrated in Fig. 5.10(a). The Park's Vector trajectory for the damaged case is elliptical, and therefore the modulus will contain a DC component and a sinusoidal component with a frequency of twice the fundamental, as shown in Fig. 5.10(b). The degree of unbalance is determined by the amplitude of this sinusoidal component. The severity factor is introduced and defined as the ratio of the magnitude of the twice-fundamental frequency to the DC component. The FFT is applied to the modulus of the Park's Vector to determine the magnitude of the twice fundamental frequency component [6], [8]. Based on its magnitude the machine may be diagnosed for the inter-turn fault. This process of detection is referred to as the Extended Park's Vector Approach (EPVA). Fig. 5.11(a) and 5.11(b) shows the frequency spectrum of the modulus Park's Vector representation of the stator currents, whereby the twice fundamental component is clearly evident for the faulted case.

$$\begin{bmatrix} id \\ iq \end{bmatrix} = \frac{2}{3}\begin{bmatrix} 1 & -\frac{1}{2} & -\frac{1}{2} \\ 0 & \frac{\sqrt{3}}{2} & -\frac{\sqrt{3}}{2} \end{bmatrix}\begin{bmatrix} ia \\ ib \\ ic \end{bmatrix} \tag{5.8}$$

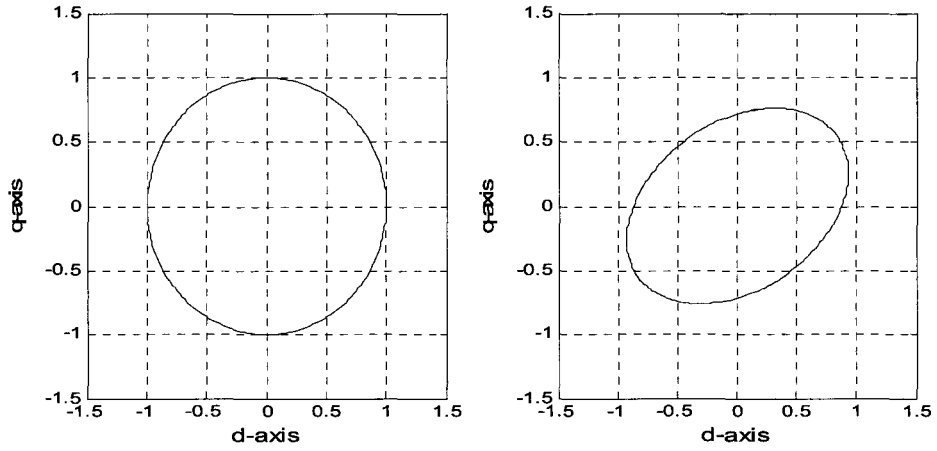

Figure 5.9: The Park's Vector representation of the stator currents for a (a) healthy machine and (b) a machine with an inter-turn fault, both operating in steady-state

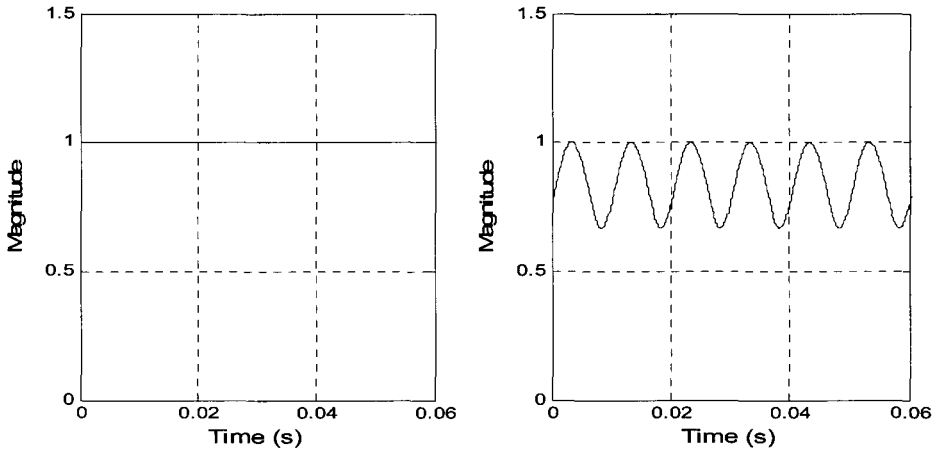

Figure 5.10: The modulus of the Park's Vector representation of the stator currents for a (a) healthy machine and (b) a machine with an inter-turn fault, both operating in steady-state

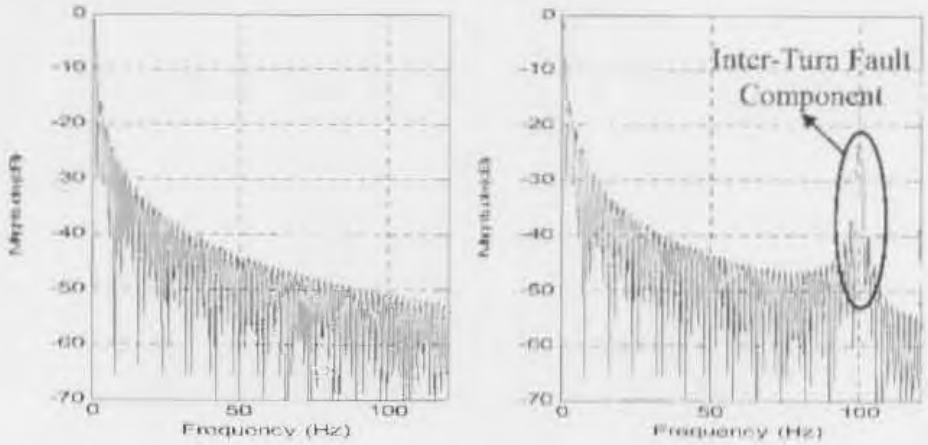

Figure 5.11: The frequency spectrum of the stator currents Park's Vector modulus for a (a) healthy machine and (b) a machine with an inter-turn fault, both operating in steady-state

5.5.2 *Analysis and Discussion of Results*

This method of detection is proven to work well under steady-state conditions, however as mentioned earlier, the behavior of these DFIG's is predominately transient. In these experiments the speed of the machine is ramped up from 1170rpm to 1880rpm (subsynchronous to supersynchronous) as shown in Fig. 5.12.

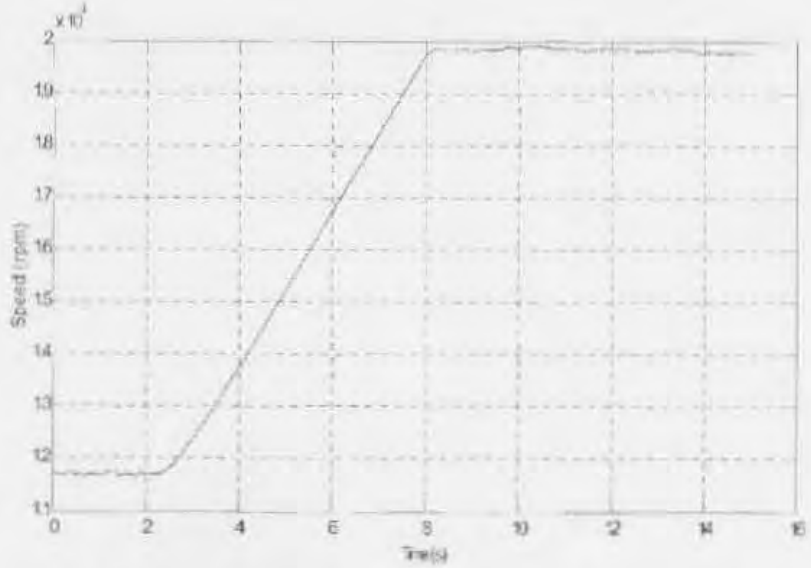

Figure 5.12: The speed profile of an undamaged machine

Observing the Park's Vector currents, of the undamaged machine in Fig. 5.13, it is clear that it does not have a constant magnitude. In fact the amplitude oscillates as time progresses. This obviously complicates the expression for the severity factor since the dc component is not a constant. The amplitude of the twice fundamental frequency component changes too, and therefore the use of Fourier analysis is questionable. Fig. 5.14 shows the frequency spectrum of the Park's Vector modulus for the healthy and faulted machines. Although there does appear to be an increase in the magnitude of the fault component (i.e. twice the fundamental) for the faulted cases, as shown in Fig. 5.13, this transient condition does not adhere to the steady-state rules for Fourier analysis, therefore the results cannot be accepted for analysis and diagnosis.

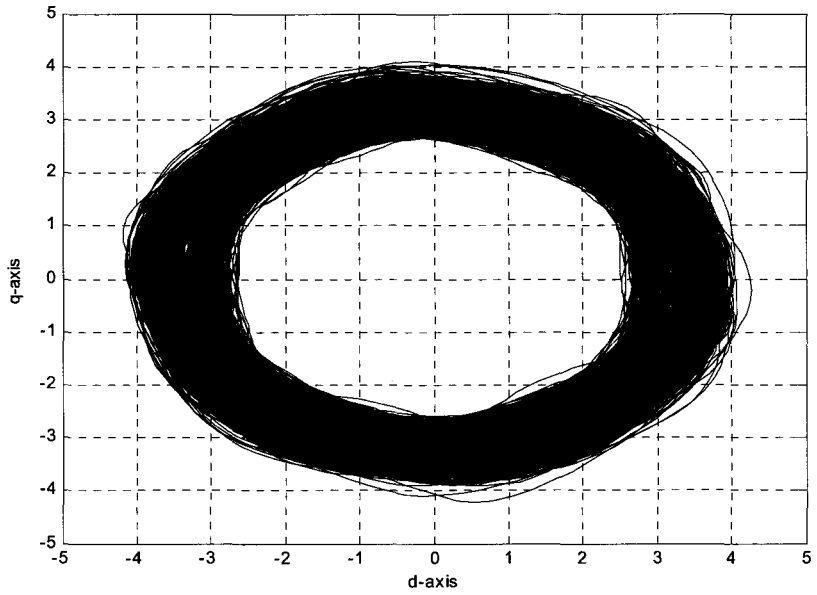

Figure 5.13: The Park's Vector of an undamaged machine

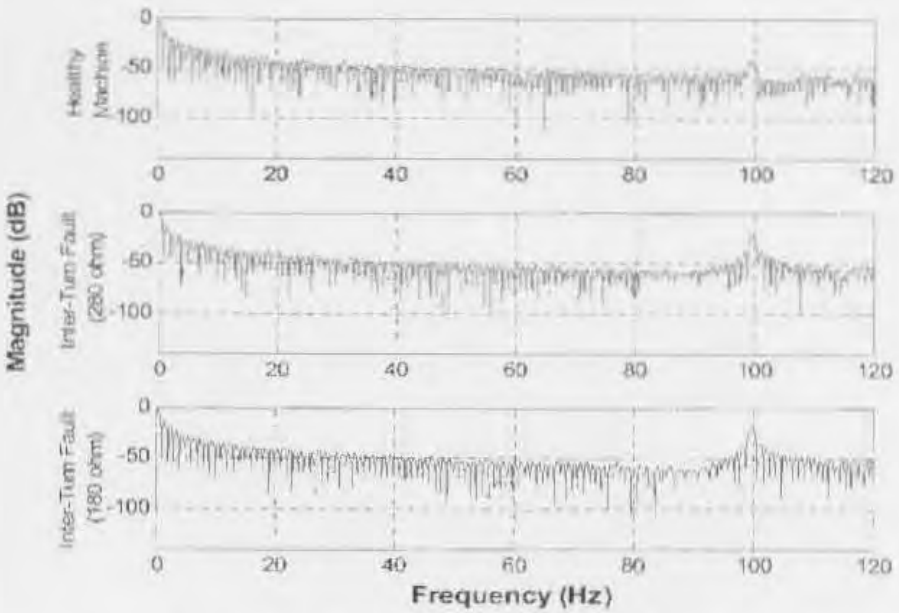

Figure 5.14: Current spectrum for the modulus of the Park's Vector for the healthy and faulted conditions under transient conditions

5.6 A New Method of Extracting the Inter-Turn Fault Associated Sinusoids

5.6.1 Theoretical Principles

As shown in EPVA, inter-turn stator faults may be identified by monitoring twice the fundamental frequency component of the Park's Vector modulus. However, the validity of using Fourier Analysis to identify this component during transients is diminished, since Fourier relies on steady-state conditions. In [2], Fourier analysis is replaced by wavelets to identify the fault condition during transients. Although this technique proved to be very successful, it lacked the ability to assess the severity of the fault while also requiring a considerable amount of processing power for real-time implementation.

Instead the use of the non-stationary adaptive algorithm, as discussed in Section 2.2, has resolved the issues faced by the previous techniques. Since the only component of interest is twice the fundamental component of the Park's Vector modulus, the fixed-frequency sinusoid-tracking algorithm, shown in Fig. 2.2, can be used to extract the non-stationary sinusoid representing the

twice fundamental component [9]-[11]. The magnitude of this sinusoid, provides insight into the inter-turn fault condition of the machine. Fig. 5.15 shows the schematic of the final fault detection algorithm.

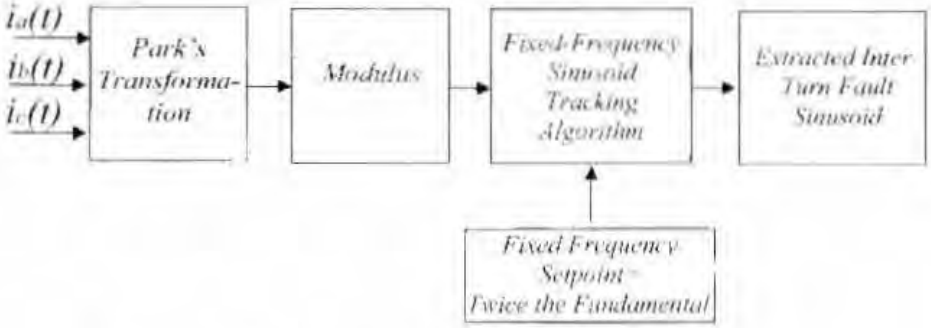

Figure 5.15: New fault detection algorithm

5.6.2 *Analysis and Discussion of Results*

Fig. 5.16 shows the extracted twice fundamental sinusoidal component (100Hz) of the Park's Vector modulus for the normal and faulted machines during a ramp up in speed from 1120rpm to1880rpm. The two faulted cases considered here were done using two different resistor values (i.e. 180Ω and 280Ω), thus representing different severities of the inter-turn fault. It is evident from the figure that there is an increase in amplitude of the extracted fault sinusoid between the healthy and the faulted machines. It is also evident that the amplitude of the sinusoid increases in proportion to the severity of the inter-turn fault and its amplitude is unaffected by changes in speed or load. Fig. 5.17 shows a magnified version of the extracted fault sinusoid for the faulted machine (180 Ω resistor), whereby the twice fundamental sinusoid (100Hz) is clearly evident. The results shown, indicate good performance by the algorithm to extract the fault associated sinusoid for this particular system. However, the gain parameters (μ_1, μ_2 and μ_3) need to be chosen so as to optimize the ability of the algorithm to track these changes for a particular system. μ_1=100, μ_2=10000 and μ_3=0.02 indicated good dynamic convergence for this case.

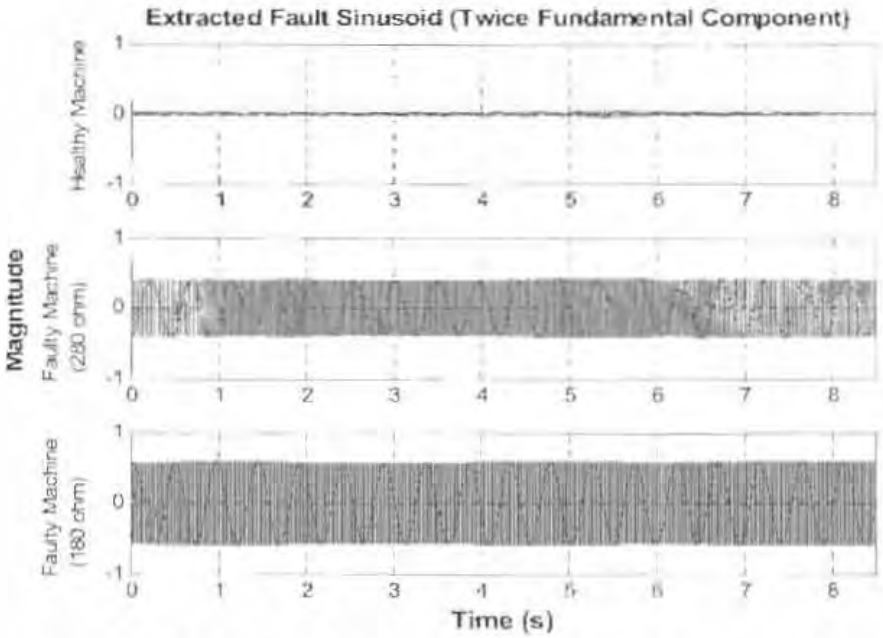

Figure 5.16: Fault sinusoid which is extracted from the Park's Vector modulus

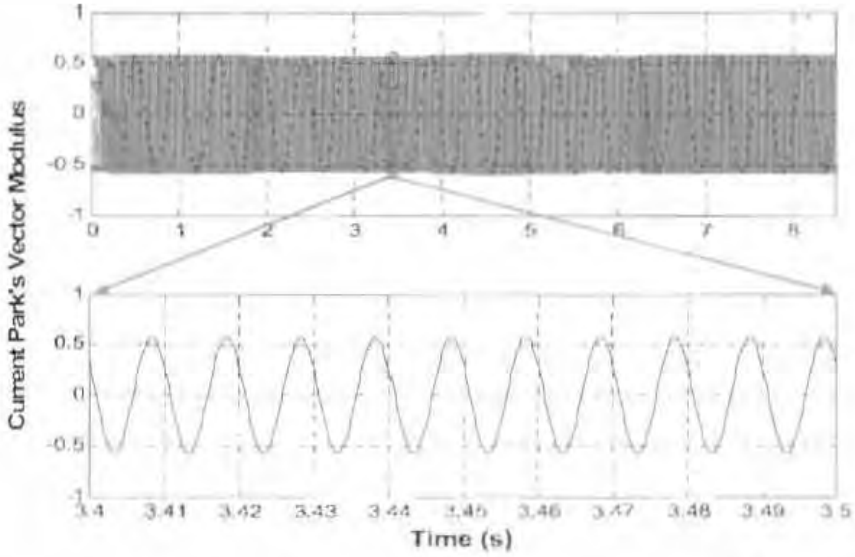

Figure 5.17: Magnified fault sinusoid for the greater fault condition

Fig. 5.18 indicates the RMS values of the extracted fault sinusoids for the normal and faulted machines during various ramps in speed. These changes in speed are listed on the horizontal axis of the figure. There is a clear difference

in magnitude between the normal and the faulted operating conditions. It is evident that there is an increase in the RMS value for an increase in the fault condition, thus indicating that the severity of the inter-turn fault may be monitored and assessed through this process. The monitoring technique also validates that the extracted fault component is unaffected by changes in speed and load since the RMS value remains relatively constant for these changes.

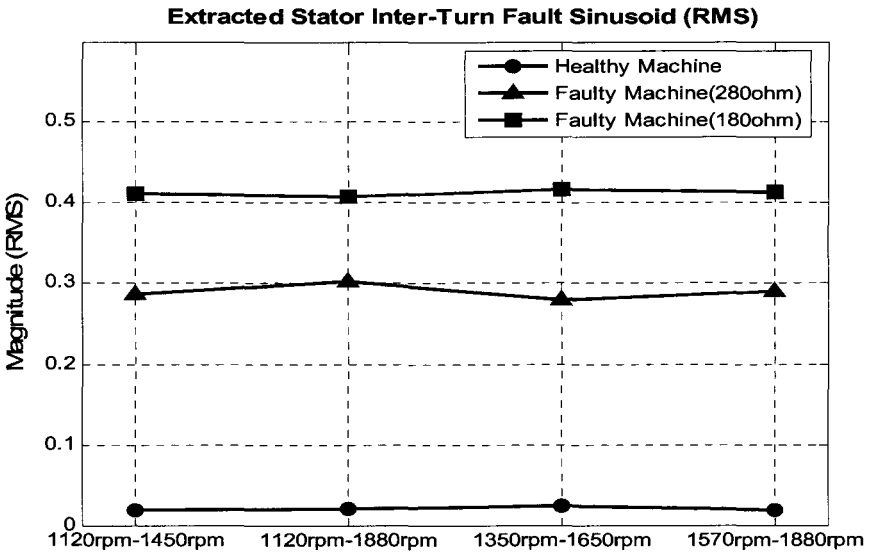

Figure 5.18: RMS value of the extracted non-stationary fault sinusoid under different operating conditions for the normal and inter-fault cases

5.7 Conclusions

The details for implementation of a DFIG system in its application to wind generation has been described. Inter-turn faults are simulated on the DFIG to provide a comparative study into various fault analysis techniques. A new algorithm for detection of inter-turn faults under non-stationary conditions has been proposed. The detection algorithm is based on the Extended Park's Vector Approach, whereby the signal processing tool used for analysis, i.e. Fourier Transform, is replaced by the non-stationary fixed-frequency sinusoid-tracking algorithm. The proposed fault detection algorithm proves to be extremely successful in its ability to unambiguously identify the inter-turn fault under non-stationary operating conditions. This is ideally suited for wind

generators since most operate predominately in the transient. It is also shown that the severity of the inter-turn fault may be assessed through the proposed fault detection technique, which other techniques have been unable to achieve. The implementation of the algorithm is also considerably simple, thus limiting the processing capabilities required to process the algorithm in real-time applications.

5.8 References

[1] Rajib Datta, V.T. Ranganathon, "Variable Speed Wind Power Generation Using Doubly Fed Wound Rotor Induction Machine-a comparison with alternative schemes," IEEE Transactions On Energy Conversion, Vol.17, No. 3, pp 414-421, September 2002.

[2] H. Douglas, P. Barendse, P. Pillay, "The Detection of Inter-Turn Stator Faults in Doubly-Fed Induction Generators", IEEE Industry Applications Conference 2005, 40th IAS Annual Meeting, vol. 2, pp 1097 – 1102, 2-6 Oct. 2005.

[3] Tomas Petru and Torbjorn Thiringer, "Modelling of Wind Turbines for Power System Studies," IEEE Transactions on Power Systems, Vol.17, No. 4, Nov 2002.

[4] R. Pena, J.C. Clare and G.M. Asher, "Doubly Fed Induction Generator using Back-to-Back PWM Converters and its Application to Variable Speed Wind Energy Generation", IEE Proc.-Electr. Power Appl., Vol. 143, No. 3, pp231-241, May 1996.

[5] P. B. Barendse, "Design and Implementation of Variable Speed Wind Energy Induction Generator Systems for Fault Studies," MSc. dissertation, University of Cape Town, Cape Town, South Africa, 2005.

[6] S. M. A. Cruz and A. J. Marques Cardoso, "Stator Winding Fault Diagnosis in Three-Phase Synchronous and Asynchronous Motors, by the Extended Park's Vector Approach", IEEE Transactions on Industry Applications, Vol. 37, No. 5, Sept/Oct 2001.

[7] L.M. Popa, B Bak-Jensen, Ewen Ritchie and Ion Boldea, "Condition Monitoring of Wind Generators", Industry Applications Conference, 2003. 38th IAS Annual Meeting, vol 3, pp 1839 - 1846, 12-16 Oct. 2003.

[8] M. E H. Benhouzid, "A Review of Induction Motor Signature Analysis as a Medium for Fault Detection", IEEE Trans. on Industry Appl., vol. 37, no. 5, Sept/Oct 2001.

[9] A. K. Ziarani, M. Karimi-Ghartemani, "On the equivalence of three independently developed phase-locked loops", IEEE Trans. on Automatic Control, vol. 50, no. 12, pp 2021 - 2027, Dec. 2005.

[10] A. K. Ziarani, A. Konrad, "A nonlinear adaptive method of elimination of power line interference in ECG signals", IEEE Trans. on Biomed. Eng, vol. 49, no. 6, pp 540 – 547, June 2002.

[11] A.K. Ziarani, "Extraction of nonstationary sinusoids," Ph.D. dissertation, University of Toronto, Toronto, Canada, 2002.

Chapter 6

6. A FAULT RIDE-THROUGH STRATEGY FOR DOUBLY-FED WIND GENERATORS DURING VOLTAGE SAGS

6.1 Introduction

Doubly-fed wind generators have seen tremendous growth over a relatively short period of time. These systems are not only susceptible to generator fault occurrences (i.e. inter-turn faults), but also power system faults. A voltage sag is a typical power system fault, which is characterized by a sudden decrease in RMS voltage magnitude. Previously, wind generators were disconnected from the grid during a voltage sag [1]. However as wind generators replace conventional generation systems, these wind systems are required to remain connected during faults [2], [3].

Although fault mitigation techniques exist for the doubly-fed induction generators (DFIG), the deciding factor that could prevent catastrophic failure is the time required to detect the sag. It is therefore imperative to incorporate a mitigation strategy based on sag detection into the control system of a DFIG for rapid response protection. Existing techniques for voltage sag detection include the root mean square (RMS), Fourier transform and peak voltage detection methods. The problem with these methods is that they use a windowing technique with historical data and can therefore be too slow when applied to detect sags for protection [4].

[5] discusses the threat of sags on the converter of the DFIG. In [6], a technique is proposed for ride-through where a set of resistors is connected to the rotor circuits. This is achieved using a thyristor to control the firing of discharge resistor that is connected in parallel with the rotor circuit. No experimental results were shown for this proposed solution. Papers which have been published prior to this have provided little or no information on their protection scheme [7]-[9].

In this chapter, a method is proposed which allows the DFIG to stay connected to the grid during voltage sags. The key component of the scheme is a sag detection algorithm which is capable of detecting sags faster than current techniques. The detection technique is formed from the non-stationary adaptive algorithm, which is presented in Section 2.2 [4]. The chapter continues by presenting a simple mitigation strategy for the DFIG once the sag is detected, thus protecting the power electronics and generator. This is achieved through the use of a discharge resistor in parallel with the DC-link capacitor for dissipating the excess currents. Experimental results show that successful ride-through can be achieved with the proposed strategy.

The chapter is organized as follows: The experimental setup of the DFIG described in Section 5.2, is used for the following study and therefore a description of the setup will not be repeated in this chapter. Section 6.2 discusses the behavioural effect voltage sags have on the DFIG system. Section 6.3 presents the detection algorithm and ride-through strategy. Based on the proposed detection and mitigation scheme, simulation and experimental results are discussed in Sections 6.4 and 6.5 respectively. The chapter concludes in Section 6.7.

6.2 Voltage Sag Characteristics of the DFIG

A drop in grid voltage will cause a rise in currents flowing through the stator circuit. Since the stator and rotor are magnetically coupled, this will result in an increase in rotor currents. The increase in rotor currents is dependant on the severity of the sag and the machine parameters. These transient currents make the power electronics of the converters vulnerable to failure [5], [6]. Failure of the system during a sag can introduce instability problems on the power network [10], [11]. It is therefore important that the wind energy conversion system is controlled in such a manner so as to protect the components from failure. Issues that need addressing are the time required to:

1) rotate the blades to reduce the power extracted from the incoming wind
2) protect the DC-link capacitor against over-voltage

3) protect the semiconductor switches against over-currents

6.3 The Fault Ride-Through Strategy

6.3.1 The Detection Algorithm

The sag detection algorithm is based on the varying-frequency adaptive algorithm, as discussed in Section 2.2. The grid voltage would serve as the input to the algorithm, whereby the amplitude is monitored and compared to a lower threshold value, which represents the sag inception value. If the threshold is surpassed, a trigger signal is activated. [4] first applied the algorithm for sag detection purposes and was able to show its superiority over other techniques, i.e. root mean square (RMS), Fourier transform and peak voltage detection methods. Some of these key advantages will be highlighted in this section. The mathematical description of the algorithm will not be repeated , since this has been covered in Section 2.2.

As mentioned previously, one of the issues that needs to be considered when using the algorithm is the setting of its parameters. The values of the parameters determine the convergence speed versus error compromise. Specifically, parameter μ_1 controls the speed of the transient response of the algorithm with respect to variations in the amplitude of the interfering signal. Parameters μ_2 and μ_3 mutually control the speed of the transient response of the algorithm with respect to variations in the frequency of the interfering signal. Speed is traded off by the steady-state error. As long as the frequency of the input signal is close to its nominal value (e.g. 50 Hz), this trade-off does not introduce a significant constraint. As the frequency of the input signal deviates from its nominal value, the algorithm introduces more significant trade-off between the speed and steady-state error; for example, within a range of Hz variations off nominal frequency, the algorithm can be adjusted to catch up a step change in the amplitude of the desired sinusoid within cycles with less than steady-state error. Fig. 6.1 shows the estimation process under different μ parameters. The higher the μ value chosen, the shorter the

convergence time becomes. The convergence time is about 20ms for the highest values of μ presented and about 200ms for the lowest values of μ, with the middle set having a convergence time of about 80ms [12].

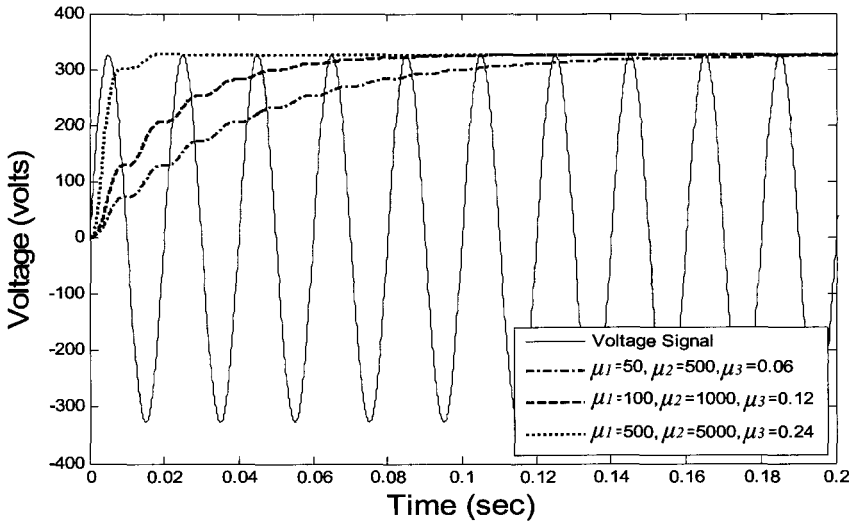

Figure 6.1: Convergence of the core algorithm under different μ parameters

Using the parameter values which gave the shortest convergence time, the algorithm is compared with two methods currently used, i.e. ½ Cycle RMS and DFT. A sag is initiated in the laboratory from cycles 4-6. The results of one of these tests are shown in Fig. 6.2. The RMS and DFT pick up the sag at point 2 (0.9 p.u as per sag definition) and the new algorithm at point 1. It is shown in more detail in [4] that the algorithm responds faster than currently used sag detection schemes.

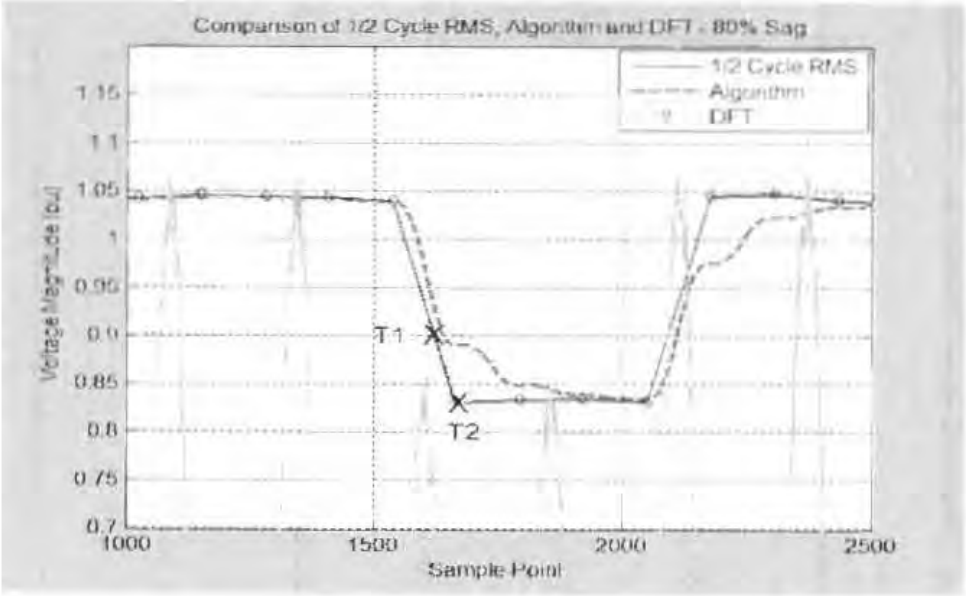

Figure 6.2: T1 shows that the algorithm is able to detect the sag much faster than the ½ cycle RMS and DFT methods

6.3.2 *The Mitigation Scheme*

Fig. 6.3 gives an overview of the proposed mitigation strategy. The stator voltage signals from the transducers serve as inputs to the algorithm. The output of the algorithm is a trigger signal that represents sag inception. The trigger signal is sent to a driver for rapidly switching the discharge resistor R_d on for the sag duration. This is achieved by opening all the power switches and transferring the excess energy into the discharge resistor, R_d. This limits the excess currents. The decrease in DC-link voltage by the mitigation scheme would be determined by the response of the filter during the sag. The filter response is established by the time constant of the discharge resistor and DC-link capacitance. The response of the filter should be selected to reduce the voltage to a satisfactory level, whereby control after the sag may still be achieved. An enhancement to the proposed mitigation technique would be to dynamically change the resistance R_d, by pulsating the switching scheme at a rate dependant on the severity of the sag. However, since the primary focus of this work is to verify the effectiveness of incorporating the detection algorithm

in the DFIG system, a fixed Ra value of 40Ω proved to provide a satisfactory filter response for the tests.

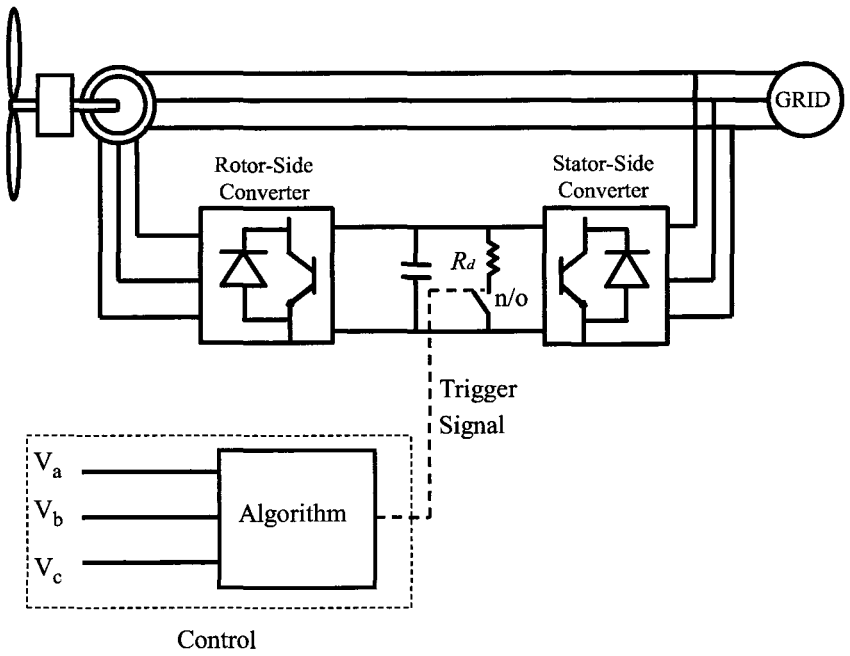

Figure 6.3: Overview of proposed ride-through strategy

6.4 Simulated Results

The following simulation results show the DFIG operating under rated conditions at 25% above synchronous speed, without the fault ride-through strategy. The machine and converter parameters used in the simulation are attained from experimental parameters. To show the effectiveness of the fault ride-through scheme, the behaviour of the DFIG during a sag without protection is firstly examined. A voltage sag of 50% is implemented at 0.5 sec and lasts for 100ms.

6.4.1 DFIG without the Fault Ride-Through Scheme

Fig. 6.4 shows the stator voltage, whereby the sag in voltage is evident. Fig. 6.5 and Fig. 6.6 show the sudden rise in the stator and rotor currents at the instant of the sag. When operating under rated conditions, the rise in rotor currents could cause damage to the power electronics in the back-to-back

converter. Fig. 6.7 shows the effect of the sag on the DC-link voltage. It is evident from the diagram that the DC-link voltage exceeds the set-point voltage of 350V, at the instant when the grid voltage recovers from the sag. This is a critical area since too large a rise in the voltage could damage the capacitors.

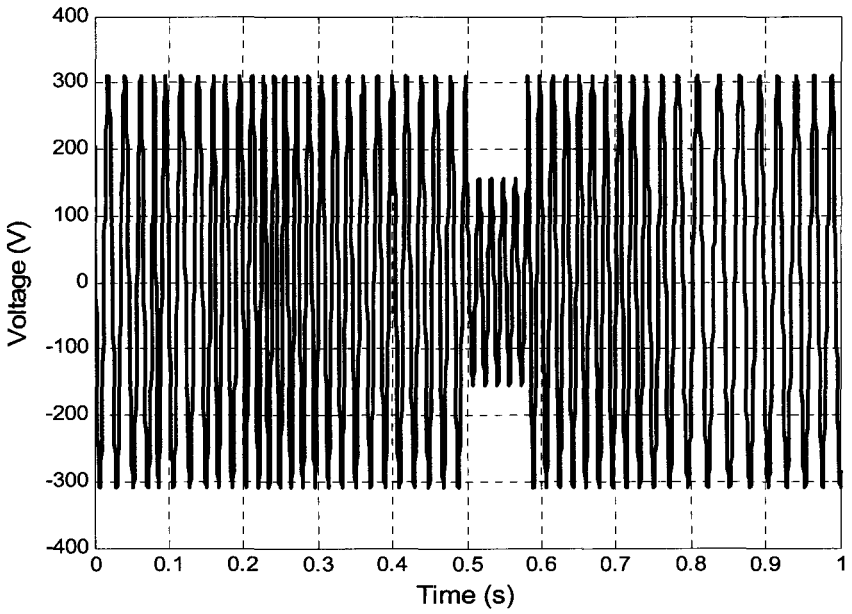

Figure 6.4: Supply voltage

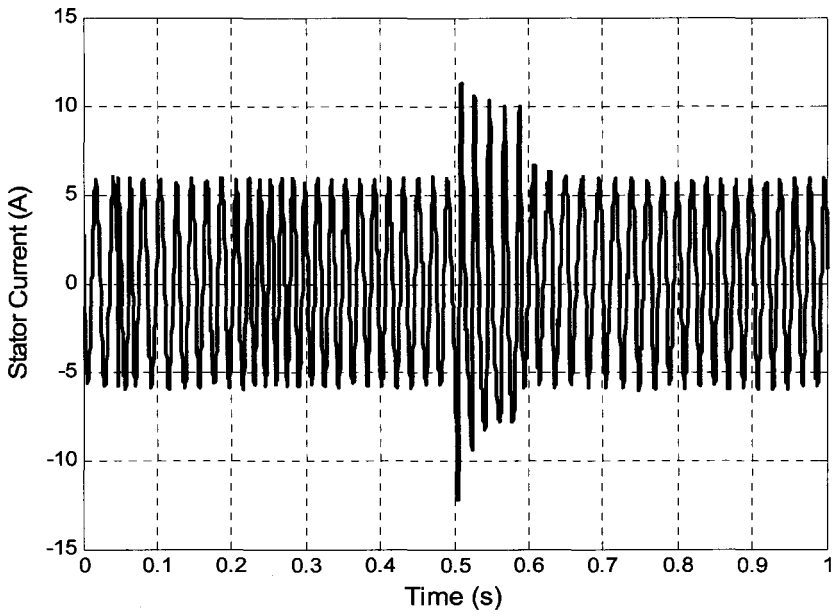

Figure 6.5: Stator current

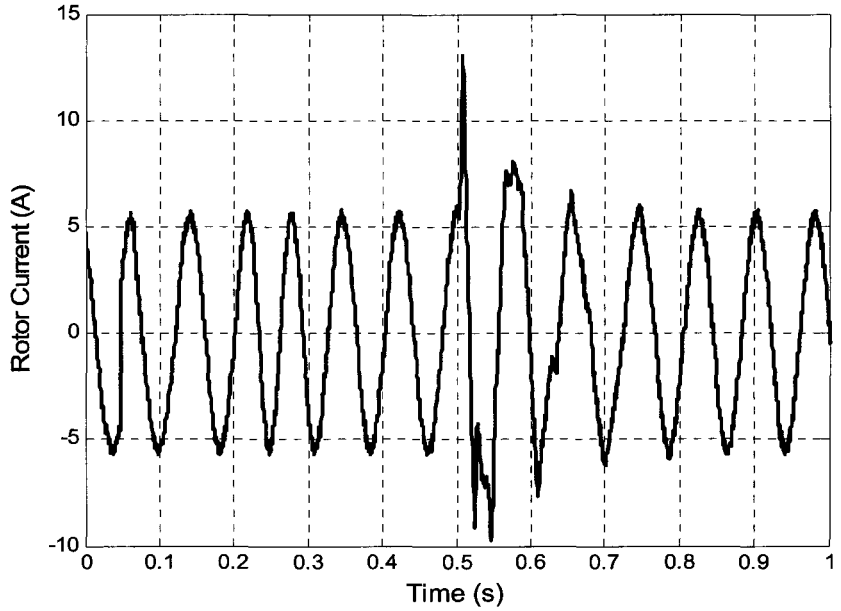

Figure 6.6: Rotor current

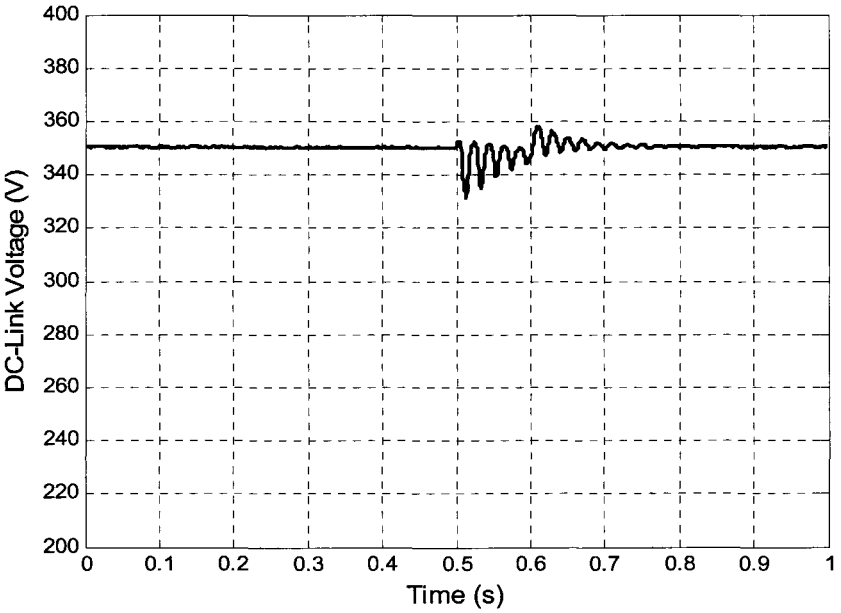

Figure 6.7: DC-link voltage

6.4.2 DFIG with the Fault Ride-Through Scheme

The simulation results shown below, illustrates the implementation of the fault ride-through strategy for the same operating conditions as discussed above. A triggered signal as shown in Fig. 6.8 is generated when a sag of below 90% of

the rated voltage is detected. This is maintained until the voltage is again recovered whereby the output goes low. It is evident from the figure that the detection and trigger happens almost instantaneously. This proves to be extremely valuable as the necessary steps may now be taken to prevent over-currents and over-voltages from occurring in the system. In [4], it was shown that the biggest influence on detection time is the point at which sag occurs. Sags that occur close to the zero crossing have the fastest detection time. For sags that occur around 90°, the detection time is marginally slower (5ms, worst case). Figures 6.9 and 6.10 show the rotor and stator currents after implementing the mitigation strategy as part of the control system. Fig. 6.11 shows the response of the DC-link voltage. It is evident through implementation of the protective strategy that overshooting of the voltage is prevented, thus safeguarding the capacitor bank. The figures illustrate the ability of the algorithm to detect sags and to implement the necessary control to limit the currents and voltages, so as to prevent damage to the machine and power electronics.

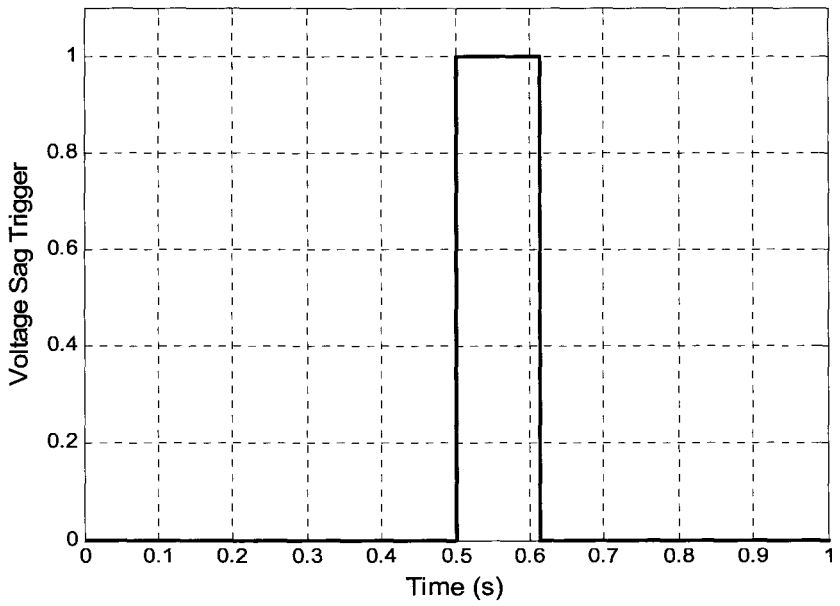

Figure 6.8: Sag trigger signal

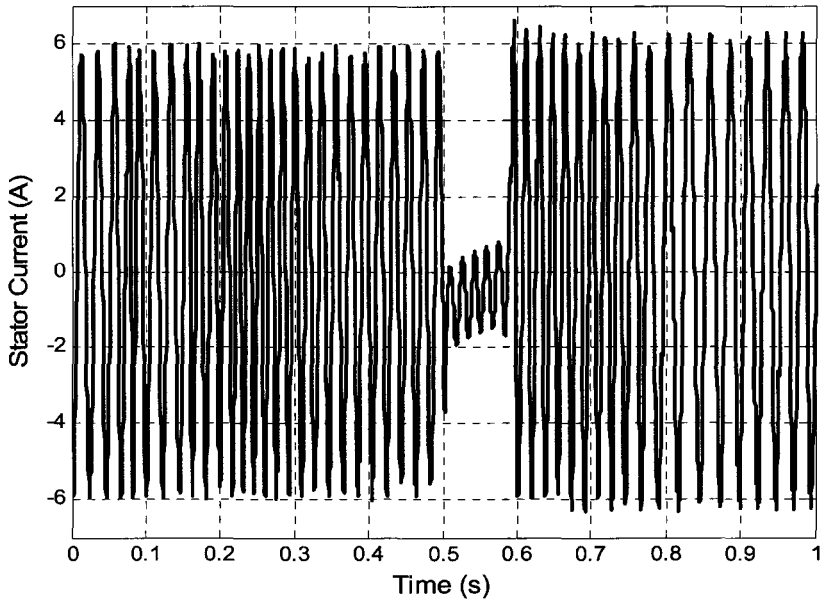

Figure 6.9: Rotor current

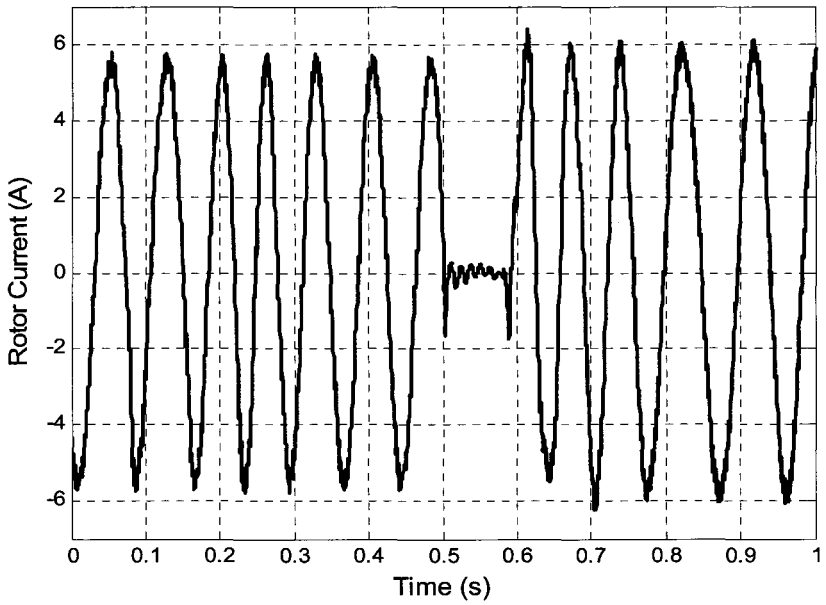

Figure 6.10: Stator current

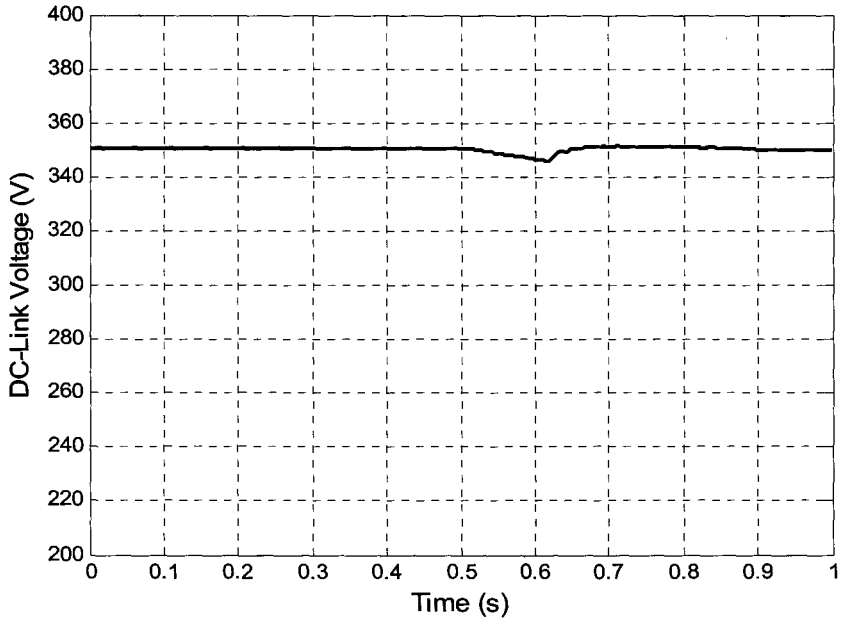

Figure 6.11: DC-link voltage

6.5 Experimental Results

The simulation system from the previous section was implemented practically. This section describes the results. The key purpose of the proposed mitigation strategy is to provide a rapid discharge path for the excess currents during the sag. The rating of the discharge resistor should be selected to carry the maximum anticipated currents. The rapid response of the controller ensures that transients, at the onset of the sag and recovery, are contained.

6.5.1 DFIG without the Fault Ride-Through Scheme

The diagrams below show the experimental results obtained with no mitigation applied. The supply voltage is reduced by 40% for a duration of 280ms to simulate a field sag, shown in Fig. 6.12. A reference voltage of 350V is set for the DC-link capacitor. Figures 6.13 and 6.14 show the increase in rotor and stator currents respectively. Fig. 6.15 shows the rise in DC-link voltage. This is a concern for the converter equipment.

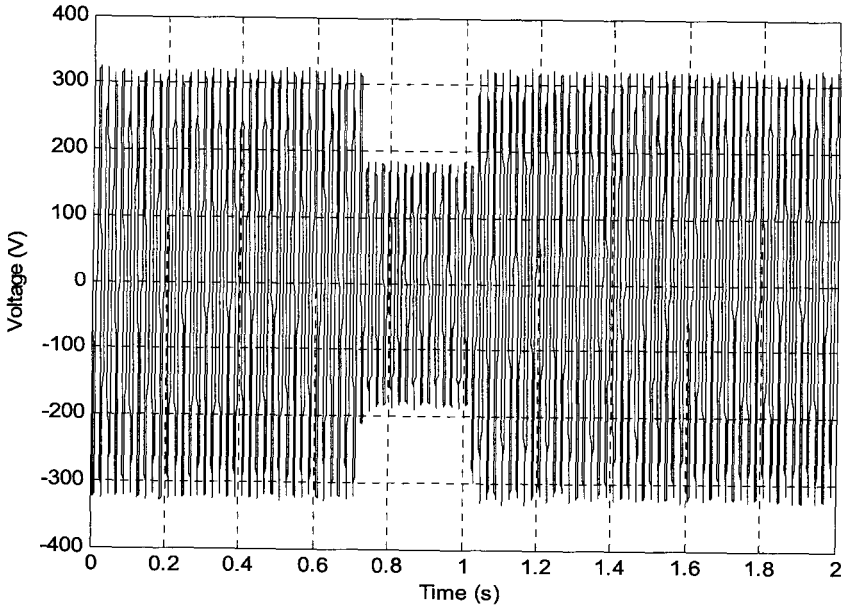

Figure 6.12: Supply voltage

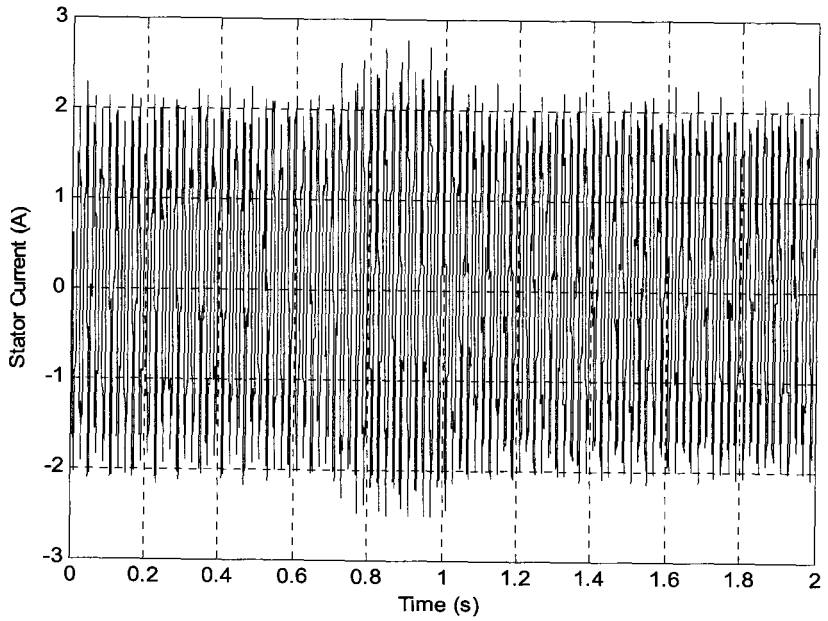

Figure 6.13: Stator current

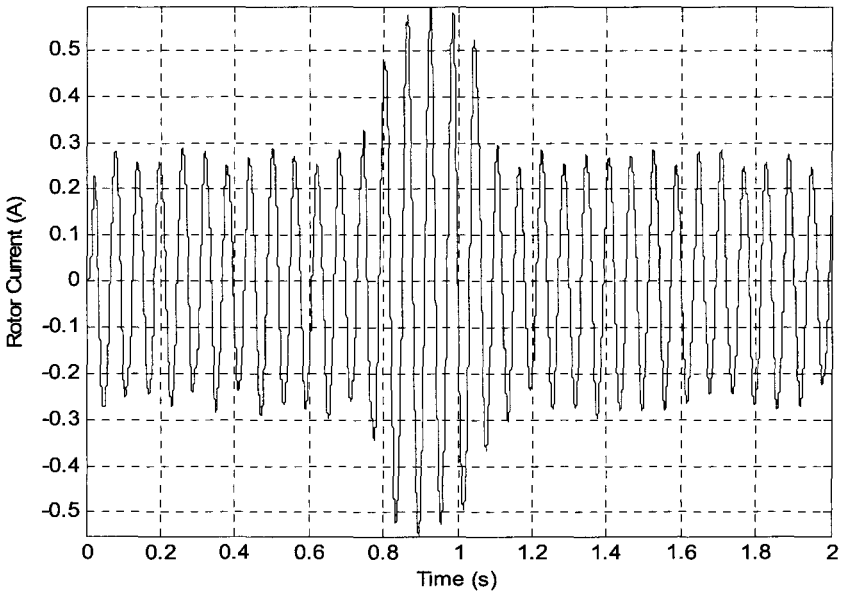

Figure 6.14: Rotor current

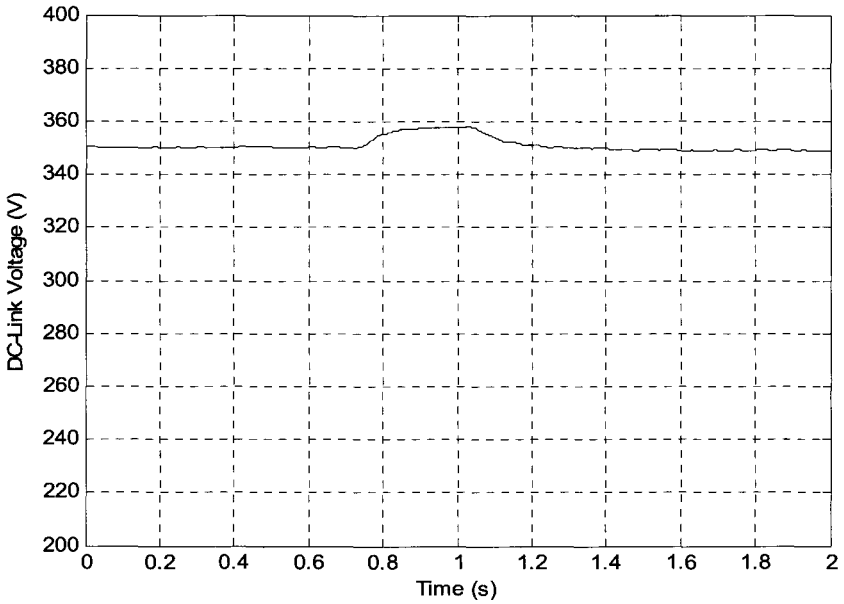

Figure 6.15: DC-link voltage

6.5.2 DFIG with the Fault Ride-Through Scheme

The system was experimentally tested using the proposed mitigation strategy. Figures 6.16 – 6.20 show the supply voltage, trigger signal, rotor current,

stator current and the DC-link voltage respectively. It is clear from the figures that the rotor and stator currents pose no danger to the power electronic converters. The DC-Link voltage is sufficiently reduced and poses no threat to the DC-link capacitor. This also compares well with the simulation results. Further research has to be done in order to incorporate the solution as part of the control system. The control must consider the mechanical torque of the turbine and ensure that the electrical torque is sufficient to provide control, especially during long duration sags. This could be done in combination with the pitch controller [6].

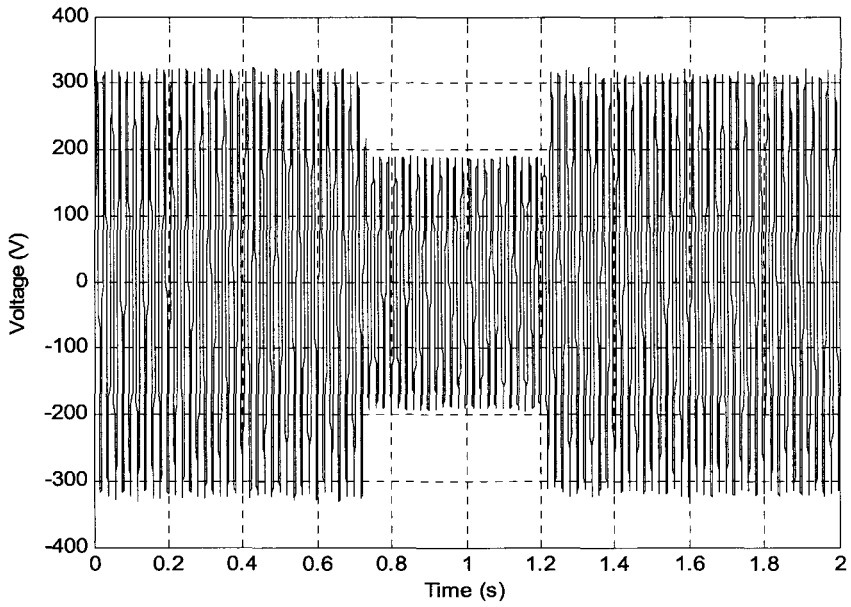

Figure 6.16: Supply voltage

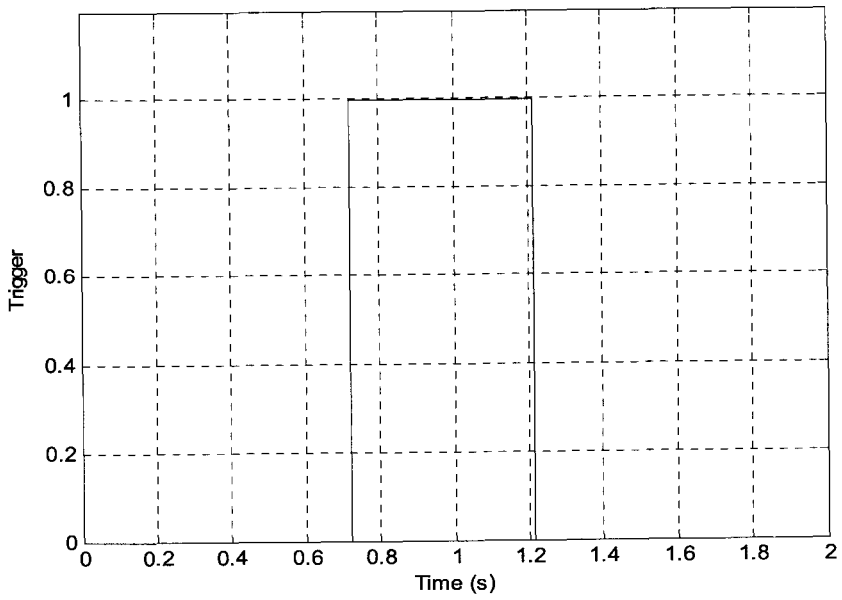

Figure 6.17: Sag trigger signal

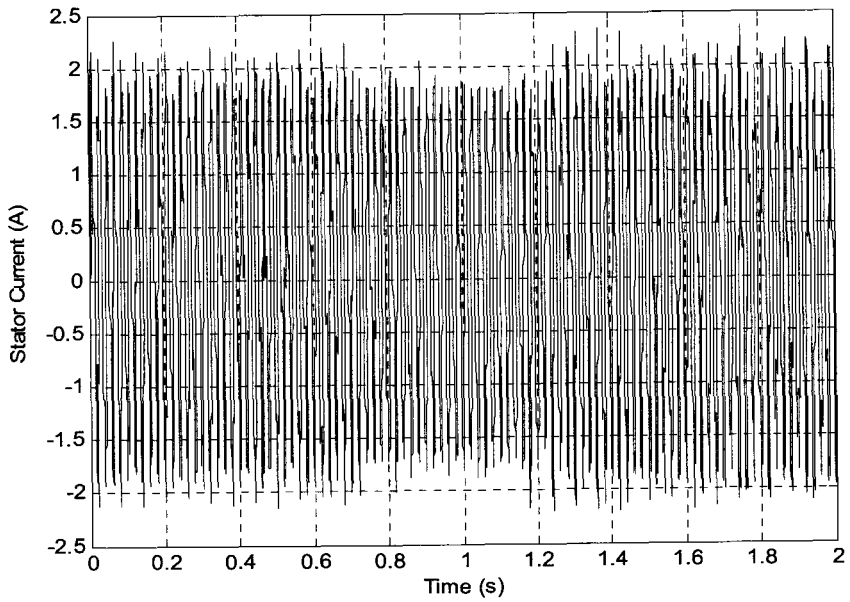

Figure 6.18: Stator current

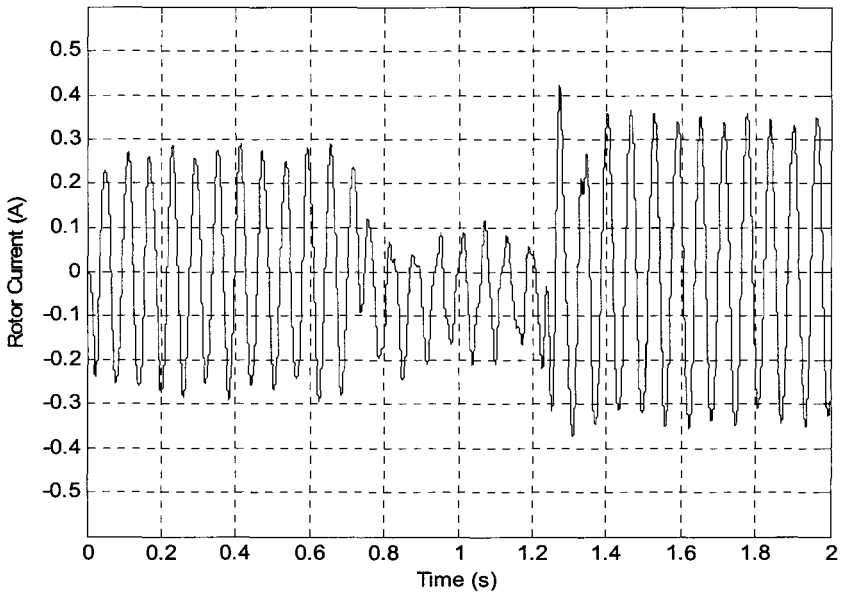

Figure 6.19: Rotor current

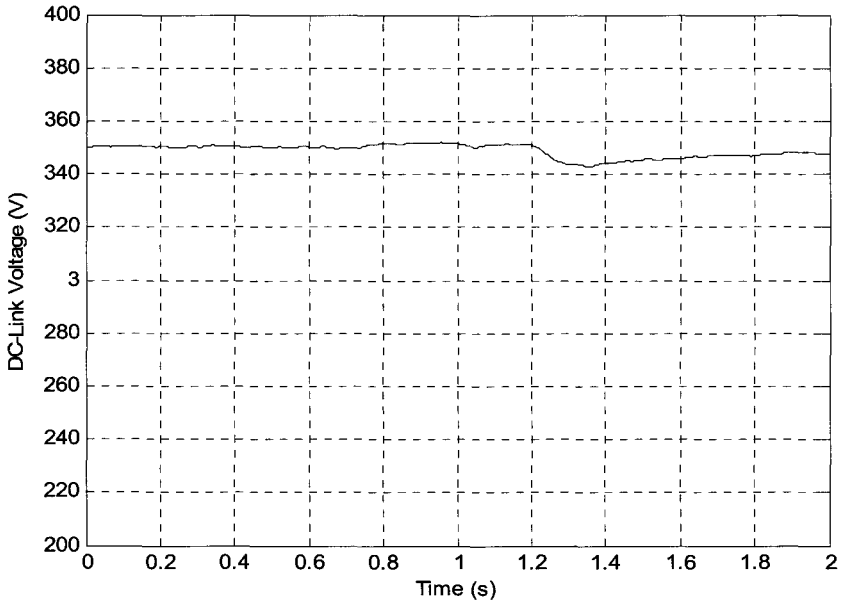

Figure 6.20: DC-link voltage

6.6 Conclusions

This chapter has shown that the impact of sags on the DFIG can be effectively mitigated through a strategy that incorporates rapid sag detection and a discharge resistor. An algorithm was proposed for rapid sag detection. It was shown to detect sags faster than existing techniques. Results showing the ability to protect the drive during sags has been presented and discussed. The proposed strategy is simple and easy to incorporate as part of an existing control system.

6.7 References

[1] J. G. Slootweg, S. W. H de Haan, H. Polinder,W. L. Kling, "General Model for Representing Variable Speed Wind Turbines in Power System Dynamics Simulations," IEEE Transactions On Power Systems, vol.18, no. 1, pp 144-151, Feb. 2003.

[2] A. Mullane, G. Lightbody, R. Yacamani, "Wind-Turbine Fault Ride-Through Enhancement," IEEE Transactions On Power Systems, vol.20, no. 4, pp 1929-1937, November 2005.

[3] M. R. Rathi, N. Mohan, "A Novel Robust Low Voltage and Fault Ride Through For Wind Turbine Application Operating in Weak Grids," Proc. IEEE Ind. Electronics Soc. (IECON'05), pp 2481-2486, 6-10 Nov. 2005.

[4] R. M. Naidoo, P. Pillay, "A New Algorithm for Voltage Sag Analysis and Mitigation", IEEE Power Engineering Society General Meeting, 2005, pp 2935 – 2938, vol. 3, 12-16 June 2005.

[5] J. M. van Coller and S. Q. Davies, "The Threat that Voltage Dips Impose on Wind Power Generation," Proc. Cigre 5th Southern African Regional Conference, Cape Town, Oct. 2005.

[6] [6] J. Morren and S. W. H. de Haan, "Ridethrough of Wind Turbines with Doubly-Fed Induction Generator during Voltage Dip," IEEE Transactions On Energy Conversion, vol.20, no. 2, pp 435-441, June 2005.

[7] J. B. Ekanayake, L. Holdsworth, X. G. Wu, N. Jenkins, "Dynamic Modeling of Doubly-Fed Induction Generator Wind Turbines," IEEE Transactions On Power Systems, vol.18, no. 2, pp 803-809, May 2003.

[8] L. Holdsworth, X. G. Wu, J. B. Ekanayake, N. Jenkins, "Comparison of Fixed Speed and Doubly-Fed Induction Wind Turbines During Power System Disturbances," Proc. Inst. Elec. Eng. Commun., vol. 150, no. 3, pp 343-352, May 2003.

[9] R. M. Hudson, F. Stadler, M. Seehuber, "Latest Developments in Power Electronic Converters for Megawatt Class Windturbines Employing Doubly-Fed Generators, " Proc. Int. Conf. Power Conversion, Intelligent Motion, Nuremberg, Germany, June 2003.

[10] G. Saccomando, J. Svennson, "Control and Operation of Grid-Connected Voltage Source Converter under Grid Disturbances in Variable-Speed Wind Turbines," Proc. European Wind Energy Conf., Copenhagen, Denmark, July 2001.

[11] S. M. Alghuwainem, R. A. Hammouda, A.R. M. Al-Farhan," Transient Analysis of a Wind-Driven Induction Generator," Proc. Canadian Conf. Electrical Computer Engineering, vol.2, pp 13-16, 2001.

[12] D. M. McNamara, "Estimation of Nonstationary Signals Comprising Harmonic-Related Components," Master's Thesis, Clarkson University, Potsdam, New York, Aug. 2005.

Chapter 7

7. CONCLUSIONS

Based on the findings of this research, the following conclusions have been drawn:

1. Time-Frequency Domain Signal Processing Techniques

The mathematical formulation and performance evaluation of a non-stationary adaptive algorithm is presented. Two versions of the non-stationary adaptive algorithm is described. The first is the varying-frequency algorithm which extracts the fundamental sinusoidal component from the input signal. The second is the fixed-frequency algorithm which extracts a sinusoidal component for a specified frequency. Some of the algorithm's key adaptive features are highlighted when evaluating the performance of the algorithm. These include the ability to track changes in amplitude, frequency and phase, while also offering immunity to noise. The gains which need to be defined within the algorithm, provide a trade-off between speed of response versus steady-state error.

The second time-frequency signal processing technique presented is Wavelet analysis. The wavelet transform has been able to overcome the resolution related problems faced by the earlier time-frequency based technique, i.e. STFT. Unlike the STFT, the resolution is varied through the use of a fully scalable modulated window. This satisfies the criterion that higher frequencies are better resolved in time and lower frequencies are better resolved in frequency. The continuous wavelet transform produces a surface in the time and scale (1/frequency) domain. The discrete wavelet transform was introduced to overcome the computing and redundancy problems faced by the wavelet series, which served as a sampled version of the continuous wavelet transform. The transform is implemented through a series of filter bank structures and downsampling/upsampling operations.

2. The Detection of Faults in Inverter-Fed Permanent Magnet Machines

The details for implementation of a low-voltage high-current PM drive for fault analysis has been described. Three of the more common faults in PM Machines (i.e. damaged PM, static eccentricity and inter-coil short) have been described and implemented on the machines.

A new algorithm for fault detection of inverter-fed PM machines operating under non-stationary conditions has been proposed. The detection technique is based on an adaptive algorithm which has been cascaded to extract fault associated sinusoids using the current signals. The results show the algorithm's capability of tracking fault sinusoids under speed and load changes of the machine. It is shown that the case of the inter-coil short produced more promising results than the other two cases, however this is attributed to the sensitivity of the inter-turn fault component and the accuracy of the algorithm to tracking the principal/dominant fault components. However the results still indicate that the algorithm's predictive capability is accurate enough to identify the faults under non-stationary conditions. The proposed fault detection algorithm proves to be extremely successful in its ability to identify different faults under non-stationary operating conditions.

3. The Detection of Mechanical Imbalances in Inverter-Fed Induction Machines

It has been shown that imbalanced faults in inverter-fed induction machines can be identified by decomposing transient inrush currents. This is significant, since most fault detection schemes fail or operate at a diminished level when drives are connected to the machine. The detection algorithm is load dependent, however it only requires a minimum load of approximately 30% at the desired speed. This is a considerable improvement from steady-state analysis techniques where heavier load conditions are required, particularly in the case of inverter-fed machines.

The methodology employed is key and further research using this technique (i.e. for different faults and machines), would only serve to extend the

knowledge base, so as to establish more complete guidelines on fault detection for machines of different designs and sizes.

4. The Detection of Inter-Turn Stator Faults in Doubly-Fed Wind Generators

The details for implementation of a DFIG system in its application to wind generation has been described. Inter-turn faults are simulated on the DFIG to provide a comparative study into various fault analysis techniques. A new algorithm for detection of inter-turn faults under non-stationary conditions has been proposed. The detection algorithm based on the Extended Parks Vector Approach, whereby the signal processing tool used for analysis, i.e. Fourier Transform, is replaced by the non-stationary fixed-frequency sinusoid-tracking algorithm. The proposed fault detection algorithm proves to be extremely successful in its ability to unambiguously identify the inter-turn fault under non-stationary operating conditions. This is ideally suited for wind generators since most operate predominately in the transient. It is also shown that the severity of the inter-turn fault may be assessed through the proposed fault detection technique, which other techniques have been unable to achieve. The implementation of the algorithm is also considerably simple, thus limiting the processing capabilities required to process the algorithm in real-time applications.

5. A Strategy for Wind Turbine Sag Mitigation Through Rapid Sag Detection

This chapter has shown that the impact of sags on the DFIG can be effectively mitigated through a strategy that incorporates rapid sag detection and a discharge resistor. An algorithm was proposed for rapid sag detection. It was shown to detect sags faster than existing techniques. Results showing the ability to protect the drive during sags has been presented and discussed. The proposed strategy is simple and easy to incorporate as part of an existing control system.

6. Closing Remarks

Condition monitoring has become a core aspect of asset management, and has progressively attracted more attention worldwide. Its increase in popularity is attributed to the realization that failure prediction forms a pivotal component in the optimum utilization of existing assets in a competitive environment.

Although steady-state techniques exist and are well established, the advancement in signal processing techniques has produced a new class of algorithms, capable of analysing nonstationary signals. These are particularly relevant to the detection of faults in electrical machines since the machine diagnostic variables typically behave as nonstationary signals.

The findings in this project, exemplifies the relevance of these new class of nonstationary signal processing tools to the condition monitoring of electrical machines. This proved to provide some prevalent findings which serves to extend the knowledge base for condition monitoring of electrical machines.

APPENDIX A: Author's Publications

A.1 Journals

A.1.1 P. Barendse, P. Pillay, "A Doubly-Fed Induction Generator Drive for a Wind Energy Conversion System", SAIEE Africa Research Journal, Vol. 97, No. 4, pp-274-280, December 2006

A.2 Conferences

A.2.1. P. Barendse, H. Douglas, P. Pillay, "Condition Monitoring of Induction Generators For Wind Energy Conversion Systems (WECS)", World Wind Energy Conference 2003, Cape Town, November 2003

A.2.2. P. Barendse, P. Pillay, "Matlab Simulation of a Doubly-Fed Induction Generator (DFIG) System in it's Application to Wind Energy Generation", SAUPEC04, Stellenbosch, January 2004

A.2.3. P. Barendse, P. Pillay, "A Doubly-Fed Induction Generator System in it's Application to Wind Energy Generation", SAUPEC05, Johannesburg 2005

A.2.4. P. Barendse, H. Douglas, P. Pillay, "Condition Monitoring of Doubly-Fed Induction Generators for Wind Energy Conversion Systems ", 2005 IEEE IAS Annual Meeting, Hong Kong

A.2.5. P. Barendse, P. Pillay, "Experimental Setup for Examining Faults in Wind Generators", SAUPEC06, Durban 2006

A.2.6. P. Barendse, P. Pillay, "A New Algorithm for the Detection of Faults in Permanent Magnet Machines", 2006 IEEE IECON Annual Meeting, Paris, France

A.2.7. P. Barendse, P. Pillay, "A New Algorithm for the Detection of Inter-Turn Stator Faults in Doubly-Fed Wind Generators", 2006 IEEE IECON Annual Meeting, Paris, France

A.2.8. P. Barendse, R. Naidoo, Dr H. Douglas, P. Pillay, "A New Algorithm for Improved Dip/Sag Detection with Application to Improved

Performance of Wind Turbine Generators", 2006 IEEE IAS Annual Meeting, Florida, USA

A.2.9. P. Barendse, P. Pillay, "A Review of Inter-Turn Stator Fault Detection Techniques for Doubly-Fed Wind Generators", SAUPEC07, Cape Town 2007

A.2.10. P. Barendse, P. Pillay, "The Detection of Unbalanced Faults in Inverter-Fed Induction Machines", IEEE SDEMPED07, 6-8 Sept 2007, Krakow, Poland